1. point-by-point response to the reviews

Reply to Referee#1' comments:

Reviewer #1: In this manuscript, the authors are trying to quantify and investigate the impact of unknown daytime HONO sources on the HO_x budget in the eastern coast of China. The authors should address the following issues before the Manuscript can be considered for publication.

Major concerns:

1. Page 808, lines 20 to 23:

The authors concluded that HONO photolysis reaches a maximum of 10 ppb/h while that of HO_2+NO is 9.38 ppb/h, which is very unlikely. The total OH initiation sources (including that of HONO) may contribute between 15-25% of the total OH production rates. OH production rate from HO_2+NO makes typically between 60-85% of the total OH production. HONO photolysis is an initiation source of OH and does not exceed (as a net source, after subtracting OH+NO=HONO) ~3 ppb/h as maximum (e.g., Kleffmann et al.,2005; Elshorbany et al.,2009) and can reach as high as 80% of the total OH initiation sources but NOT the total OH production rate.

(i) The major reason is that we have not subtracted OH+NO=HONO. According to your suggestions, we recalculated the net OH production rate from HONO photolysis: $P(OH)_{HONOnet} = P(OH)_{HONO+hv} – L(OH)_{OH+NO}$, where P and L are the production and loss rates, respectively (Figs. R1 and R2). As shown in Fig. R1, when the additional HONO sources were inserted into the WRF-Chem model, the diurnal peak of $P(OH)_{HONO+hv}$ was 10.01 ppb $h^{–1}$ in Beijing, 2.63 ppb $h^{–1}$ in Shanghai, and 2.60 ppb $h^{–1}$ in Guangzhou, while the diurnal peak of $L(OH)_{OH+NO}$ was 6.90 ppb $h^{–1}$ in Beijing, 1.73 ppb $h^{–1}$ in Shanghai, and 1.54 ppb $h^{–1}$ in Guangzhou. The net contribution of the HONO photolysis to OH (after subtracting OH+NO=HONO) reached a maximum of 3.72 ppb h^{-1} in Beijing, 0.89 ppb h^{-1} in Shanghai, and 0.97 ppb h^{-1} in Guangzhou respectively (Fig. R3), consistent with the result (3 ppb h^{-1}) of Hofzumahaus et al. (2009) mentioned above.

(ii) The revised OH budgets are shown in Table R1. The contribution of the total OH initiation sources to the total OH production rates was 19.68% in Beijing, 23.28% in Shanghai, and 13.38% in Guangzhou, in the range of 15-25%

mentioned by Reviewer #1. The contribution of HO_2+NO was 61.95-73.34% of the total OH production rates (Table R1), in the range of 60-85% mentioned by Reviewer #1. Additionally, among all the OH initiation sources, HONO photolysis contributed 39.85%-71.87% of the total OH initiation sources (NOT the total OH production rate), with the largest being close to the 80% mentioned above.

2. Hofzumahaus et al. (2009) investigated the OH budget in one of this study's domains (PRD) and measured maximum OH production rates of about 35 and 2 ppb/h from HO_2+NO and HONO photolysis, respectively. How the authors would explain these large differences between their model results and these measurements?

(i) The contribution of HONO photolysis was revised (see the response to question 1 of Reviewer #1).

(ii) The contribution of HO_2+NO in this study was not as high as ~35 ppb h^{-1} (Hofzumahaus's results). The major reason is the underestimation of HO_2 in our study (Fig. R5). This underestimation was partially associated with the underestimation of anthropogenic VOCs (AVOCs) emissions (Wang et al., 2014), Wang et al. (2014) demonstrated that a 68% increase in the AVOCs emissions [the uncertainty of the AVOCs emissions could be ±68% (Zhang et al., 2009)] led to significant improvements in the HO_2. We added one case simulation (Case S in Fig. R4) by increasing the AVOCs emissions by 68%. When the AVOCs emissions were increased by 68%, the conversion rate of HO_2+NO was increased to 11.43 ppb h^{-1} from 9.38 ppb h^{-1} in Beijing, 3.34 ppb h^{-1} from 2.63 ppb h^{-1} in Shanghai, 5.78 ppb h^{-1} from 4.88 ppb h^{-1} in Guangzhou respectively (Fig. R4).

(iii) Although the anthropogenic VOCs emissions were increased by 68%, the simulated hourly HO_2 concentrations were still considerably underestimated by comparison with the observations in the period of July 5-25, 2006 (Fig. R5). So the contribution of HO_2+NO to OH was still lower than that (35 ppb h^{-1}) of

Hofzumahaus et al. (2009). Further studies are needed for HO_2 simulations.

3. Page 808, lines 24 to 28:
What is this OH production rate, daytime mean? Even then, HONO contribution is almost similar to HO_2+NO (about 4 ppb/h). That is also very unlikely, see above. Further the loss terms due to CO is very high. If CO loss term is very high in the region, you would probably have also so much VOC loss and therefore also high HO_2+NO to compensate, given the high NO_x levels in eastern China.
(i) We used "*the daytime average OH production rate***" instead of "***the OH production rate***", and used "***the daytime average OH loss rate***" instead of "***the OH loss rate***", and added necessary "***daytime average***" in the whole revised version.**

(ii) After recalculating the net OH production rate from HONO photolysis (subtracting OH+NO=HONO), the contribution of HO_2+NO to the OH production rate was much higher than that of HONO photolysis (Fig. R3). The former reached a maximum of 9.38 ppb h^{-1} in Beijing, 2.63 ppb h^{-1} in Shanghai, and 4.88 ppb h^{-1} in Guangzhou, respectively, while the maximum of the later was 3.72 ppb h^{-1} in Beijing, 0.89 ppb h^{-1} in Shanghai, and 0.97 ppb h^{-1} in Guangzhou, respectively (Fig. R3).

(iii) The contribution of HO_2+NO in this study was not high. The major reason is the underestimation of HO_2 in our study (see the response to question 2 of Reviewer#1).

4. Page 813, line 13:
By referring to the mentioned study, it is HONO/NO_x and not HONO/NO_2.
We have revised our description in the Introduction section: "*This is the reason why the recent CalNex 2010 (California Research at the Nexus of Air Quality and Climate Change) study found a very strong positive correlation (R^2= 0.985) between HONO flux and the product of NO_2 concentration and solar radiation at Bakersfield site (Ren et al., 2011).***"**

5. Page 813, line 17:
The authors mentioned they used data from 13 field measurement campaigns around

the globe. Why data from around the globe if the study domain is located only on eastern coast of China?

We used the data from 13 field measurement campaigns around the globe. The reasons are below:

(i) We want to know whether the correlations of the $P_{unknown}$ with NO_2 mixing ratios and $[NO_2]\cdot J(NO_2)$ are consistent around the globe.

(ii) The measurement campaigns of HONO are still limited around the world，especially in China, but a statistical result needs large samples.

(iii) Fig. R6 shows the correlations of the $P_{unknown}$ with $[NO_2]$ and $[NO_2]\cdot J(NO_2)$ in the coastal areas of China, the other countries, and the globe, respectively. Compared with that around the globe (Fig. R6ef), the correlation coefficient (R^2) between the $P_{unknown}$ and $[NO_2]$ was decreased to 0.38 from 0.75, while the correlation coefficient between the $P_{unknown}$ and $[NO_2]\cdot J(NO_2)$ was decreased to 0.48 from 0.80 (Fig. R6abef). However, the linear regression slope of the latter was 17.37 (Fig. R6b), very close to the 19.60 based on the data around the globe (Fig. R6f).

The correlation coefficients between the $P_{unknown}$ and $[NO_2]$ and between the $P_{unknown}$ and $[NO_2]\cdot J(NO_2)$ were 0.15 and 0.33, respectively (Fig. R6cd), much lower than those in the coastal areas of China (Fig. R6ab).

(iv) The description was added in section 2.2: *"For the coastal regions of China, the correlation between the $P_{unknown}$ and* $NO_2\cdot J(NO_2)$ *was 0.48, with a linear regression slope of 17.37 (Fig. S2b in the Supplement), which is within the maximum $P_{unknown}$ uncertainty range of 25% (Table S1)."*

(v) The uncertainties in the observed data were added in the Table R2. In the study of Su et al. (2008, 2011), the uncertainty in the $P_{unknown}$ values calculated by the PSS (see the response to question 8 of Reviewer #1) is 10-25%. Sörgel et al.

(2011) suggested the uncertainty in the PSS mainly originated from OH measurements with an accuracy of ±18 %. With the same method (PSS), Wong et al. (2012) also proposed an uncertainty of 10-20% in the $P_{unknown}$ values. To assess the impacts of the uncertainty in the $P_{unknown}$ parameterization on production and loss rates of HONO, two sensitivity cases (Case R_{inc} and Case R_{dec}) were performed. Case R_{inc} includes case R_p with an increase of 25% (the maximum uncertainty range according to the previous studies above) in the slope factor (19.60); Case R_{dec} is the same as case R_p with a decrease of 25% in the slope factor (19.60). The sensitivity results show that a 25% increase (25% decrease) in the slope factor (19.60) led to a 9.19-18.62% increase (12.69-14.32% decrease) in the maximum HONO production rate and a 0-17.64% increase (8.40-14.07% decrease) in the maximum HONO loss rate (Fig.R7) (section 3.2 in the revised version).

6. Page 815, line 1:
Which studies? Please write the reference(s).
The references were added in section 2.2: "*Previous studies (Sörgel et al., 2011; Villena et al., 2011; Wong et al., 2012) have shown $P_{unknown} \propto [NO_2]\cdot J(NO_2)$.***"**

7. Page 815, line 5:
Figure 2 is not clear at all; references are almost not readable. Which good correlation the authors mean? The slop and the correlation coefficient in these two plots are calculated based on the high NO_2 points! The low NO_2 points do not correlate at all and should have been plotted in another plot? And would have probably results in negative slope.
(i) The data and related references used in Figure 2 were added in Table R2 (were also added in the revised Supplement).

(ii) According to your suggestions, we calculated the correlations of the $P_{unknown}$ with $[NO_2]$ and $[NO_2]\cdot J(NO_2)$ in China (corresponding to the high NO_2 points) and in the other countries (corresponding to the low NO_2 points) as shown in Fig. R6. Please see the response to question 5 of Reviewer #1, the correlation

coefficients calculated based on the high NO_2 points located mainly in China were higher than those based on the low NO_2 points located mainly in the other countries.

8. Also, How the authors define the data selection criteria (for Fig 2), e.g., did the authors used J-values near sunrise and sunset? What type of data (mean, median, max, min, ..etc.), measurements techniques, ..etc..?

Please see Table R2.

(i) The $P_{unknown}$ in this study was calculated by the daytime HONO budget analysis below.

$$\frac{d[HONO]}{dt} = \left(P_{OH+NO} + P_{emission} + P_{transport} + P_{unknown}\right) - \left(L_{HONO+hv} + L_{OH+HONO} + L_{deposition} + L_{transport}\right)$$

(Sörgel et al., 2011; Wong et al., 2012; Spataro et al., 2013)

where $\frac{d[HONO]}{dt}$ is the instantaneous rate of HONO, P_{OH+NO} is HONO production rate from R1, $P_{transport}$ is HONO transport processes including horizontal and vertical transports, $P_{emission}$ is direct emissions of HONO from vehicles, $P_{unknown}$ is the additional unknown daytime HONO source(s). In the sink terms, $L_{HONO+hv}$ is HONO photolysis rate, $L_{HONO+OH}$ is HONO loss rate by HONO+OH, $L_{deposition}$ is HONO deposition rate, and $L_{transport}$ is dilution effects through transport processes. When the photolysis frequency of HONO (J_{HONO}) is greater than 1.0×10^{-3} s^{-1}, the lifetime of HONO is less than 17 minutes. Then the influences of transport and deposition on HONO ($P_{transport}$, $L_{deposition}$ and $L_{transport}$) are weak, can be omitted from the equation above. Therefore, the equation could be expressed:

$$P_{unknown} + P_{OH+NO} + P_{emission} \approx L_{HONO+hv} + L_{OH+HONO}$$

To obtain reasonable $P_{unknown}$ values, we must ensure that all of $J(NO_2)$ values we used are higher than 1.0×10^{-3} s^{-1}. The data used in this study were in the daytime (from 8:00 to 15: 30), and the $J(NO_2)$ values near sunrise and sunset were

eliminated (Table R2).

(ii) Mean values of the data were used, and related references as well as the measurement techniques were added in Table R2.

9. Since the study of the impact of the unknown HONO sources is limited to China, why do not you limit the analysis and the parameterization to these regions. This way, the authors would be able to better parameterize this unknown source, given the knowledge of all controlling factors, e.g., surface areas, topography, radiation and dynamics. Limiting the parameterization to the measurement location would also help elucidate and shed some light on the sources and nature of this unknown source.

(i) Although our studied areas are focused on the coastal areas of China, very useful is a general parameterization of the $P_{unknown}$ used in different regions of the world. For the correlation between the $P_{unknown}$ and $[NO_2] \cdot J(NO_2)$ the linear regression slope was 17.37 in China (Fig. R6b), very close to the value of 19.60 around the globe (Fig. R6f), indicating that the $P_{unknown}$ parameterization can be used in different regions of the world, where NO_x emissions are high.

(ii) Your suggestions are very important. However, some controlling factors, e.g., measured surface areas and radiation are not available from the references (Wu et al., 2013, Villena et al., 2011, N. Zhang et al., 2012, ……) (Table R2), except for Su et al. (2011) and Spataro et al. (2013); Your suggestions will be considered in the future.

10. The authors need to first determine the correct parameterization for this region before investigating the impacts on HO_x, which would also require reasonable estimation of HO_x budgets.

According to your suggestions, we have shown the details about the parameterization for China and other countries (see above).

Reply to Referee#2' comments:

Reviewer #2: General comments:
The manuscript tried to quantify the impact of the unknown HONO source on the concentrations and budgets of HONO, HO_x radicals and RO_2 radicals in the eastern coast of China by utilizing a model simulation and parameterized unknown HONO source strength. To fulfill this meaningful aim, reasonable parameterization of HONO source and uncertainty analysis of the results are important. However, the uncertainty analysis is not found in the manuscript and the parameterization is not fully justified. Hence, this manuscript is recommended to be published in Atmos. Chem. Phys. unless both parameterization justification and uncertainty analysis are well addressed.

Specific comments:
1. parameterization justification:
A. HONO emission is considered. In page 812, line 6-7, you stated that an emission ratio of 2.3% for $HONO/NO_2$ used in other study is relatively high. However, in page 814, line 15, you choose to use the same ratio of 0.023 in your model. Please explain.

As shown in the Introduction section, Li et al. (2010) used the $HONO/NO_2$ ratio of 2.3%. The ratio of 2.3% is only applicable for diesel vehicles, so we used the formula ($[0.023 \times f_{DV} + 0.008 \times (1 - f_{DV})] \times f_{TS}$) to calculate HONO emissions. Where f_{DV} denotes the NO_x emission ratio of diesel vehicles to total vehicles, and f_{TS} is the NO_x emission ratio of the traffic source to all anthropogenic sources (Li et al., 2011; An et al., 2013; Tang et al., 2014). The final ratio for $HONO/NO_x$ as HONO emissions was 1.18% in the BTH.

B. You noticed that HONO chemistry is different near the surface and over the surface within 1000 m. Is this difference explained by the NO_2, $J(NO_2)$ and aerosol surface density? Why NO_2 heterogeneous reactions on ground surface is not considered in your model?

(i) The differences of HONO concentrations near the surface and over the surface within 1000 m can be calculated from the formula $P_{unknown} \approx 19.60 [NO_2] \cdot J(NO_2)$ when those of NO_2 mixing ratios and $J(NO_2)$ are known. However, the specific chemistry for HONO formation near the surface and over the surface within 1000 m is still unknown because this formula is a statistical result. The specific chemistry for HONO formation near the surface and over the surface within 1000 m is beyond the aim of this paper, and will be investigated in

the future.

(ii) Whether NO_2 heterogeneous reactions on ground surface is a source of HONO is still argued. Several model studies (e.g., Li et al., 2010; Wong et al., 2013) have suggested that the NO_2 heterogeneous reactions on ground surface were a possible source of daytime HONO, however, field experiments showed a good correlation between concentrations of particulate matter and HONO (An et al., 2009), or between aerosol surface area and HONO concentrations (Ziemba et al., 2010), suggesting that aerosol surface is the dominant reaction substrate and that stationary sources (e.g., buildings and soils) are likely insignificant (Ziemba et al., 2010). So more field experiments are needed to validate this mechanism, which could be discussed in the future.

C. In page 811, photo-enhanced heterogeneous reactions and photolysis of surface-adsorbed HNO_3 are summarized as HONO sources. Why these two sources are excluded in your model?

(i) For photolysis of surface-adsorbed HNO_3, only one laboratory study about this reaction was conducted (Zhou et al., 2002b, 2003). A chamber study demonstrated that the photolysis of nitrate which was recently postulated for the observed photolytic HONO formation on snow, ground, and glass surfaces, can be excluded in the chamber (Rohrer et al., 2005). So more laboratory and field studies are required to validate this mechanism, which could be considered in our future work.

(ii) For photo-enhanced heterogeneous reactions, our formula $P_{unknown} \approx 19.60[NO_2] \cdot J(NO_2)$ has some implications.

D. The unknown source strength ($19.60*NO_2*S/V$) is fitted using HONO measurement globally. Is it good for China eastern coast?

We used the data from 13 field measurement campaigns around the globe.

The reasons are below:

(i) We want to know whether the correlations of the $P_{unknown}$ with NO_2 mixing ratios and $[NO_2] \cdot J(NO_2)$ are consistent around the globe.

(ii) The measurement campaigns of HONO are still limited around the world， especially in China, but a statistical result needs large samples.

(iii) Fig. R6 shows the correlations of the $P_{unknown}$ with $[NO_2]$ and $[NO_2] \cdot J(NO_2)$ in the coastal areas of China, the other countries, and the globe, respectively. Compared with that around the globe (Fig. R6ef), the correlation coefficient (R^2) between the $P_{unknown}$ and $[NO_2]$ was decreased to 0.38 from 0.75, while the correlation coefficient between the $P_{unknown}$ and $[NO_2] \cdot J(NO_2)$ was decreased to 0.48 from 0.80 (Fig. R6abef). However, the linear regression slope of the latter was 17.37 (Fig. R6b), very close to the 19.60 based on the data around the globe (Fig. R6f).

2. uncertainty analysis

A. How the uncertainty in parameterization on HONO source impact the model simulation? What kind of improvement have you made compared to previous model work?

(i) The $P_{unknown}$ in this study was calculated by the daytime HONO budget analysis (Photo Stationary State (PSS) approach) below.

$$\frac{d[HONO]}{dt} = \left(P_{OH+NO} + P_{emission} + P_{transport} + P_{unknown}\right) - \left(L_{HONO+hv} + L_{OH+HONO} + L_{deposition} + L_{transport}\right)$$

(Sörgel et al., 2011; Wong et al., 2012; Spataro et al., 2013)

where $\frac{d[HONO]}{dt}$ is the instantaneous rate of HONO, P_{OH+NO} is HONO production rate from R1, $P_{transport}$ is HONO transport processes including horizontal and vertical transports, $P_{emission}$ is direct emissions of HONO from vehicles, $P_{unknown}$ is the additional unknown daytime HONO source(s). In the sink terms, $L_{HONO+hv}$ is HONO photolysis rate, $L_{HONO+OH}$ is HONO loss rate by HONO+OH, $L_{deposition}$ is HONO deposition rate, and $L_{transport}$ is dilution effects

through transport processes. When the photolysis frequency of HONO (J_{HONO}) is greater than 1.0×10^{-3} s^{-1}, the lifetime of HONO is less than 17 minutes. Then the influences of transport and deposition on HONO ($P_{transport}$, $L_{deposition}$ and $L_{transport}$) are weak, can be omitted from the equation above. Therefore, the equation could be expressed:

$$P_{unknown}+P_{OH+NO}+P_{emission}\approx L_{HONO+hv}+L_{OH+HONO}$$

The uncertainties in the observed data were added in the Table R2. In the study of Su et al. (2008, 2011), the uncertainty in the $P_{unknown}$ values calculated by the PSS is 10-25%. Sörgel et al. (2011) suggested the uncertainty in the PSS mainly originated from OH measurements with an accuracy of ±18 %. With the same method (PSS), Wong et al. (2012) also proposed an uncertainty of 10-20% in the $P_{unknown}$ values. To assess the impacts of the uncertainty in the $P_{unknown}$ parameterization on production and loss rates of HONO, two sensitivity cases (Case R_{inc} and Case R_{dec}) were performed. Case R_{inc} includes case R_p with an increase of 25% (the maximum uncertainty range according to the previous studies above) in the slope factor (19.60); Case R_{dec} is the same as case R_p with a decrease of 25% in the slope factor (19.60). The sensitivity results show that a 25% increase (25% decrease) in the slope factor (19.60) led to a 9.19-18.62% increase (12.69-14.32% decrease) in the maximum HONO production rate and a 0-17.64% increase (8.40-14.07% decrease) in the maximum HONO loss rate (Fig.R7) (section 3.2 in the revised version).

(ii) Unexpected high HONO concentrations have been observed in recent years. However, most current air quality models have underestimated HONO observations, particularly in the daytime (Czader et al., 2012; Gonçalves et al., 2012; Li et al., 2011). Although some of modeling studies have improved HONO

daytime simulations by incorporating the new HONO formation mechanisms, e.g., HNO_3 surface photolysis (Sarwar et al., 2008), the NO_2 heterogeneous reaction on aerosols and ground surface (Li et al., 2010; Wong et al., 2013) into air quality models, these HONO daytime formation mechanisms are still under discussion (see the responses to question 1B and 1C of Reviewer #2). Different from these modeling studies above, we derived a formula ($P_{unknown} \approx 19.60[NO_2] \cdot J(NO_2)$) based on the observation data from 13 different field campaigns to quantify the unknown daytime HONO source, and then coupled the $P_{unknown}$ into the WRF-Chem model based on our previous studies (Li et al., 2011; An et al., 2013; Tang et al., 2014). We found that the $P_{unknown}$ significantly improved the daytime HONO simulations. We also assessed the impacts of the $P_{unknown}$ on the concentrations and production and loss rates of HONO, OH, HO_2, and organic peroxy radicals (RO_2).

For modeling study, this is a new and simple method to help quantify the daytime HONO source if the detailed formation mechanism of HONO in the daytime is unknown. However, needed are more field and laboratory studies for the detailed formation mechanism of HONO in the future .

B. How the model itself and these inputs affect the model output?

In general, the main influencing factors for model output are meteorological fields and the emissions inventory.

(i) Comparison of simulated and observed meteorological factors has been made in our previous study (Wang et al., 2014). The RMSE was 2.5°C for air temperature (TA), 16.3% for relative humidity (RH), 2.5 m s^{-1} for wind speed (WS), and 99.3° for wind direction (WD), whereas the IOA was 0.90 for TA, 0.78 for RH, 0.56 for WS, and 0.65 for WD (Table R3). These statistical metrics indicated that the simulations of TA and RH were much better than those of WS

and WD. The results were very similar to the studies of Wang et al. (2010) and Li et al. (2012) using the fifth-generation Pennsylvania State University/National Center for Atmospheric Research Mesoscale Model (MM5), and those of H. Zhang et al. (2012) using the WRF model (Table R3). The definitions of root-mean-square error (RMSE), mean bias (MB), normalized mean bias (NMB), correlation coefficient (RC), and index of agreement (IOA) are available in Simon et al. (2012).

(ii) As for the emissions inventory, monthly anthropogenic emissions of SO_2, NO_x, CO, VOCs, PM_{10}, $PM_{2.5}$, BC, and OC in 2006/2007 were obtained from Zhang et al. (2009) and those of NH_3 from Streets et al. (2003) and monthly emissions of other species were derived from Zhang et al. (2009). The anthropogenic and biogenic emissions were the same as those used by An et al. (2011, 2013), Li et al. (2011, 2014), Tang et al. (2014), and Wang et al. (2014).

(iii) The uncertainty of anthropogenic VOCs (AVOCs) emissions in China is large (Wang et al., 2014). Wang et al. (2014) demonstrated that AVOCs emissions in 2006 from Zhang et al. (2009) were underestimated by ~68% in suburban areas and by more than 68% in urban areas. The substantial underestimation of AVOCs emissions is one of the main reasons for low simulations of HO_2 and low contributions of HO_2+NO in this study. This will be improved in our future work.

C. The model-observation difference is quite considerable in Fig. 4-6. How to make sure your results is a trustful one?

(i) The model performance for O_3 and NO_x in Beijing was good and comparable with other applications of the CMAQ model by Li et al. (2012). However, the model performance in Guangzhou of the PRD region was not as good as that in Beijing. The model-observation difference in Guangzhou is mainly caused by the

underestimation of the emissions inventory. If the emissions are improved, the WRF-Chem model will well simulate the mixing ratios of considered chemical species. Take Beijing as an example, we added the comparison of simulated and observed O_3 at six sites in the BTH (Fig. R8), with an RC of 0.84, NMB of -4.0%, NME of 35.0%, and IOA of 0.91 , better than the results of Li et al. (2012) and Wang et al. (2010).

(ii) Although there are some differences in HONO simulations, we have significantly improved the HONO simulations in both daytime and nighttime.

(iii) The model performance for OH in Guangzhou was good; whereas, that for HO_2 was underestimated. This underestimation was mainly associated with the underestimation of the AVOCs emissions (Wang et al., 2014).

3. In page 809, line 15-17: other OH primary sources, such as HCHO photolysis, is widely accepted. Add them!

According to the previous studies (Alicke et al., 2003; Ren et al., 2003; Lu et al., 2012), the HCHO photolysis is not the direct source of OH. The reaction product of HCHO photolysis is HO_2, which contributes to the OH formation via the reaction of HO_2 with NO. The photochemistry of HCHO is below (Meller and Moortgart, 2000),

$$\mathrm{HCHO+hv \rightarrow H+HCO} \quad (1)$$

$$\mathrm{HCHO+hv \rightarrow H_2+CO} \quad (2)$$

$$\mathrm{H+O_2 \rightarrow HO_2} \quad (3)$$

$$\mathrm{HCO+O_2 \rightarrow HO_2+CO} \quad (4)$$

$$\mathrm{HO_2+NO \rightarrow OH+NO_2} \quad (5)$$

So we have added "the HO_2 to OH conversion process (HO_2+NO)"in the Introduction section: "*OH is formed primarily through the photolysis of O_3, nitrous acid (HONO), hydrogen peroxide (H_2O_2), the reactions of O_3 with alkenes, and the HO_2 to OH conversion process (HO_2+NO) (Platt et al., 1980; Crutzen and*

Zimmermann,1991; Atkinson and Aschmann, 1993; Fried et al., 1997; Paulson et al., 1997)."

4. In page 809, line 27: if daytime HONO could reach ppb level, it is within the detect limit of most HONO measurement instruments. Do you mean specific instrument here?

According to your suggestions, we have revised them in the Introduction section:

"*After sunrise, HONO mixing ratios are usually in low concentrations due to the strong photolysis of HONO.*"

5. In page 813, line 10-14: ambient HONO is correlated with NO_2 as a result of secondary HONO formation instead of HONO direct emission since HONO photolysis lifetime is only about 15 min in the noontime. So why the correlation is the reason for that $HONO/NO_x$ ratio is used as a HONO emission factor?

According to your suggestions, we have revised them in the Introduction section:

"*This is the reason why the recent CalNex 2010 (California Research at the Nexus of Air Quality and Climate Change) study found a very strong positive correlation (R^2= 0.985) between HONO flux and the product of NO_2 concentration and solar radiation at Bakersfield site (Ren et al., 2011).*"

6. In page 814, line 4-7: an annular denuder and an absorption photometer were used for HONO measurement. How are their results comparing to, such as DOAS? How are they compared to each other?

As described in Section 2.1: "*HONO observations were conducted using two annular denuders at the campus of Peking University (PKU) (39°59'N, 116°18'E) in Beijing on 17–20 August 2007 (Spataro et al., 2013) and a long path absorption photometer at the Backgarden (BG) supersite (23°30'N, 113°10'E), about 60 km northwest of Guangzhou on 3–31 July 2006 (X. Li et al., 2012).*"

(i) HONO can be measured by various techniques, e.g., spectroscopic techniques and wet chemical techniques Differential optical absorption spectroscopy (DOAS) detects HONO by its specific UV absorption ranges with detection limits in the order of 100 ppt (Platt et al., 1980). Wet chemical techniques, which operate

HONO sampling on humid/aqueous surfaces, include rotated wet annular denuders and the long path absorption photometer (LOPAP). The techniques have detection limits in the order of few ppt, but suffer from chemical interferences caused by, e.g., NO_2 and phenol reaction or by NO_2 and SO_2 (Gutzwiller et al., 2002; Spindler et al., 2003). However, since the LOPAP instrument collects HONO even at low pH, these chemical interferences are minimized (Kleffmann et al., 2002, 2006). That means the HONO measured by the wet chemical techniques (e.g., annular denuder and LOPAP) could be compared to that by the DOAS.

(ii) Both being the wet chemical techniques, the annular denuder and the LOPAP could be comparable.

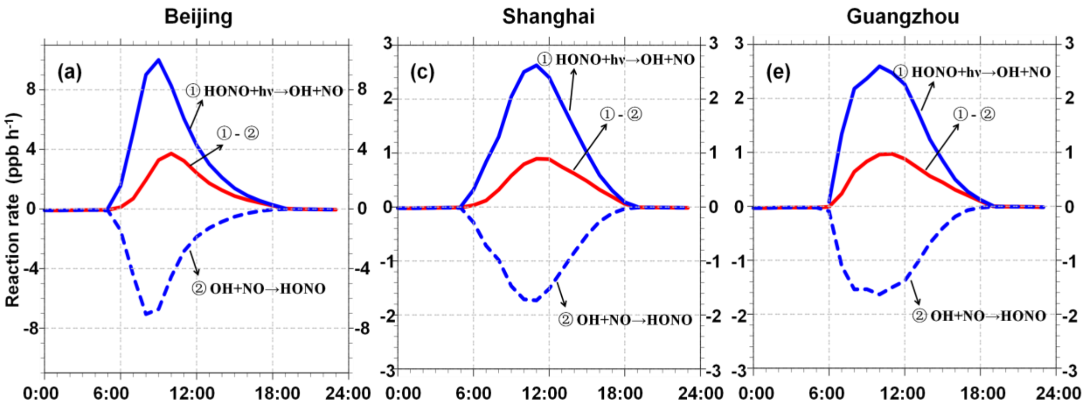

Fig. R1 Averaged reaction rates of HONO+hv→OH+NO（①）, and OH+NO→HONO（②）, and the net OH production rate by HONO photolysis (①-②) for case R_p in (a) Beijing, (b) Shanghai, and (c) Guangzhou in August 2007.

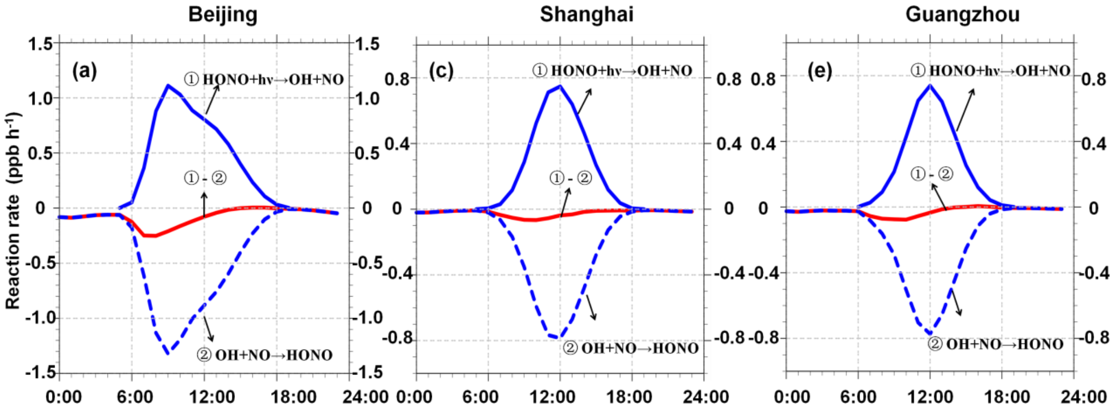

Fig. R2 Averaged reaction rates of HONO+hv→OH+NO（①）, and OH+NO→HONO（②）, and the net OH production rate by HONO photolysis (①-②) for case R in (a) Beijing, (b) Shanghai, and (c) Guangzhou in August 2007.

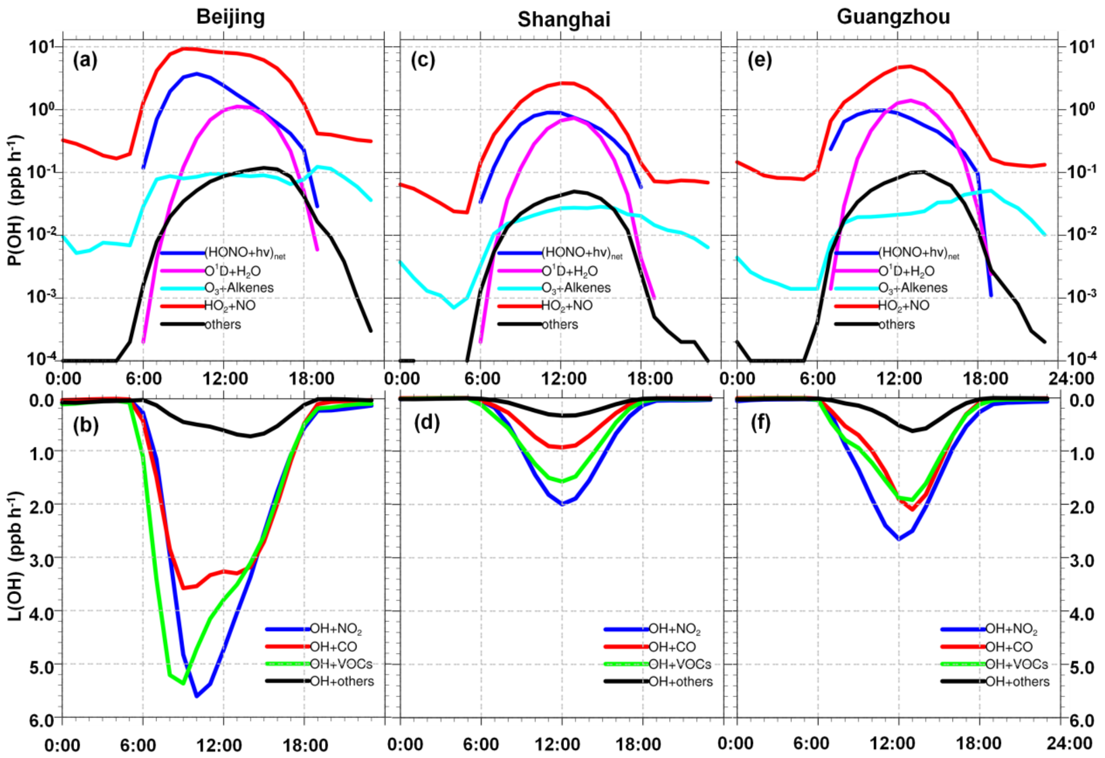

Fig. R3. Averaged production [P(OH)] and loss [L(OH)] rates of OH for case R_p in (a, b) Beijing, (c, d) Shanghai, and (e, f) Guangzhou in August 2007. $(HONO+hv)_{net}$ means the net OH production rate from HONO photolysis (subtracting OH + NO = HONO).

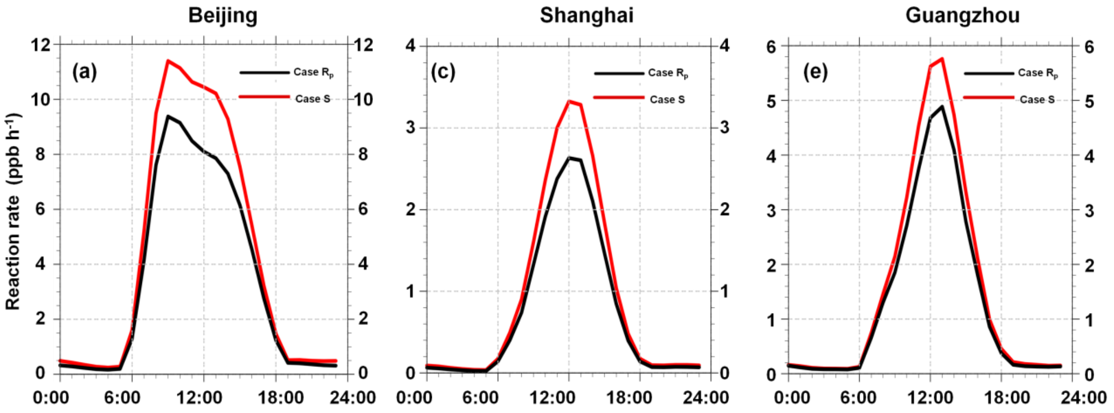

Fig. R4. Comparison of averaged conversion rates of HO_2 to OH between case R_p and case S (increasing the anthropogenic VOCs emissions by 68%) in (a) Beijing, (b) Shanghai, and (c) Guangzhou in August 2007.

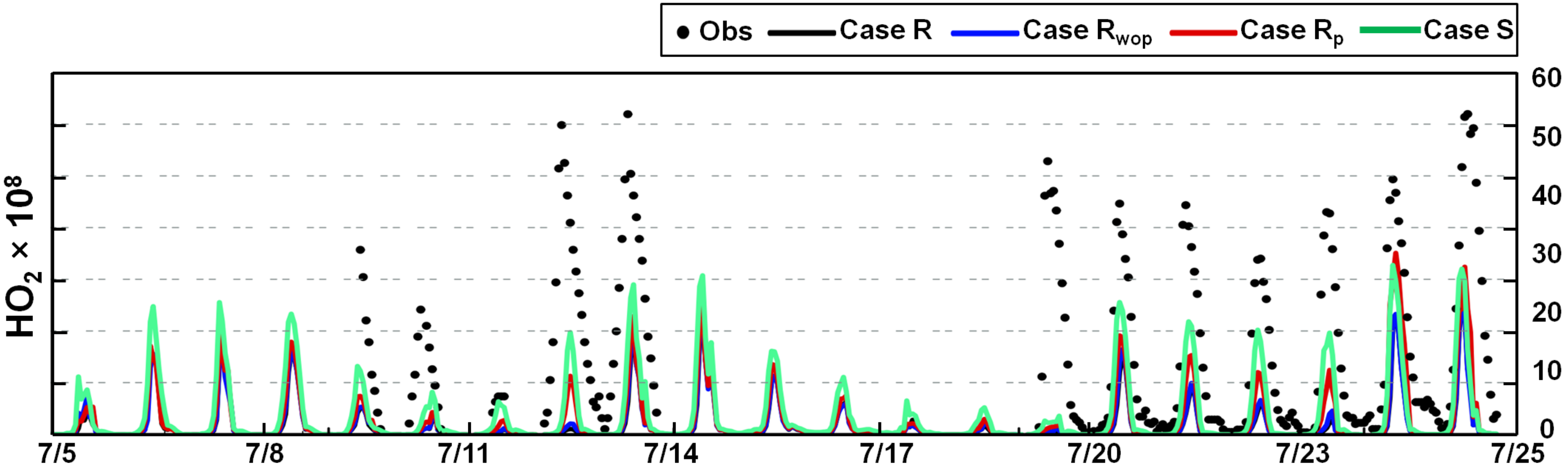

Fig. R5. Comparison of simulated and observed hourly-mean mixing ratios of HO_2 (molecules cm^{-3}) at the Backgarden site in Guangzhou in July 2006 (Lu et al., 2012). (Case S: a 68% increase in the anthropogenic emissions of VOCs for Case R_p).

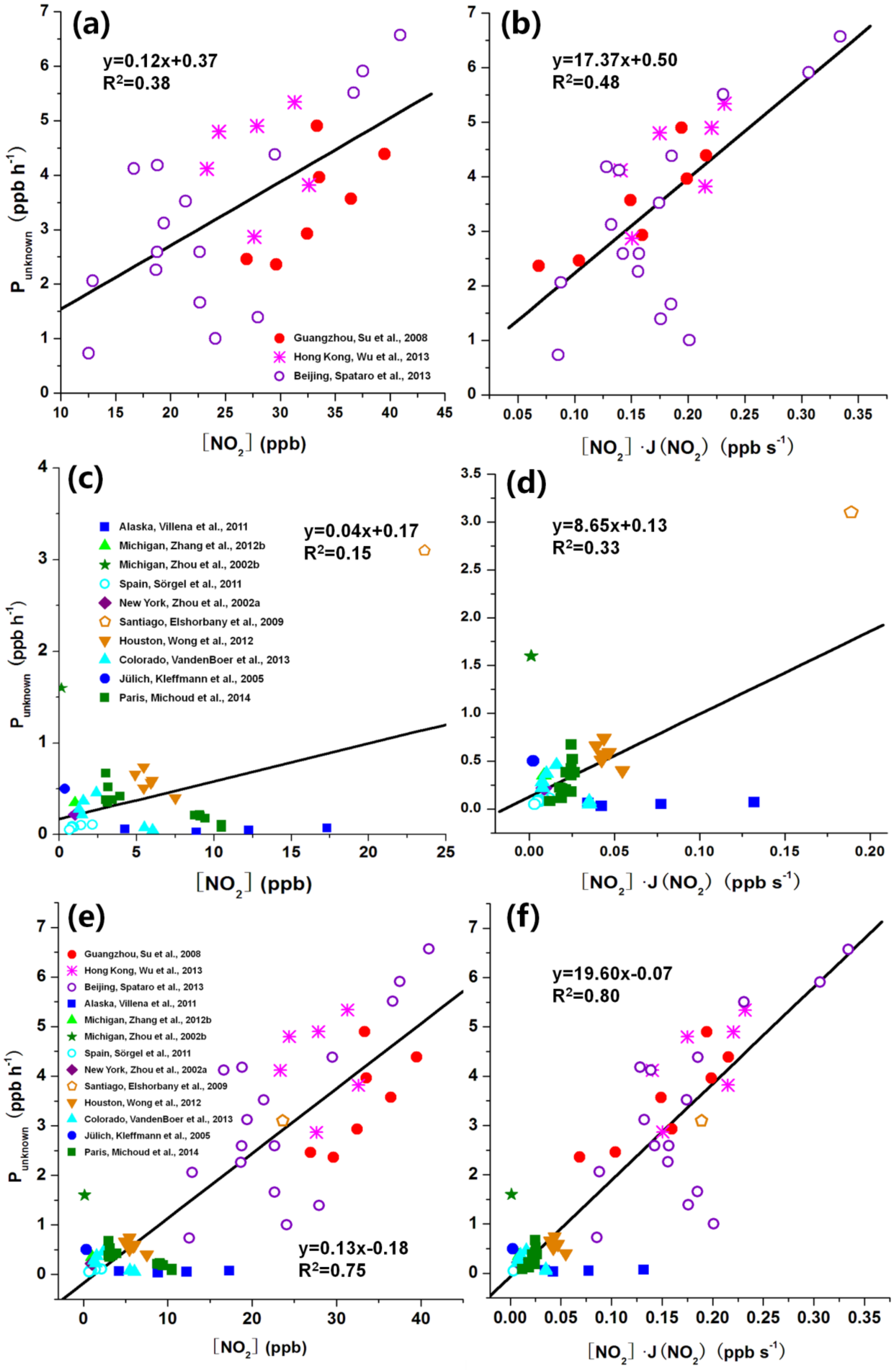

Fig. R6. Correlations of the unknown daytime HONO source ($P_{unknown}$) (ppb h^{-1}) with NO_2 mixing ratios (ppb) and $[NO_2]\cdot J(NO_2)$ (ppb s^{-1}) in (a), (b) the coastal regions of China, (c), (d) the other countries, and (e), (f) the globe, respectively, based on the field experiment data shown in Fig. 1 in the revised version.

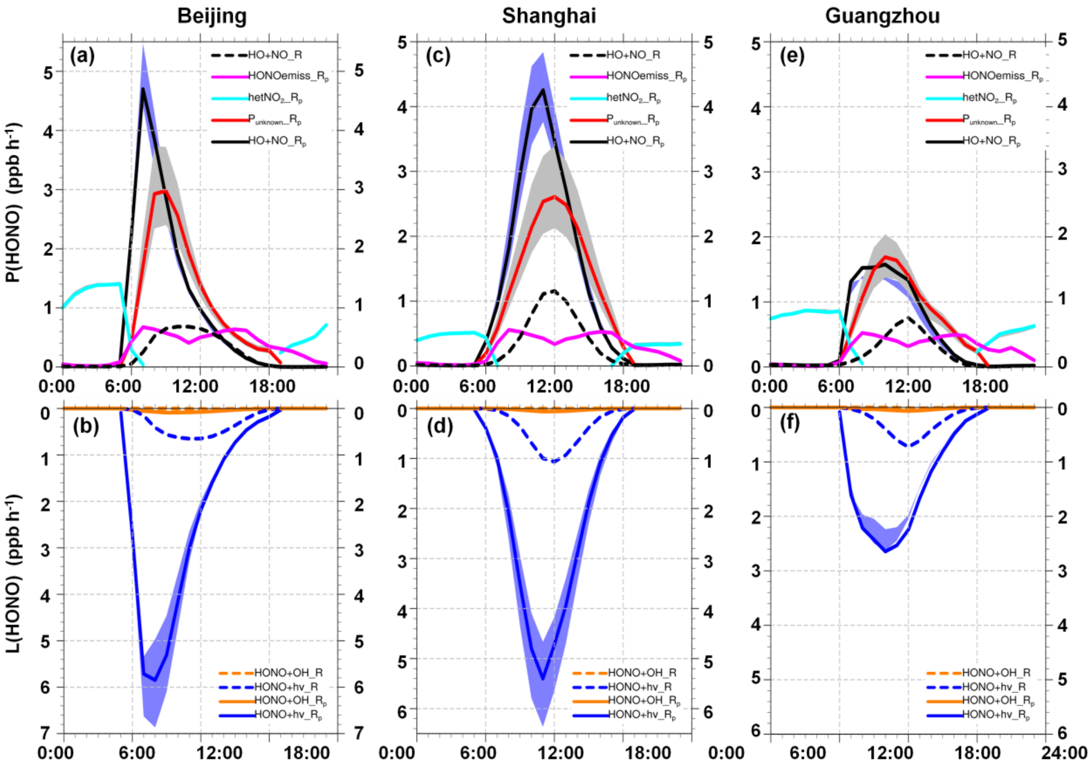

Fig. R7. Production [P(HONO)] and loss [L(HONO)] rates of HONO for cases R (dashed lines), R_p(solid lines) and sensitivity ranges (based on R_{inc} and R_{dec}) in (a), (b) Beijing, (c), (d) Shanghai, and (e), (f) Guangzhou in August 2007. Case R_{inc} includes case R_p with an increase of 25% (the maximum uncertainty range according to the previous studies above) in the slope factor (19.60); Case R_{dec} is the same as case R_p with a decrease of 25% in the slope factor (19.60).

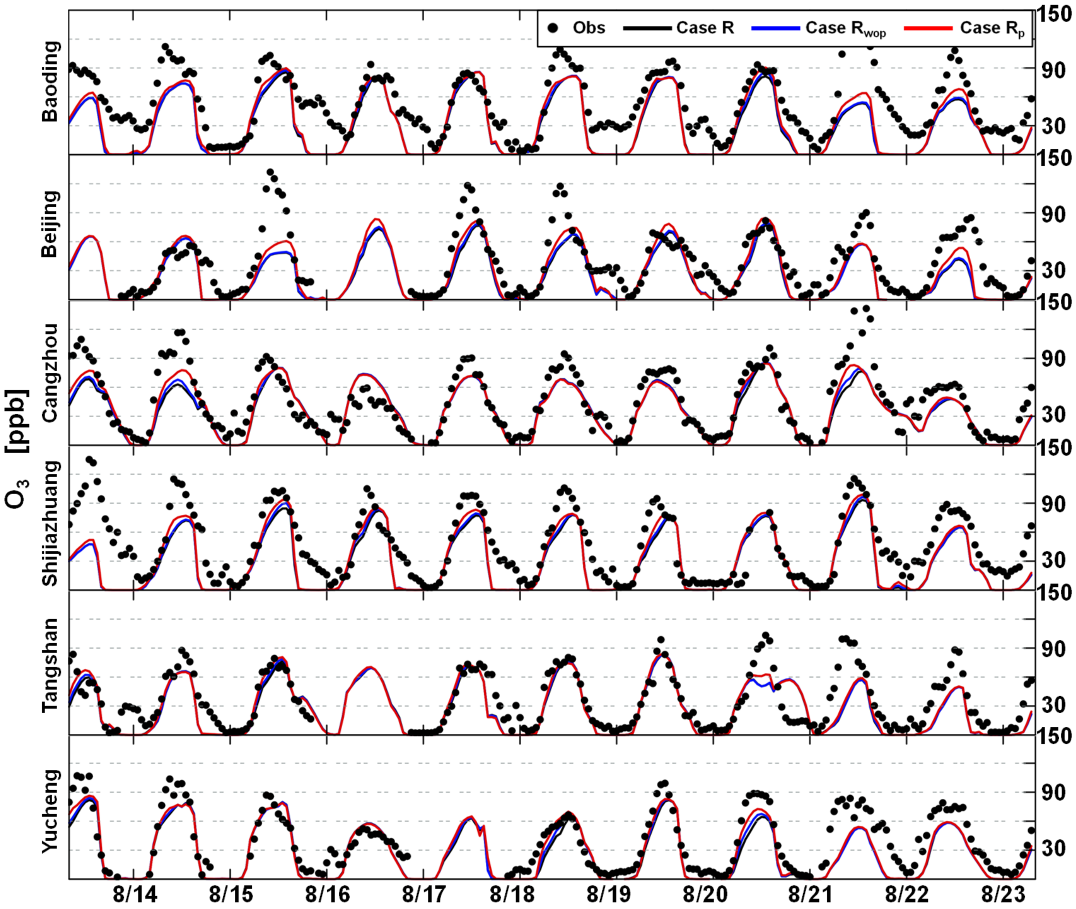

Fig. R8. Comparison of simulated and observed hourly-mean mixing ratios of O_3 (ppb) at six sites in the Beijing-Tianjin-Hebei region (BTH) in August 14-22 of 2007.

Table R1. Daytime (06:00–18:00 LST) average OH budgets in Beijing/Shanghai/Guangzhou in August 2007.

Reaction	Case R		Case R_{wop}		Case R_p	
	Rate (ppb h^{-1})	Contribution (%)	Rate (ppb h^{-1})	Contribution (%)	Rate (ppb h^{-1})	Contribution (%)
			OH production			
HO_2+NO	**2.778/0.732/1.748**	**81.73/67.09/71.54**	**3.242/0.760/1.871**	**83.74/68.00/72.02**	**7.101/1.402/2.553**	**73.34/61.95/67.55**
$^*(HONO+hv)_{net}$	**--/--/--**	**--/--/--**	**--/--/0.017**	**--/--/0.66**	**1.855/0.497/0.489**	**19.16/21.98/12.93**
O^1D+H_2O	**0.465/0.307/0.617**	**13.68/28.17/25.27**	**0.479/0.306/0.630**	**12.36/27.38/24.24**	**0.568/0.312/0.651**	**5.86/13.80/17.23**
O_3+OLET/OLEI	0.101/0.024/0.027	2.98/2.16/1.11	0.095/0.023/0.027	2.45/2.08/1.03	0.080/0.021/0.025	0.83/0.91/0. 65
$^*(H_2O_2+hv)_{net}$	0.035/0.023/0.029	1.02/2.07/1.17	0.035/0.023/0.030	0.91/2.03/1.16	0.037/0.022/0.032	0.38/0.97/0.19
HO_2+O_3	0.009/0.001/0.014	0.28/0.07/0.59	0.010/0.001/0.015	0.26/0.06/0.58	0.026/0.001/0.019	0.27/0.05/0.51
$^*(HNO_3+hv)_{net}$	0.005/0.001/0.002	0.15/0.06/0.10	0.005/0.001/0.002	0.13/0.06/0.09	0.007/0.001/0.003	0.07/0.04/0.07
ROOH+hv	0.003/0.004/0.005	0.09/0.36/0.19	0.003/0.004/0.005	0.09/0.38/0.19	0.007/0.007/0.007	0.07/0.29/0.19
O_3+ETH	0.002/<0.001/<0.001	0.05/0.02/0.01	0.002/<0.001/<0.001	0.04/0.02/0.01	0.001/<0.001/<0.001	0.02/0.01/0.01
HO_2+NO_3	<0.001/<0.001/<0.001	<0.01/<0.01/0.01	<0.001/<0.001/<0.001	<0.01/<0.01/<0.01	<0.001/<0.001/<0.001	<0.01/<0.01/<0.01
O_3+ISOP	<0.001/<0.001/<0.001	0.01/<0.01/<0.01	<0.001/<0.001/<0.001	0.01/<0.01/<0.01	<0.001/<0.001/<0.001	<0.01/<0.01/<0.01
Total	3.399/1.091/2.443	100/100/100	3.873/1.118/2.598	100/100/100	9.683/2.263/3.779	100/100/100
			OH loss			
$OH+NO_2$	**1.116/0.474/0.770**	**39.31/46.63/38.33**	**1.225/0.501/0.844**	**38.11/45.86/38.86**	**3.146/1.045/1.424**	**38.08/44.29/40.76**
OH+CO	**0.785/0.203/0.576**	**27.65/19.97/28.67**	**0.932/0.227/0.637**	**29.00/20.78/29.33**	**2.573/0.506/1.001**	**31.14/21.45/28.65**
OH+OLET/OLEI	**0.192/0.054/0.059**	**6.76/5.31/2.94**	**0.264/0.065/0.077**	**8.21/5.95/3.55**	**0.537/0.206/0.095**	**6.50/8.73/2.72**
OH+HCHO	**0.150/0.050/0.146**	**5.28/4.92/7.27**	**0.166/0.053/0.156**	**5.16/4.85/7.18**	**0.544/0.096/0.242**	**6.59/4.07/6.93**
$OH+CH_4$	0.103/0.057/0.135	3.63/5.61/6.72	0.109/0.059/0.142	3.39/5.40/6.54	0.260/0.115/0.223	3.15/4.87/6.38
OH+ALD2/MGLY/ANOE	0.092/0.018/0.045	3.24/1.77/2.24	0.109/0.020/0.049	3.39/1.83/2.26	0.323/0.047/0.081	3.91/1.99/2.32
$OH+SO_2$	0.054/0.030/0.035	1.90/2.95/1.74	0.064/0.034/0.041	1.99/3.11/1.89	0.172/0.116/0.072	2.08/4.92/2.06

OH+XYL	0.052/0.022/0.023	1.83/2.16/1.14	0.066/0.026/0.029	2.05/2.38/1.34	0.141/0.078/0.045	1.71/3.31/1.29
OH+H_2	0.038/0.021/0.050	1.34/2.07/2.49	0.040/0.022/0.052	1.24/2.01/2.39	0.095/0.027/0.075	1.15/1.14/2.15
OH+TOL	0.027/0.007/0.011	0.95/0.69/0.55	0.034/0.008/0.014	1.06/0.73/0.64	0.086/0.025/0.024	1.04/1.06/0.69
OH+HONO	0.003/0.003/0.005	0.11/0.30/0.25	0.006/0.004/0.007	0.19/0.37/0.32	0.069/0.023/0.032	0.84/0.97/0.92
OH+HNO_x	0.005/0.001/0.005	0.18/0.10/0.25	0.005/0.001/0.005	0.16/0.09/0.23	0.015/0.002/0.008	0.18/0.08/0.23
OH+O_3	0.028/0.006/0.035	0.99/0.59/1.70	0.029/0.006/0.036	0.90/0.55/1.66	0.072/0.005/0.046	0.87/0.21/1.32
OH+H_2O_2	0.015/0.008/0.027	0.53/0.79/1.34	0.016/0.008/0.029	0.50/0.73/1.34	0.040/0.010/0.043	0.48/0.42/1.23
OH+ETH/OPEN	0.007/0.002/0.004	0.25/0.20/0.20	0.008/0.002/0.005	0.25/0.18/0.23	0.036/0.009/0.011	0.44/0.38/0.31
OH+CH_3OOH/ROOH	0.010/0.011/0.014	0.35/1.08/0.70	0.011/0.012/0.014	0.34/1.10/0.64	0.022/0.020/0.022	0.27/0.85/0.63
OH+ISOP	0.019/0.004/0.002	0.67/0.39/0.10	0.020/0.004/0.003	0.62/0.37/0.14	0.017/0.007/0.003	0.21/0.30/0.09
OH+PAR	0.005/0.002/0.004	0.18/0.20/0.20	0.007/0.003/0.005	0.22/0.27/0.23	0.015/0.005/0.007	0.18/0.21/0.20
OH+ONIT /ISOPRD	0.028/0.005/0.016	0.99/0.49/0.80	0.030/0.005/0.018	0.93/0.46/0.83	0.077/0.013/0.025	0.93/0.55/0.72
OH+C_2H_6	0.002/0.001/0.002	0.07/0.10/0.10	0.003/0.001/0.002	0.09/0.09/0.09	0.008/0.002/0.004	0.10/0.08/0.11
OH+CH_3OH/ANOL/CRES	0.002/0.001/0.002	0.07/0.10/0.10	0.002/0.001/0.002	0.06/0.09/0.09	0.007/0.002/0.003	0.08/0.08/0.09
OH+HO_2	0.001/<0.001/0.004	0.04/0.05/0.20	0.002/<0.001/0.005	0.06/0.05/0.23	0.006/<0.001/0.008	0.07/0.02/0.23
OH+NO	0.105/0.036/0.039	3.70/3.54/1.94	0.066/0.030/--	2.05/2.75/--	--/--/--	--/--/--
Total	2.839/1.017/2.009	100/100/100	3.214/1.093/2.172	100/100/100	8.261/2.360/3.495	100/100/100

OLET: internal olefin carbons (C=C); OLEI: terminal olefin carbons (C=C); ROOH: higher organic peroxide; ETH: ethene; ISOP: isoprene; ALD2: acetaldehyde; MGLY: methylglyoxal; ANOE: acetone; XYL: xylene; TOL: toluene; HNO_x: HNO_3 + HNO_4; OPEN: aromatic fragments; PAR: paraffin carbon –C–; ONIT: organic nitrate; ISOPRD: lumped intermediate species; ANOL: ethanol; CRES: cresol and higher molar weight phenols.

Table R2.The calculated unknown daytime HONO source ($P_{unknown}$), NO_2 mixing ratios and photolysis frequency of NO_2 [$J(NO_2)$] from field experiments in Figure 1.

Site	Date	Time	$P_{unknown}$ (ppb h^{-1})	[NO_2] (ppb)	$J(NO_2)$ ($\times10^{-3}$ s^{-1})	Measurement techniques /Uncertainties	Reference
Xinken (22.6 °N, 113.6 °E)	2004.10.23- 2004.10.30	09:30	2.36	29.65	2.31	HONO: WD/IC; NO_2: estimated from NO and NO_y (measured by the NO-O_3 chemiluminescence detector (Kondo et al., 1997))/22%; $J(NO_2)$: TUV/18%; $P_{unknown}$: 10~30%.	Su et al. (2008) Su et al. (2011)
		10:30	3.57	36.46	4.09		
		11:30	4.39	39.51	5.46		
		12:30	4.90	33.33	5.83		
		13:30	3.96	33.54	5.93		
		14:30	2.93	32.43	4.92		
		15:30	2.46	26.94	3.85		
Beijing (39.99 °N, 116.30 °E)	2007.08.17	8:00	2.59	22.66	6.29	HONO: Annular denuders; NO_2: means of commercial ECOTECH Ltd. (Australia analyzer)/ 1%; $J(NO_2)$: calculated by J(HONO);	Spataro et al. (2013)
		10:00	1.66	22.67	8.16		
		12:00	1.00	24.09	8.35		
		14:00	3.12	19.39	6.82		
	2007.08.18	8:00	1.39	27.96	6.29		
		10:00	3.52	21.37	8.16		
		12:00	4.12	16.66	8.35		
		14:00	2.06	12.90	6.82		
	2007.08.19	8:00	4.38	29.50	6.29		
		10:00	5.91	37.53	8.16		
		12:00	2.26	18.67	8.35		

		14:00	0.73	12.54	6.82		
	2007.08.20	8:00	5.51	36.69	6.29		
		10:00	6.57	40.94	8.16		
		12:00	2.59	18.78	8.35		
		14:00	4.18	18.79	6.82		
Tung Chung (22.30 °N, 113.93 °E)	2011.08.25- 2011.08.31	10:00	2.87	27.62	5.45	HONO: LOPAP; NO_2: TEI; $J(NO_2)$: Optical actinometer.	Wu et al. (2013)
		11:00	3.82	32.62	6.59		
		12:00	5.34	31.31	7.41		
		13:00	4.90	27.86	7.92		
		14:00	4.80	24.40	7.17		
		15:00	4.12	23.33	6.02		
Alaska (71.32 °N, 156.65 °W)	2009.03.13- 2009.04.14	10:30	0.03	-	4.73	HONO: LOPAP; NO_2: estimated from NO and NO_y (measured by the NO-O_3 chemiluminescence detector; $J(NO_2)$: estimated as a function of solar zenith angle using the TUV radiative transfer model.	Villena et al. (2011)
		11:00	0.03	-	6.03		
		11:30	0.06	4.23	8.16		
		12:00	0.09	-	8.81		
		12:30	0.05	-	9.46		
		13:00	0.08	-	8.69		
		13:30	0.07	17.31	7.63		
		14:00	0.05	12.24	6.33		
		14:30	0.03	8.85	4.79		
Michigan (45.50 °N,	2008.07.17- 2008.08.07	noon	0.35	1.00	8.48	HONO: LOPAP; NO_2: Custom-built analyzer using the	N. Zhang et al. (2012)

84.70 °W)						chemiluminescence technique; J(NO_2): estimated as a function of UV measured by the TUV radiative transfer model/10%.	
Michigan (45.50 °N, 84.70 °W)	2000.07.27	noon	1.60	0.13	8.48	HONO: Two-channel measurement system (Zhou et al., 1999); NO_2: TEI Model.	Zhou et al. (2002a)
Spain (37.10 °N, 6.74 °W)	2008.07.17-2008.08.07 (cloud-free)	10:00	0.11	2.15	5.39	HONO: LOPAP/12%; NO_2: Droplet Measurement Technologies (Hosaynali-Beygi et al., 2011) /8%; J(NO_2): Filter radiometers/5%; $P_{unknown}$: 18%.	Sörgel et al. (2011)
		11:00	0.10	1.38	6.26		
		12:00	0.08	0.95	6.76		
		13:00	0.09	0.84	6.68		
		14:00	0.08	0.79	6.03		
		15:00	0.05	0.66	4.62		
New York (42.09 °N, 77.21 °W)	1998.06.26-1998.07.14	noon	0.22	1.00	8.48	HONO: Two-channel measurement system (Zhou et al., 1999); NO_2: TEI Model.	Zhou et al. (2002b)
Santiago (33.45 °S, 70.67 °W)	2005.03.08-2005.03.20	noon	1.70	10.00	8.00	HONO: LOPAP; NO_2: DOAS-OPSIS optical system; J(NO_2): Filter radiometers.	Elshorbany et al. (2009)
Houston (29.76 °N, 95.37 °W)	2009.04.21	10:00	0.40	7.50	7.29	HONO: LP-DOAS/5%; NO_2: LP-DOAS /3%; J(NO_2): SAFS;	Wong et al. (2012)
		11:00	0.59	6.02	7.77		
		12:00	0.74	5.45	8.03		

		13:00	0.66	4.89	8.03	$P_{unknown}$: 10~20%.	
		14:00	0.51	5.45	7.76		
		15:00	0.57	5.91	7.18		
Colorado (40.05 °N, 105.00 °W)	2011.02.19-2011.02.25	10:00	0.05	6.04	5.84	HONO: NI-PT-CIMS; NO_2: a cavity ring-down spectrometer (Wagner et al., 2011)/5%; $J(NO_2)$: Filter radiometers.	VandenBoer et al. (2013)
		11:00	0.08	5.49	6.39		
		12:00	0.46	2.39	6.64		
		13:00	0.37	1.55	6.39		
		14:00	0.28	1.27	6.02		
		15:00	0.22	1.47	5.22		
Jülich (50.92 °N, 6.36 °E)	2003.07.29	noon	0.50	0.35	6.63	HONO: LOPAP; NO_2: Chemiluminescence analyzer equipped with a photolytic converter for NO_2 to NO conversion; $J(NO_2)$: derived from actinic flux spectra measured by a scanning spectroradiometer.	Kleffmann et al. (2005)
Paris (40.72 °N, 2.21 °E)	2009.07.09-2009.07.27	10:00	0.42	3.91	6.31	HONO: Wet chemical derivatization (SA/NED), HPLC detection (NitroMAC)/12%; NO_2: Luminol chemiluminescence/5%; $J(NO_2)$: filter radiometer/ 20–25%.	Michoud et al. (2014)
		11:00	0.38	3.42	7.76		
		12:00	0.52	3.14	8.08		
		13:00	0.67	3.00	8.24		
		14;00	0.38	3.00	7.29		
		15:00	0.35	3.11	7.88		

2010.01.15-2010.02.15	10:00	0.08	10.49	1.16
	11:00	0.11	10.49	1.80
	12:00	0.18	9.44	2.60
	13:00	0.21	8.76	2.20
	14;00	0.20	9.12	2.34
	15:00	0.22	9.07	1.99

WD/IC: Wet Denuder sampling/Ion Chromatograph analysis system; TUV: Ultraviolet-Visible Model; TEI: Thermo Environmental Instruments; LOPAP: Long path absorption photometer; LP-DOAS: Long path Differential Optical Absorption Spectroscopy instrument; SAFS: scanning actinic flux spectroradiometer; NI-PT-CIMS: Negative-Ion Proton-Transfer Mass Spectrometer; SA/NED: an aqueous sulphanilamide/ N-(1-naphthyl)-ethylenediamine solution; NitroMAC: an instrument developed at the laboratory (Afif et al., 2014); HPLC: High Performance Liquid Chromatography.

Note that: Since J(NO_2) data of Wu et al. (2012), N. Zhang et al. (2012), Zhou et al. (2002b), VandenBoer et al. (2013), Kleffmann et al. (2005) were not measured, they were calculated from the J(HONO) measurement data (J(NO_2) = 5.3J(HONO)) (Kraus and Hofzumahaus, 1998); J(NO_2) data of Zhou et al. (2002ab) were derived from the campaign of N. Zhang et al. (2012) (The experiments were conducted in summer and the studied sites were close to each other). J(NO2) data of Spataro et al. (2013) were also calculated from the J(HONO) at noon (J(NO_2) = 5.3J(HONO)), then we computed the hourly J(NO_2) (8:00~14:00 LST) through multiplying by the cosine of solar zenith angle. The NO_2 mixing ratios of N. Zhang et al. (2012) and Zhou et al. (2002b) were not shown and derived from NO_x mixing ratios. Similarly, NO_2 mixing ratios of Kleffmann et al. (2005) were inferred from NO mixing ratios.

Table R3. Performance metrics of WRF-Chem meteorology simulations in August 2007 (Wang et al., 2014)

Temperature(℃)			Relative Humidity(%)			Wind Speed(m/s)			Wind direction(deg)			Reference
RMSE	MB	IOA	RMSE	MB	IOA	RMSE	MB	IOA	RMSE	MB	IOA	
2.54	0.23	0.90	16.30	-5.46	0.78	2.46	1.61	0.56	99.25	2.59	0.65	This work
	-0.88	0.90		-1.30	0.78	2.06	0.89	0.65		2.47		(Wang et al., 2010b)
	0.53	0.88		-1.06	0.86	1.47	0.64	0.62		2.59		(Li et al., 2012)
3.1	0.8		17.4	-5.7		2.2	1.1		60.9	8.2		(H. Zhang et al., 2012)

References

Afif, C., Jambert, C., Colomb, A., Eyglunent, G., Borbon, A., Daële, V., Doussin, J. F., and Perros, P. E.: NitroMAC: an instrument for the measurement of HONO. Intercomparison with LOPAP, Water Air Soil Poll., in preparation, 2014.

An, J., Zhang, W., Qu Y.: Impacts of a strong cold front on concentrations of HONO, HCHO, O_3, and NO_2 in the heavy traffic urban area of Beijing, Atmospheric Environment, 43, 3454–3459, 2009.

An, J., Li, Y., Wang, F., and Xie, P.: Impacts of photoexcited NO_2 chemistry and heterogeneous reactions on concentrations of O_3 and NO_y in Beijing, Tianjin and Hebei province of China, Air Quality-Models and Applications, Prof. Dragana Popovic (Ed.), InTech, ISBN: 978-953-307-307-1, doi: 10.5772/16858, 2011.

An, J., Li, Y., Chen, Y., Li, J., Qu, Y., Tang, Y.: Enhancements of major aerosol components due to additional HONO sources in the North China Plain and implications for visibility and haze, Advances in Atmospheric Science, 30, 57-66, 2013.

Alicke, B., Geyer, A., Hofzumahaus, A., Holland, F., Konrad, S., Pätz, H. W., Schäfer, J., Stutz, J., Volz-Thomas, A., Platt, U.: OH formation by HONO photolysis during the BERLIOZ experiment, Journal of Geophysical Research, 108, D4, 8247, doi:10.1029/2001JD000579, 2003.

Czader, B. H., Rappenglück, B., Percell, P., Byun, D. W., Ngan, F., and Kim, S.: Modeling nitrous acid and its impact on ozone and hydroxyl radical during the Texas Air Quality Study 2006, Atmos. Chem. Phys., 12, 6939–6951, doi:10.5194/acp-12-6939-2012, 2012.

Elshorbany, Y. F., Kurtenbach, R., Wiesen, P., Lissi, E., Rubio, M., Villena, G., Gramsch, E., Rickard, A. R., Pilling, M. J., Kleffmann, J.: Oxidation capacity of the city air of Santiago, Chile. Atmospheric Chemistry and Physics, 9(6), 2257-2273, 2009.

Gonçalves, M., Dabdub, D., Chang, W. L., Jorba, O., and Baldasano, J. M.: Impact of HONO sources on the performance of mesoscale air quality models, Atmos. Environ., 54, 168–176, 2012.

Gutzwiller L, Arens F, Baltensperger U, Gäggeler HW, Ammann M. Significance of semivolatile diesel exhaust organics for secondary HONO formation, Environ Sci Technol, 36, 677-682, 2002.

Hofzumahaus, A., Rohrer, F., Lu, K., Bohn, B., Brauers, T., Chang, C.C.: Amplified trace gas removal in the troposphere, Science, 324, 1702-1704, 2009.

Hosaynali Beygi, Z., Fischer, H., Harder, H. D., Martinez, M., Sander, R., Williams, J., Brookes, D. M., Monks, P. S., and Lelieveld, J.: Oxidation photochemistry in the Southern Atlantic boundary layer: unexpected deviations of photochemical steady state, Atmos. Chem. Phys., 11, 8497–8513, doi:10.5194/acp-11-8497-2011, 2011.

Kleffmann, J., Heland, J., Kurtenbach, R., Lörzer, J., Wiesen, P.: A new instrument for the detection of nitrous acid (HONO), Environ Sci Pollut Res, 4(Special Issue 4), 48–54. 2002.

Kleffmann, J., Gavriloaiei, T., Hofzumahaus, A., Holland, F., Koppmann, R., Rupp, L.,Schlosser, E., Siese, M., and Wahner, A.: Daytime formation of nitrous acid: a major source of OH radicals in a forest, J. Geophys. Res. Lett., 32(5), doi: 10.1029/2005GL022524, 2005.

Kleffmann, J., Lorzer, J. C., Wiesen, P., Kern, C., Trick, S., Volkamer, R.: Intercomparison of the DOAS and LOPAP techniques for the detection of nitrous acid (HONO), Atmos Environ, 40, 3640-3652, 2006.

Kondo, Y., S. Kawakami, M. Koike, D. Fahey, H. Nakajima, Y. Zhao, N. Toriyama, M. Kanada, G. Sachse, and G. Gregory.: The performance of an aircraft instrument for the measurement of NO_y. J. Geophys. Res., 102, 28,663–28,671, 1997.

Li, G., Lei, W., Zavala, M., Volkamer, R., Dusanter, S., Stevens, P., Molina, L.T.: Impacts of HONO sources on the photochemistry in Mexico City during the MCMA-2006/MILAGO Campaign, Atmos. Chem. Phys. 10, 6551-6567, 2010.

Li, L., Chen, C. H., Huang, C., Huang, H. Y., Zhang, G. F., Wang, Y. J., Wang, H. L., Lou, S. R., Qiao, L. P., Zhou, M., Chen, M. H., Chen, Y. R., Fu, J. S., Streets, D. G., Jang, C. J.: Process analysis of regional ozone formation over the Yangtze River Delta, China using the Community Multi-scale Air Quality modeling system, Atmospheric Chemistry and Physics, 12, 10971-10987, 2012.

Li, Y., An, J., Min, M., Zhang, W., Wang, F., Xie, P.: Impacts of HONO sources on the air quality in Beijing, Tianjin and Hebei Province of China, Atmospheric Environment, 45(27), 4735-4744, 2011.

Li, Y., An, J., Gultepe I.: Effects of additional HONO sources on visibility over the North China Plain, Adv. Atmos. Sci., 31(5), 1221–1232, doi: 10.1007/s00376-014-4019-1, 2014.

Lu, K. D., Rohrer, F., Holland, F., Fuchs, H., Bohn, B., Brauers, T., Chang, C. C., Haseler, R., Hu, M., Kita, K., Kondo, Y., Li, X., Lou, S. R., Nehr, S., Shao, M., Zeng, L. M., Wahner, A., Zhang, Y. H., Hofzumahaus, A.: Observation and modelling of OH and HO_2 concentrations in the Pearl River Delta 2006: a missing OH source in a VOC rich atmosphere, Atmospheric Chemistry and Physics, 12(3), 1541-1569, 2012.

Meller, R. and Moortgat, G. K.: Temperature dependence of the absorption cross sections of formaldehyde between 223 and 323 k in the wavelength range 225–375 nm, J. Geophys. Res.-Atmos., 105, 7089–7101, 2000.

Michoud, V., Colomb, A., Borbon, A., Miet, K., Beekmann, M., Camredon, M., Aumont, B., Perrier, S., Zapf, P., Siour, G., Ait-Helal, W., Afif, C., Kukui, A., Furger, M., Dupont, J. C., Haeffelin, M., Doussin, J. F.: Study of the unknown HONO daytime source at a European suburban site during the MEGAPOLI summer and winter field campaigns. Atmospheric Chemistry and Physics, 14(6), 2805-2822, 2014.

Platt, U., Perner, D., Harris, G. W., Winer, A. M., Pitts, J. N.: Observations of nitrous acid in an urban atmosphere by differential optical absorption, Nature 285, 312-314 (29 May 1980); doi: 10.1038/285312a0, 1980.

Ren, X., Harder, H., Martinez, M., Lesher, R. L., Oliger, A., Simpas, J. B., Brunea, W. H., Schwab, J. J., Demerjian, K. L., He, Y., Zhou, X., Gao, H.: OH and HO_2 Chemistry in the urban atmosphere of New York City, Atmospheric Environment, 37(26), 3639-3651, 2003.

Rohrer, F., Bohn, B., Brauers, T., Brüning, D., Johnen, F. J., Wahner, A., Kleffmann, J.: Characterisation of the photolytic HONO-source in the atmosphere simulation chamber SAPHIR, Atmospheric Chemistry and Physics, 5(8), 2189-2201, 2005.

Sörgel, M., Regelin, E., Bozem, H., Diesch, J. M., Drewnick, F., Fischer, H., Harder, H., Held, A., Hosaynali-Beygi, Z., Martinez, M., Zetzsch, C.: Quantification of the unknown HONO daytime source and its relation to NO_2, Atmospheric Chemistry and Physics, 11(20), 10433-10447, 2011.

Sarwar, G., Roselle, S. J., Mathur, R., Appel, W., Dennis, R. L., Vogel, B.: A comparison of CMAQ HONO predictions with observations from the Northeast Oxidant and Particle Study, Atmospheric Environment, 42(23), 5760-5770, 2008.

Spataro, F., Ianniello, A., Esposito, G., Allegrini, I., Zhu, T., Hu, M.: Occurrence of atmospheric nitrous acid in the urban area of Beijing (China), Science of the Total Environment, 447, 210-224, 2013.

Simon, H., Baker, K. R., Phillips, S.: Compilation and interpretation of photochemical model performance statistics published between 2006 and 2012, Atmos. Environ., 61, 124-139, 2012.

Spindler, G., Hesper, J., Brüggemann, E., Dubois, R., Müller, Th., Herrmann, H.: Wet annular denuder measurements of nitrous acid: laboratory study of the artifact reaction of NO2 with S(IV) in aqueous solutions and comparison with field measurements, Atmos Environ, 37, 2643-2662, 2003.

Streets, D. G., Bond, T. C., Carmichael, G. R., Fernandes, S. D., Fu, Q., He, D., Klimont, Z., Nelson, S. M., Tsai, N. Y., Wang, M. Q., Woo, J. H., Yarber, K. F.: An inventory of gaseous and primary aerosol emissions in Asia in the year 2000, Journal of Geophysical Research, Atmospheres 108, 8809, 2003.

Su, H., Cheng, Y., Oswald, R., Behrendt, T., Trebs, I., Meixner, F. X., Andreae, M. O., Cheng, P., Zhang, Y., Pöschl, U.: Soil nitrite as a source of atmospheric HONO and OH radicals, Science, 333(6049), 1616-1618, 2011.

Su, H., Cheng, Y. F., Shao, M., Gao, D. F., Yu, Z. Y., Zeng, L. M., Slanina, J., Zhang, Y. H., Wiedensohler, A.: Nitrous acid (HONO) and its daytime sources at a rural site during the 2004 PRIDE-PRD experiment in China, Journal of Geophysical Research: Atmospheres (1984–2012), 113(D14), 2008.

Tang, Y., An, J., Li, Y., Wang, F.: Uncertainty in the uptake coefficient for HONO formation on soot and its impacts on concentrations of major chemical components in the Beijing–Tianjin–Hebei region, Atmospheric Environment, 84, 163-171, 2014.

VandenBoer, T. C., Brown, S. S., Murphy, J. G., Keene, W. C., Young, C. J., Pszenny, A. A. P., Kim, S., Warneke, C., de Gouw, J. A., Maben, J. R., Wagner, N. L., Riedel, T. P., Thornton, J. A., Wolfe, D. E., Dubé, W. P., Öztürk, F., Brock, C. A., Grossberg, N., Lefer, B., Lerner, B. Middlebrook, A. M., Roberts, J. M.: Understanding the role of the ground surface in HONO vertical structure: High resolution vertical profiles during NACHTT-11. Journal of Geophysical Research: Atmospheres, 118, 10,155–10,171, doi:10.1002/jgrd.50721, 2013.

Villena, G., Wiesen, P., Cantrell, C. A., Flocke, F., Fried, A., Hall, S. R., Hornbrook, R. S., Knapp, D., Kosciuch, E., Mauldin, R. L., McGrath, J. A., Montzka, D., Richter, D., Ullmann, K., Walega, J., Weibring, P., Weinheimer, A., Staebler, R. M., Liao, J., Huey, L. G., and Kleffmann, J.: Nitrous acid (HONO) during polar spring in Barrow, Alaska: a net source of OH radicals?, J. Geophys. Res.

–Atmos., 116(D14), doi: 10.1029/2011JD016643, 2011.

Wagner, N. L., Dubé, W. P., Washenfelder, R. A., Young, C. J., Pollack, I. B., Ryerson, T. B., Brown S. S.: Diode laser-based cavity ring-down instrument for NO_3, N_2O_5, NO, NO_2 and O_3 from aircraft, Atmos. Meas. Technol., 4, 1227–1240, 2011.

Wang, F., An, J., Li, Y., Tang, Y., Lin, J., Qu, Y., Cheng, Y., Zhang, B., Zhai, J.: Impacts of Uncertainty in AVOC Emissions on the Summer RO_x Budget and Ozone Production Rate in the Three Most Rapidly-Developing Economic Growth Regions of China, Advances in Atmospheric Sciences, 31, 1331–1342, 2014.

Wang, X., Zhang, Y., Hu, Y., Zhou, W., Lu, K., Zhong, L., Zeng, L., Shao, M., Hu, M., Russell, A. G.: Process analysis and sensitivity study of regional ozone formation over the Pearl River Delta, China, during the PRIDE-PRD2004 campaign using the Community Multiscale Air Quality modeling system, Atmospheric Chemistry and Physics, 10(9), 4423-4437, 2010.

Wong, K. W., Tsai, C., Lefer, B., Haman, C., Grossberg, N., Brune, W. H., Ren, X., Luke, W., Stutz, J.: Daytime HONO vertical gradients during SHARP 2009 in Houston, TX, Atmospheric Chemistry and Physics, 12(2), 635-652, 2012.

Wong, K. W., Tsai, C., Lefer, B., Grossberg, N., Stutz, J.: Modeling of daytime HONO vertical gradients during SHARP 2009, Atmospheric Chemistry and Physics, 13(7), 3587-3601, 2013.

Wu, J., Xu, Z., Xue, L., and Wang, T.: Daytime nitrous acid at a polluted suburban site in Hong Kong: indication of heterogeneous production on aerosol, in: Proceedings of 12th international conference on atmospheric sciences and applications to air quality, Seoul, Korea, 3–5 June 2013, 52, 2013.

Zhang, Q., Streets, D. G., Carmichael, G. R., He, K., Huo, H., Kannari, A., Klimont, Z., Park, I., Reddy, S., Fu, J. S., Chen, D., Duan, L., Lei, Y., Wang, L., Yao, Z.: Asian emissions in 2006 for the NASA INTEX-B mission, Atmospheric Chemistry and Physics, 9, 5131-5153, 2009.

Zhang, H., Li, J., Ying, Q., Yu, J. Z., Wu, D., Cheng, Y., Kebin Hed, Jiang, J.: Source apportionment of $PM_{2.5}$ nitrate and sulfate in China using a source-oriented chemical transport model. Atmospheric Environment, 62, 228-242, 2012.

Zhang, N., Zhou, X., Bertman, S., Tang, D., Alaghmand, M., Shepson, P. B., Carroll, M. A.: Measurements of ambient HONO concentrations and vertical HONO flux above a northern Michigan forest canopy. Atmospheric Chemistry and Physics, 12(17), 8285-8296, 2012.

Zhou, X., Qiao, H., Deng, G., Civerolo, K.: A method for the measurement of atmospheric HONO based on DNPH derivatization and HPLC analysis. Environ. Sci. Technol., 33, 3672–3679, 1999

Zhou, X., Civerolo, K., Dai, H., Huang, G., Schwab, J., Demerjian, K. Summertime nitrous acid chemistry in the atmospheric boundary layer at a rural site in New York State, Journal of Geophysical Research: Atmospheres (1984–2012), 107(D21), ACH-13, 2002a.

Zhou, X., He, Y., Huang, G., Thornberry, T. D., Carroll, M. A., and Bertman, S. B.: Photochemical production of nitrous acid on glass sample manifold surface, Geophys. Res. Lett., 29, 26-1 – 26-4, doi: 10.1029/2002GL015080, 2002b.

Zhou, X., Gao, H., He, Y., Huang, G., Bertman, S. B., Civerolo, K., Schwab, J.: Nitric acid photolysis on surfaces in low-NO_x environments.: Significant atmospheric implications, Geophysical Research Letters, 30(23), 2003.

Ziemba, L. D., Dibb, J. E., Griffin, R. J., Anderson, C. H., Whitlow, S. I., Lefer, B. L., Rappenglück, B., Flynn, J.: Heterogeneous conversion of nitric acid to nitrous acid on the surface of primary organic aerosol in an urban atmosphere, Atmos. Environ. 44, 4081-4089, 2010

2. The list of all relevant changes made in the manuscript

A. Changes for "Abstract"

1) We have revised our description in the Abstract section: "*When the additional HONO sources were included, the photolysis of HONO was the second source in the OH production rate in Beijing, Shanghai and Guangzhou before 10:00 LST with a maximum of 3.72 [3.06 due to the $P_{unknown}$] ppb h^{-1} in Beijing, whereas the reaction of HO_2 + NO (nitric oxide) was dominated after 10:00 LST with a maximum of 9.38 [7.23] ppb h^{-1} in Beijing.*"

2) We have revised our description in the Abstract section: "*The daytime average OH production rate was enhanced by 0.67 [0.64] to 4.32 [3.86] ppb h^{-1} via the reaction of HO_2 + NO, and by 0.49 [0.47] to 1.86 [1.86] ppb h^{-1} via the photolysis of HONO, and the OH daytime average loss rate was enhanced by 0.58 [0.55] to 2.03 [1.92] ppb h^{-1} via the reaction of OH + NO_2 and by 0.31 [0.28] to 1.78 [1.64] ppb h^{-1} via the reaction of OH + CO (carbon monoxide) in Beijing, Shanghai and Guangzhou.*"

3) We have added "daytime average" in the Abstract section: "*Similarly, the additional HONO sources produced an increase of 0.31 [0.28] to 1.78 [1.64] ppb h^{-1} via the reaction of OH + CO and 0.10 [0.09] to 0.63 [0.59] ppb h^{-1} via the reaction of CH_3O_2 [methylperoxy radical] + NO in the daytime average HO_2 production rate, and 0.67 [0.61] to 4.32 [4.27] ppb h^{-1} via the reaction of HO_2 + NO in the daytime average HO_2 loss rate in Beijing, Shanghai and Guangzhou.*"

B. Changes for "1. Introduction"

1) We have added "the HO_2 to OH conversion process (HO_2+NO)"in the Introduction section: "*OH is formed primarily through the photolysis of O_3, nitrous acid (HONO), hydrogen peroxide (H_2O_2), the reactions of O_3 with alkenes, and the HO_2 to OH conversion process (HO_2+NO) (Platt et al., 1980; Crutzen and Zimmermann,1991; Atkinson and Aschmann, 1993; Fried et al., 1997; Paulson et al., 1997).*"

2) We used "*After sunrise, HONO mixing ratios are usually in low concentrations due to the strong photolysis of HONO.***" instead of** *"After sunrise, HONO mixing ratios are usually below the detection limit due to the strong photolysis of HONO."*

3) We used "*This is the reason why the recent CalNex 2010 (California Research at the Nexus of Air Quality and Climate Change) study found a very strong positive correlation (R^2= 0.985) between HONO flux and the product of NO_2 concentration and solar radiation at Bakersfield site (Ren et al., 2011).***" instead of** *"This is the reason why some researchers have adopted the HONO/NO_2 ratio as a HONO emission factor to assess its implications (Elshorbany et al., 2012)."*

C. Changes for "2.2 Parameterization of HONO sources"

1) We have added references in the section 2.2: "*Previous studies (Sörgel et al., 2011; Villena et al., 2011; Wong et al., 2012) have shown* $P_{unknown} \propto [NO_2] \cdot J(NO_2)$*.*"

2) We have added the description in the section 2.2: *"For the coastal regions of China, the correlation between the $P_{unknown}$ and* $NO_2 \cdot J(NO_2)$ *was 0.48, with a linear regression slope of 17.37 (Fig. S2b in the Supplement), which is within the* *maximum $P_{unknown}$ uncertainty range of 25% (Table S1).”*

D. Changes for “3.2 $P_{unknown}$ simulations and its impacts on production and loss rates of HONO”

1) We have added uncertainty analysis in the section 3.2: *“The maximum $P_{unknown}$ uncertainty range of 25% (Table S1), a 25% increase (decrease) in the slope factor (19.60) led to a 9.19−18.62% increase (12.69−14.32% decrease) in the maximum HONO production rate and a 0−17.64% increase (8.40−14.07% decrease) in the maximum HONO loss rate (Fig. S3 in the Supplement).”*

E. Changes for “3.4 $P_{unknown}$ impacts on the budgets of OH, HO_2 and RO_2”

1) We have revised our description in the section 3.4: *“OH radicals are produced mainly through the reaction of HO_2 + NO, the photolysis of O_3 and HONO, and the reactions between O_3 and alkenes (Fig. 11).”*

2) We have revised our results in the section 3.4: *“The photolysis of O_3 was the second most important sources of OH, which was dominant (0.91 ppb h^{-1} in Beijing, 0.52 ppb h^{-1} in Shanghai, and 1.20 ppb h^{-1} in Guangzhou) at noon (Fig. S1a, c, e). Compared with the two OH sources above, the contributions of the reactions of O_3 + alkenes, HONO photolysis and others were small, lower than 0.15 ppb h^{-1} (Fig. S1a, c, e). When the additional HONO sources were added, the most important source was the reaction of HO_2 + NO, with a diurnal maximum conversion rate reaching 9.38 [7.23 due to the $P_{unknown}$] ppb h^{-1} in Beijing, 2.63 [1.15] ppb h^{-1} in Shanghai, and 4.88 [1.43] ppb h^{-1} in Guangzhou near noon (Fig. 11a, c, e). The photolysis of HONO became the second important source of OH in Beijing and Guangzhou before*

10:00 LST, and in Shanghai before 12:00 LST; the diurnal peaks were 3.72 [3.06] ppb h^{-1} in Beijing at 09:00 LST, 0.89 [0.62] ppb h^{-1} in Shanghai at 11:00 LST, and 0.97 [0.78] ppb h^{-1} in Guangzhou at 09:00 LST (Fig. 11a, c, e), which were comparable to or lower than the 3.10 ppb h^{-1} reported by Elshorbany et al. (2009).”

3) We have revised our results in the section 3.4: *“For case R, the reaction of HO_2 + NO was the major source of OH [2.78 ppb h^{-1} (81.73% of the total daytime average production rate of OH) in Beijing, 0.73 ppb h^{-1} (67.09%) in Shanghai, and 1.75 ppb h^{-1} (71.54%) in Guangzhou] (Fig. 12a and Table 4). The second largest source of OH was the photolysis of O_3 [0.47 ppb h^{-1} (13.68%) in Beijing, 0.31 ppb h^{-1} (28.17%) in Shanghai, and 0.62 ppb h^{-1} (25.27%) in Guangzhou] (Table 4).”*

4) We have revised our results in the section 3.4: *“When the additional HONO sources were inserted into the WRF-Chem model (case R_p), the daytime average OH production rate was enhanced by 4.32 (= 7.10 − 2.78) [3.86 due to the $P_{unknown}$] ppb h^{-1} in Beijing, 0.67 (= 1.40 − 0.73) [0.64] ppb h^{-1} in Shanghai, and 0.80 (= 2.55 − 1.75) [0.68] ppb h^{-1} in Guangzhou via the reaction of HO_2 + NO, and by 1.86 (= 1.86 − 0) [1.86] ppb h^{-1} in Beijing, 0.50 (= 0.50 − 0) [0.50] ppb h^{-1} in Shanghai, and 0.49 (= 0.49 − 0) [0.47] ppb h^{-1} in Guangzhou via the photolysis of HONO, respectively (Table 4). The enhancements of the daytime average OH production rate due to the photolysis of HONO were comparable to or lower than the 2.20 ppb h^{-1} obtained by Liu et al. (2012).”*

5) We have revised our results in the section 3.4: *“Overall, the net daytime production rate of RO_x was increased to 3.48 (= 2.56 + 0.71 + 0.21) [2.06 due to the*

$P_{unknown}$] from 1.20 (= 0.60 + 0.43 + 0.17) ppb h^{-1} in Beijing, 1.09 (= 0.86 + 0.19 + 0.04) [0.45] from 0.54 (= 0.36 + 0.14 + 0.04) ppb h^{-1} in Shanghai, and 1.52 (= 1.21 + 0.26 + 0.05) [0.58] from 0.92 (= 0.68 + 0.20 + 0.04) ppb h^{-1} in Guangzhou (Fig. 12) due to the additional HONO sources, indicating that the RO_x source was mainly from OH production, especially via the photolysis of HONO (Tables 4, S2 and S3). This result is different from the conclusion of Liu et al. (2012) that the photolysis of HONO and oxygenated VOCs is the largest RO_x source. One of the primary reasons for this is the underestimation of anthropogenic VOCs (Wang et al., 2014). For Beijing, the net production rate of RO_x was 3.48 ppb h^{-1}, lower than the 6.60 ppb h^{-1} from the field studies of Liu et al. (2012).”

6) We have added “daytime average” in the necessary positions of the section 3.4 in the revised Manuscript.

F. Changes for “4. Conclusions”

1)We have revised our conclusion in the Conclusion section: *“(6) When the additional HONO sources were added, the photolysis of HONO became the second important source of OH in Beijing and Guangzhou before 10:00 LST, and in Shanghai before 12:00 LST, with a maximum of 3.72 [3.06 due to the $P_{unknown}$] ppb h^{-1} in Beijing, 0.89 [0.62] ppb h^{-1} in Shanghai, and 0.97 [0.78] ppb h^{-1} in Guangzhou; whereas, the reaction of HO_2 + NO was the most important source of OH, dominated in Beijing and Guangzhou after 10:00 LST and in Shanghai after 12:00 LST, with a maximum of 9.38 [7.23] ppb h^{-1} in Beijing, 2.63 [1.15] ppb h^{-1} in*

Shanghai, and 4.88 [1.43] ppb h^{-1} in Guangzhou. "

2) We have revised our conclusion in the Conclusion section: *"(7) The additional HONO sources, especially the $P_{unknown}$, accelerated the whole RO_x cycle. The daytime average OH production rates were enhanced by 4.32 [3.86 due to the $P_{unknown}$] ppb h^{-1} in Beijing, 0.67 [0.64] ppb h^{-1} in Shanghai, and 0.80 [0.68] ppb h^{-1} in Guangzhou via the reaction of HO_2 + NO, and by 1.86 [1.86] ppb h^{-1} in Beijing, 0.50 [0.50] ppb h^{-1} in Shanghai, and 0.49 [0.47] ppb h^{-1} in Guangzhou via the photolysis of HONO. The daytime average OH loss rates were increased by 2.03 [1.92 due to the $P_{unknown}$] ppb h^{-1} in Beijing, 0.58 [0.55] ppb h^{-1} in Shanghai, and 0.65 [0.58] ppb h^{-1} in Guangzhou via the reaction of OH + NO_2, and by 1.78 [1.64] ppb h^{-1} in Beijing, 0.31 [0.28] ppb h^{-1} in Shanghai, and 0.42 [0.36] ppb h^{-1} in Guangzhou via the reaction of OH + CO."*

6) We have added "daytime average" in the necessary positions of the conclusion in the revised Manuscript.

G. Changes for "References"

1) We have added the reference: *"Ren, X., Sanders, J. E., Rajendran, A., Weber, R. J., Goldstein, A.H., Pusede, S. E., Browne, E. C., Min, K.-E., and Cohen, R.C.: A relaxed eddy accumulation system for measuring vertical fluxes of nitrous acid, Atmos. Meas. Tech., 4, 2093–2103, doi:10.5194/amt-4-2093-2011, 2011."*

H. Changes for Tables and Figures

We have revised the Figs. 11 and 12 and Table 4 in the revised Manuscript.

3. The marked-up manuscript version (Changes are in red font)

Impacts of an unknown daytime nitrous acid source on its daytime concentration and budget, as well as those of hydroxyl, hydroperoxyl, and organic peroxy radicals, in the coastal regions of China

Yujia Tang[1,2], Junling An[1*], Feng Wang[1,2,3], Ying Li[1], Yu Qu[1], Yong Chen[1], Jian Lin[1,2]

[1]State Key Laboratory of Atmospheric Boundary Layer Physics and Atmospheric Chemistry (LAPC), Institute of Atmospheric Physics (IAP), Chinese Academy of Sciences, Beijing 100029, China

[2]University of the Chinese Academy of Sciences, Beijing 100049, China

[3]Anhui Meteorological Bureau, Hefei 230061, China

[*]Corresponding author: anjl@mail.iap.ac.cn

Abstract

Many field experiments have found high nitrous acid (HONO) mixing ratios in both urban and rural areas during daytime, but these high daytime HONO mixing ratios cannot be explained well by gas-phase production, suggesting that an unknown daytime HONO source ($P_{unknown}$) could exist. The formula $P_{unknown} \approx 19.60[NO_2] \cdot J(NO_2)$ was obtained using observed data from 13 field experiments across the globe. The additional HONO sources [i.e. the $P_{unknown}$, HONO emissions, and nighttime hydrolysis conversion of nitrogen dioxide (NO_2) on aerosols] were coupled into the WRF-Chem model (Weather Research and Forecasting model coupled with Chemistry) to assess the $P_{unknown}$ impacts on the

concentrations and budgets of HONO and peroxy (hydroxyl, hydroperoxyl, and organic peroxy) radicals (RO_x) (= OH + HO_2 + RO_2) in the coastal regions of China. Results indicated that the additional HONO sources produced a significant improvement in HONO and OH simulations, particularly in the daytime. Elevated daytime average $P_{unknown}$ values were found in the coastal regions of China, with a maximum of 2.5 ppb h^{-1} in the Beijing–Tianjin–Hebei region. The $P_{unknown}$ produced a 60%–250% increase of OH, HO_2 and RO_2 near the ground in the major cities of the coastal regions of China, and a 5–48% increase of OH, HO_2 and RO_2 in the daytime meridional-mean mixing ratios within 1000 m above the ground. When the additional HONO sources were included, the photolysis of HONO was the second source in the OH production rate in Beijing, Shanghai and Guangzhou before 10:00 LST with a maximum of 3.72 [3.06 due to the $P_{unknown}$] ppb h^{-1} in Beijing, whereas the reaction of HO_2 + NO (nitric oxide) was dominated after 10:00 LST with a maximum of 9.38 [7.23] ppb h^{-1} in Beijing. The whole RO_x cycle was accelerated by the additional HONO sources, especially the $P_{unknown}$. The daytime average OH production rate was enhanced by 0.67 [0.64] to 4.32 [3.86] ppb h^{-1} via the reaction of HO_2 + NO, and by 0.49 [0.47] to 1.86 [1.86] ppb h^{-1} via the photolysis of HONO, and the OH daytime average loss rate was enhanced by 0.58 [0.55] to 2.03 [1.92] ppb h^{-1} via the reaction of OH + NO_2 and by 0.31 [0.28] to 1.78 [1.64] ppb h^{-1} via the reaction of OH + CO (carbon monoxide) in Beijing, Shanghai and Guangzhou. Similarly, the additional HONO sources produced an increase of 0.31 [0.28] to 1.78 [1.64] ppb h^{-1} via the reaction of OH + CO and 0.10 [0.09] to 0.63 [0.59] ppb h^{-1} via the reaction of CH_3O_2 [methylperoxy radical] + NO in the daytime average HO_2 production rate, and 0.67 [0.61] to 4.32 [4.27] ppb h^{-1} via the reaction of HO_2 + NO in the daytime average HO_2 loss rate in Beijing, Shanghai and Guangzhou. The above results suggest that the $P_{unknown}$ considerably enhanced the RO_x concentrations and accelerated RO_x cycles in the coastal regions of China, and could produce significant increases in concentrations of inorganic aerosols and secondary organic aerosols and further aggravate haze events in these regions.

1. Introduction

The hydroxyl radical (OH) is the dominant oxidant in the troposphere, initiating daytime photochemistry, removing the majority of reactive gases, and leading to the formation of secondary products [e.g. ozone (O_3), peroxyacyl nitrates (PANs) and aerosols] that can affect air quality, climate, and human health (Stone et al., 2012). OH is formed primarily through the photolysis of O_3, nitrous acid (HONO), hydrogen peroxide (H_2O_2), the reactions of O_3 with alkenes, and the HO_2 to OH conversion process (HO_2+NO) (Platt et al., 1980; Crutzen and Zimmermann, 1991; Atkinson and Aschmann, 1993; Fried et al., 1997; Paulson et al., 1997). Recent field experiments have found the contribution of the photolysis of HONO to daytime OH production can reach up to 56, 42, and 33% in urban, rural and forest areas, respectively (Ren et al., 2003; Kleffmann et al., 2005; Acker et al., 2006), more than that of the photolysis of O_3. However, most current air quality models fail to predict observed HONO concentrations, underestimating daytime HONO in particular

(Czader et al., 2012; Gonçalves et al., 2012; Li et al., 2011), due to the incomplete knowledge of HONO sources.

It is generally accepted that the photolysis of HONO (Reaction R2) in the early morning could be a major source of OH. After sunrise, HONO mixing ratios are usually in low concentrations due to the strong photolysis of HONO. However, many field experiments have found daytime HONO mixing ratios that are unexpectedly higher than the theoretical steady value (~10 ppt), in both urban and rural areas: e.g. 0.15–1.50 ppb higher in Asia (Su et al., 2008; Wu et al.,2013; Spataro et al., 2013), 0.01–0.43 ppb higher in Europe (Kleffmann et al., 2005; Acker et al., 2007; Sörgel et al., 2011; Michoud et al., 2014), 0.02–0.81 ppb higher in North America (Zhou et al., 2002a,b; Ren et al., 2010; Villena et al., 2011; N. Zhang et al., 2012; Wong et al., 2012; VanderBoer et al., 2013), 2.00 ppb higher (maximum) in South America (Elshorbany et al., 2009), and 0.015–0.02 ppb higher in Antarctica (Kerbrat et al., 2012) (Fig. 1). These high HONO mixing ratios, particularly in the daytime, cannot be explained well by gas-phase production (Reaction R1), suggesting that an unknown daytime HONO source ($P_{unknown}$) could exist.

$$OH + NO \rightarrow HONO \qquad (R1)$$

$$HONO + h\nu \rightarrow OH + NO \qquad (R2)$$

$$HONO + OH \rightarrow NO_2 + H_2O \qquad (R3)$$

The $P_{unknown}$ was calculated by Su et al. (2008) at Xinken (Guangzhou, China), with a maximum of 4.90 ppb h^{-1}. Spataro et al. (2013) proposed a $P_{unknown}$ value of 2.58 ppb h^{-1} in Beijing. In fact, $P_{unknown}$ values, ranging from 0.06 to 4.90 ppb h^{-1} have been obtained from many field studies across the globe, as shown in Fig. 1, suggesting $P_{unknown}$ could contribute greatly to the daytime production of OH and hydroperoxyl radical (HO_2).

The most important formation pathway for nocturnal HONO could be the hydrolysis reaction of nitrogen dioxide (NO_2) on humid surfaces (Reaction R4) (Kleffmann et al., 1999; Alicke et al., 2002; Finlayson-Pitts et al., 2003):

$$2NO_2 + H_2O \rightarrow HONO + HNO_3 \qquad \text{(R4)}$$

Ammann et al. (1998) found HONO formation via the heterogeneous reduction of NO_2 on the surface of soot (Reaction R5), and Reaction (R5) can be enhanced by irradiation (Monge et al., 2010):

$$NO_2 + red_{ads} \rightarrow HONO + ox_{ads} \qquad \text{(R5)}$$

George et al. (2005) and Stemmler et al. (2006, 2007) showed the heterogeneous reduction of NO_2 on organic surfaces (Reaction R6) (e.g. humic acid) to produce HONO:

$$NO_2 + HC_{red} \rightarrow HONO + HC_{ox} \qquad \text{(R6)}$$

Li et al. (2008) proposed a homogeneous reaction of photolytically excited NO_2 with H_2O (Reaction R7), but this reaction has been proven to be unimportant in the real atmosphere (Carr et al., 2009; Wong et al., 2011; Amedro et al., 2011). Zhang and Tao (2010) suggested the homogeneous nucleation of NO_2, H_2O and ammonia (NH_3) for the production of HONO (Reaction R8), but Reaction (R8) has not yet been tested in laboratory studies, nor observed in field experiments:

$$NO_2 + h\upsilon\ (\lambda > 420\ \text{nm}) \rightarrow NO_2^{*}$$

$NO_2^* + H_2O \rightarrow HONO + OH$ (R7)

$NO_2^* + M \rightarrow NO_2 + M$

$2NO_2 + H_2O(g) + NH_3 \rightarrow HONO + NH_4NO_3(s)$ (R8)

Zhou et al. (2002b, 2003, 2011) demonstrated that the photolysis of adsorbed nitric acid (HNO_3) and nitrate (NO_3^-) at ultraviolet wavelengths (~300 nm) (Reaction R9) can produce HONO:

$HNO_3/NO_3^- + h\upsilon \rightarrow HONO/ NO_2^- + O$ (R9)

Additionally, HONO could be emitted from soils (Su et al., 2011; Oswald et al., 2013), and may be important in farmland and forest areas.

Based on these mechanisms outlined above, some modeling studies have been carried out to simulate HONO concentrations (e.g. An et al., 2011; Czader et al., 2012; Gonçalves et al., 2012). Sarwar et al. (2008) incorporated Reactions (R4), (R9) and HONO emissions into the Community Multiscale Air Quality (CMAQ) model, but still underestimated HONO mixing ratios during daytime. Li et al. (2010) considered both aerosol and ground surface reactions, and HONO emissions in the WRF-Chem model (Weather Research and Forecasting model coupled with Chemistry), and found that HONO simulations were significantly improved. However, Li et al. (2010) used a relatively high emission ratio of 2.3% for $HONO/NO_2$ to compute the direct emissions of HONO, which could have overestimated the HONO concentrations in the air (An et al., 2013). Czader et al. (2012) added Reactions (R6), (R7) and HONO emissions into the CMAQ model. The HONO simulations matched well with observations at night, but were significantly lower than observations at noon. Wong et al. (2013) reported good agreement between simulated and observed daytime HONO when HONO emissions, photolytically enhanced daytime formation mechanisms on both aerosols and the ground, and Reaction R7 were included. However, according to our recent studies (Tang et al., 2014), this result depended heavily on the selection of uptake coefficients of NO_2 heterogeneous chemistry. Overall, the topic of HONO sources remains under discussion today, and so it is a challenge for modelers to decide which mechanism(s) to be coupled into an air quality model.

To investigate the importance of the mechanisms described above, correlation tests between the $P_{unknown}$ and NO_2, HNO_3, irradiation or the photolysis frequency of NO_2 [$J(NO_2)$] were conducted in field experiments (Acker et al., 2007; Sörgel et al., 2011; Villena et al., 2011; Wong et al., 2012). Many of these studies demonstrated that there is a clear dependency of the $P_{unknown}$ on irradiation/$J(NO_2)$ during daytime, particularly at noon. Rohrer et al. (2005) proposed that the photolytic HONO source at the surface of the chamber strongly depended on light intensity. Acker et al. (2007) summarized field experiments in several European countries and showed a strong correlation (R^2=0.81) between the $P_{unknown}$ and $J(NO_2)$. Wong et al. (2012) also indicated that the $P_{unknown}$ showed a clear symmetrical diurnal variation with a maximum around noontime, closely correlated with actinic flux (NO_2 photolysis frequency) and solar irradiance; the correlation coefficient was over 0.70.

Besides irradiation/$J(NO_2)$, good correlations between the $P_{unknown}$ and NO_2 mixing ratios have been found from both field and laboratory studies, supporting the viewpoint that NO_2 is the primary precursor of HONO. Through estimating the $P_{unknown}$, Acker et al. (2007) speculated that the daytime HONO levels might be explained by a fast electron transfer onto adsorbed NO_2. Sörgel et al. (2011) indicated that the conversion of NO_2 most likely accounted for light-induced HONO formation, about an order of magnitude stronger than HONO formation during nighttime. High correlations between the $P_{unknown}$ and NO_2 mixing ratios have also been found [e.g. $R^2 = 0.77$ in Qin et al. (2006), $R^2 = 0.80$ in Villena et al. (2011), and $R^2 = 0.62$ in Elshorbany et al. (2009)], indicating that the photosensitized conversion of NO_2 is more likely to be the daytime HONO source. This is the reason why the recent CalNex 2010 (California Research at the Nexus of Air Quality and Climate Change) study found a very strong positive correlation ($R^2= 0.985$) between HONO flux and the product of NO_2 concentration and solar radiation at the Bakersfield site (Ren et al., 2011).

Based on the studies introduced above, the $P_{unknown}$ calculated from field experiments may be a practical method to help quantify the daytime HONO source. In this study, field experiment data from 13 different field campaigns across the globe were used to express the $P_{unknown}$ as a function of NO_2 mixing ratios and $J(NO_2)$ (see Sect. 2.2). We then added the $P_{unknown}$ into the WRF-Chem model to assess the impacts of the $P_{unknown}$ on the concentrations and production and loss rates of HONO, OH, HO_2, and organic peroxy radicals (RO_2).

2. Data and methods

2.1 Observed data

Observed air temperature (TA), relative humidity (RH), wind speed (WS) and direction (WD) near the ground were obtained from the National Climatic Data Center, China Meteorological Administration (H. Zhang et al., 2012). Surface mixing ratios of O_3 and NO_2 in Beijing were obtained from the Beijing Atmospheric Environmental Monitoring Action carried out by the Chinese Academy of Sciences (Li et al., 2011; Wang et al., 2014), except those in Guangzhou, which were sourced from Qin et al. (2009). HONO observations were conducted using two annular denuders at the campus of Peking University (PKU) (39°59′N, 116°18′E) in Beijing on 17–20 August 2007 (Spataro et al., 2013) and a long path absorption photometer at the Backgarden (BG) supersite (23°30′N, 113°10′E), about 60 km northwest of Guangzhou on 3–31 July 2006 (X. Li et al., 2012). The measurement systems are described in detail in Spataro et al. (2013) and X. Li et al. (2012). OH and HO_2 were measured by laser induced fluorescence at the BG supersite on 3–30 July 2006 (Lu et al., 2012).

2.2 Parameterization of HONO sources

Besides HONO gas-phase production from Reaction (R1), three additional HONO sources [HONO emissions, Reaction (R4) (nighttime), and the $P_{unknown}$] were coupled into the WRF-Chem model in this work.

HONO emissions were calculated using $[0.023 \times f_{DV} + 0.008 \times (1 - f_{DV})] \times f_{TS}$, where f_{DV} denotes the nitrogen oxides (NO_x) emission ratio of diesel vehicles to total vehicles, and f_{TS} is the NO_x emission ratio of the traffic source to all anthropogenic sources (Li et al., 2011; An et al., 2013; Tang et al., 2014). Reaction (R4) was inserted into the Carbon-Bond Mechanism Z (CBM-Z) during nighttime only. The heterogeneous reaction rate was parameterized by $k = \left(\frac{a}{D_g} + \frac{4}{v\gamma} \right)^{-1} A_s$ (Jacob, 2000), where a is the radius of aerosols, v is the mean molecular speed of NO_2, D_g is a gas-phase molecular diffusion coefficient taken as 10^{-5} m^2 s^{-1}(Dentener and Crutzen, 1993), and A_s is the aerosol surface area per unit volume of air, calculated from aerosol mass concentrations and number density in each bin set by the Model for Simulating Aerosol Interactions and Chemistry (MOSAIC). Hygroscopic growth of aerosols was considered (Li et al., 2011).

Previous studies (Sörgel et al., 2011; Villena et al., 2011; Wong et al., 2012) have shown $P_{unknown} \propto [NO_2] \cdot J(NO_2)$. To quantify the relationship between the $P_{unknown}$ and NO_2 mixing ratios and irradiation, daytime $P_{unknown}$, NO_2 mixing ratios and $J(NO_2)$, based on all the available data sets from 13 different field campaigns across the globe (Table S1), were plotted in Fig. 2. As expected, good correlation (R^2 = 0.75) between the $P_{unknown}$ and NO_2 mixing ratios was obtained (Fig. 2a). Furthermore, the correlation between the $P_{unknown}$ and $NO_2 \cdot J(NO_2)$ was increased to 0.80, with a linear regression slope of 19.60 (Fig. 2b). For the coastal regions of China, the correlation between the $P_{unknown}$ and $NO_2 \cdot J(NO_2)$ was 0.48, with a linear regression slope of 17.37 (Fig. S2b in the Supplement), which is within the maximum $P_{unknown}$ uncertainty range of 25% (Table S1). The $P_{unknown}$ cloud be expressed as a function of NO_2 mixing ratios and $J(NO_2)$, i.e., $P_{unknown} \approx 19.60[NO_2] \cdot J(NO_2)$. This formula is very similar to $P_{unknown} \approx \alpha \cdot J(NO_2) \cdot [NO_2] \cdot [H_2O] \cdot (S/V_g + S/V_a)$ proposed by Su et al. (2008), and $P_{unknown} \approx 3.3 \times 10^{-8}[NO_2] \cdot Q_s$ suggested by Wong et al. (2012) as an additional daytime source of HONO through analysis of observed data, where S/V_a is the aerosol surface area-to-volume ratio, S/V_g is the ground surface area-to-volume ratio, α is a fitting parameter, and Q_s is solar visible irradiance.

2.3 Model setup

Used in this study was the WRF-Chem model version 3.2.1 (Grell et al., 2005; Fast et al., 2006), with the CBM-Z (Zaveri and Peters, 1999) and the MOSAIC (Zaveri et al., 2008). The detailed physical and chemical schemes for the simulations can be found in Tang et al. (2014). Two domains with a horizontal resolution of 27 km were employed in this study: domain 1 covered East Asia, whereas domain 2 covered the coastal regions of China, including the Beijing–Tianjin–Hebei region (BTH), the Yangtze River delta (YRD), and the Pearl River delta (PRD) (Fig. 3). There were 28 vertical model layers from the ground to 50 hPa, and the first model layer was ~28 m above the ground. Meteorological initial and boundary conditions were obtained from the National Centers for Environmental Prediction (NCEP) 1 °×1 ° reanalysis dataset. Chemical initial and boundary conditions were constrained with the output of the Model for Ozone and Related chemical Tracers, version 4 (MOZART-4) (Emmons et al., 2010) every 6 h. Monthly anthropogenic emissions in 2006/2007 and biogenic emissions were the same as those used by Li et al. (2011)

and An et al. (2013).

Six simulations (cases R, R_{wop}, and R_p performed for the entire months of August 2007 and July 2006) with a spin-up period of seven days were conducted in this study to assess the $P_{unknown}$ effects on the concentrations and budgets of HONO, OH, HO_2, and RO_2. Case R only considered Reaction (R1) as a reference; Case R_{wop} included case R with HONO emissions, and Reaction (R4) only at night; case R_p contained case R_{wop} with the $P_{unknown}$ $[\approx 19.60[NO_2]\cdot J(NO_2)]$. The $P_{unknown}$ and Reaction (R4) were added to the CBM-Z, and diagnostic variables (i.e. production and loss rates of HONO, OH, HO_2, RO_2, O_3, and other species) were inserted into the CBM-Z to quantify the $P_{unknown}$ impacts on the budgets of HONO, OH, HO_2, and RO_2 (Wang et al., 2014).

3. Results and discussion

3.1 Comparison of simulations and observations

Simulations of TA, RH, WS and WD were compared with observations, as shown in Wang et al. (2014). The statistical metrics, i.e. mean bias (MB), mean error (ME), root-mean-square error (RMSE), normalized mean bias (NMB), normalized mean error (NME), index of agreement (IOA), and correlation coefficient (CC), were comparable with those of Wang et al. (2010) and L. Li et al. (2012) using the fifth-generation Pennsylvania State University/National Center for Atmospheric Research Mesoscale Model (MM5) and H. Zhang et al. (2012) using the WRF model. For O_3 in Beijing of the BTH region and Guangzhou of the PRD region, the NMB, NME and IOA were −22.80%, 58.70% and 0.79, respectively (Table 1 for case R), comparable to the values of 30.2% for NMB, 55.8% for NME and 0.91 for IOA reported in L. Li et al. (2012) using the CMAQ model. When HONO emissions, Reaction (R4) and the $P_{unknown}$ were included, the NMB, NME and IOA increased to −2.20%, 66.10% and 0.80, respectively (Table 1 for case R_p). The NO_2 fluctuations were generally captured (Fig. 4) but the simulated amplitude of NO_2 was underestimated in some cases (Fig. 4). This underestimation could be related with the uncertainty of NO_x emissions. For case R, the NMB, NME and IOA for NO_2 were −13.50%, 42.10% and 0.57, respectively (Table 1), similar to the results of Wang et al. (2010) using the CMAQ model (NMB of −33.0%, NME of 50.0%, and IOA of 0.61). Compared with case R, NO_2 simulations were further underestimated for case R_p (Table 1 for case R_p) due to the underestimation of NO_x emissions in Guangzhou.

HONO simulations with the gas-phase production only (case R) were always substantially underestimated compared with observations (Fig. 5), similar to the results of Sarwar et al. (2008), Li et al. (2011) and An et al. (2013). When HONO emissions and Reaction (R4) were included, HONO simulations were significantly improved, especially at night (Fig. 5 and Table 2 for case R_{wop}). For Beijing, the nighttime RMSE and NME were reduced by 0.90×10^6 molecules cm^{-3} and 44.70%, whereas the NMB and IOA were increased by 50.00% and 0.29, respectively (Table 2). For Guangzhou, the nighttime RMSE and NME were reduced by 0.44×10^6 molecules cm^{-3} and 32.90%, and the NMB and IOA were enhanced by 58.80% and 0.18, respectively. When the $P_{unknown}$ was included, daytime HONO simulations were considerably improved (Fig. 5 and Table 2 for case R_p). Compared with case R_{wop}, the daytime NME in Beijing was reduced by 19.60%, and the NMB and IOA in Beijing were increased to −24.30% from −62.00% and 0.73 from 0.64, respectively (Table 2); the daytime NME in Guangzhou was reduced by 8.10%, and the NMB in Guangzhou was increased to −61.20% from −76.50% (Table 2).

Simulated diurnal variations of OH and HO_2 showed consistent patterns with the observed data (Fig. 6). When HONO emissions and Reaction (R4) were considered (case R_{wop}), OH and HO_2 enhancements were minor in most cases compared with case R (Fig. 6 and Table 3), but the $P_{unknown}$ led to noticeable improvements in OH simulations on 5–12 July 2006 (Fig. 6). Substantial overestimation of OH mixing ratios on 20–25 July 2006 (Fig. 6) needs further investigation. Compared with case R, the NME was reduced by 79.60%, whereas the NMB was increased by 105.40%, and the IOA was improved to 0.84 from 0.79 (Table 3). When the $P_{unknown}$ was considered, HO_2 simulations were substantially improved (Fig. 6), the IOA was improved to 0.61 from 0.54 and the CC was improved to 0.66 from 0.57 (Table 3). However, HO_2 simulations were still substantially underestimated (Fig. 6). One of the major reasons for the HO_2 underestimation could be related to the considerable underestimation of anthropogenic volatile organic compounds (VOCs) (Wang et al., 2014).

3.2 $P_{unknown}$ simulations and its impacts on production and loss rates of HONO

High $P_{unknown}$ values were found in the coastal regions of China (Fig. 7), especially in the BTH, YRD and PRD regions due to elevated emissions of NO_x

(Zhang et al., 2009). For the BTH region, the largest daytime average $P_{unknown}$ values reached 2.5 ppb h^{-1} in Tianjin (Fig. 7a). Elevated daytime average $P_{unknown}$ values were found in the YRD region, with a maximum of 2.0 ppb h^{-1} in Shanghai (Fig. 7b). Daytime average $P_{unknown}$ values reached 1.2 ppb h^{-1} in Guangzhou and Shenzhen of the PRD (Fig. 7c). The simulated $P_{unknown}$ values in the PRD region were lower than those in the BTH and YRD regions. One major reason is the underestimation of daytime NO_2 mixing ratios in the PRD (Fig. 4b).

For case R, daytime HONO production was primarily from the reaction of OH and NO (Reaction R1), with a maximum production rate of 0.69 ppb h^{-1} in Beijing, 1.20 ppb h^{-1} in Shanghai, and 0.72 ppb h^{-1} in Guangzhou near noon due to high OH mixing ratios (Fig. 8a, c, e). The loss rate of HONO was 0.62 ppb h^{-1} in Beijing, 1.09 ppb h^{-1} in Shanghai, and 0.65 ppb h^{-1} in Guangzhou via Reaction (R2), much higher than the 0.01–0.02 ppb h^{-1} in Beijing, Shanghai and Guangzhou via Reaction (R3) (Fig. 8b, d, f), indicating that Reaction (R2) accounted for approximately 99% of the total loss rate of HONO.

When the additional HONO sources [HONO emissions, Reaction (R4), and the $P_{unknown}$] were coupled into the WRF-Chem model, nighttime HONO was formed mainly via Reaction (R4) (0.30–1.42 ppb h^{-1} in Beijing, 0.20–0.45 ppb h^{-1} in Shanghai, and 0.25–0.84 ppb h^{-1} in Guangzhou) (Fig. 8a, c, e). HONO emissions contributed 0.04–0.62 ppb h^{-1} to HONO production (Fig. 8a, c, e). Simulated $P_{unknown}$ values ranged from 0.42 to 2.98 ppb h^{-1} in Beijing, from 0.18 to 2.58 ppb h^{-1} in Shanghai, and from 0.06 to 1.66 ppb h^{-1} in Guangzhou (Fig. 8a, c, e). The simulated $P_{unknown}$ values in Beijing (Fig. 8a) were in good agreement with the results of Spataro et al. (2013), with an average unknown daytime HONO production rate of 2.58 ppb h^{-1} in the studied summer period. However, the simulated $P_{unknown}$ values in Guangzhou (Fig. 8e) were lower than the 2.36–4.90 ppb h^{-1} reported by Su et al (2008), due mainly to the underestimation of the daytime NO_2 mixing ratios in the PRD region. The additional HONO sources produce more HONO, which subsequently photolyzes to yield more OH. Therefore, the formation of HONO through Reaction (R1) was greatly enhanced, with a maximum of 4.70 [1.44 due to the $P_{unknown}$] ppb h^{-1} in Beijing, 4.25 [3.13] ppb h^{-1} in Shanghai, and 1.58 [0.40] ppb h^{-1} in Guangzhou in the morning (Fig. 8a, c, e), much higher than the 0.69 ppb h^{-1} in Beijing, 1.20 ppb h^{-1} in Shanghai, and 0.72 ppb h^{-1} in Guangzhou, respectively, for case R (Fig. 8a, c, e). Meanwhile, the loss rate of HONO via Reaction (R2) was significantly enhanced, with a maximum enhancement of 5.20 (= 5.82 − 0.62) [1.97 due to the $P_{unknown}$] ppb h^{-1} in Beijing, 4.31 (= 5.40 − 1.09) [1.44] ppb h^{-1} in Shanghai, and 1.96 (= 2.61 − 0.65) [1.18] ppb h^{-1} in Guangzhou (Fig. 8b, d, f). The HONO loss rate via dry deposition ranged from 0.28 to 0.45 ppb h^{-1} (not shown), roughly equivalent to the contribution of HONO emissions, suggesting that dry deposition of HONO cannot be neglected in high NO_x emission areas. The maximum $P_{unknown}$ uncertainty range of 25% (Table S1), a 25% increase (decrease) in the slope factor (19.60) led to a 9.19−18.62% increase (12.69−14.32% decrease) in the maximum HONO production rate and a 0−17.64% increase (8.40−14.07% decrease) in the maximum HONO loss rate (Fig. S3 in the Supplement).

3.3 $P_{unknown}$ impacts on concentrations of OH, HO_2 and RO_2

Incorporation of the $P_{unknown}$ into the WRF-Chem model led to substantial enhancements in the daytime average mixing ratios of OH in the coastal regions of China, e.g. 60–190% in the BTH region, 60–210% in the YRD region, and 60–200% in the PRD region (Fig. 9a). The maximum enhancement of HO_2 reached 250% in the BTH region, 200% in the YRD region, and 140% in the PRD region (Fig. 9b). Similarly, a maximum increase of 180, 150 and 80% in RO_2 [= CH_3O_2 (methylperoxy radical) + ETHP (ethylperoxy radical) + C_2O_3 (peroxyacyl radical) + others] were found in the BTH, YRD and PRD regions, respectively (Fig. 9c).

Vertically, the $P_{unknown}$ enhanced the monthly meridional-mean daytime (06:00–18:00 LST) mixing ratios of OH, HO_2 and RO_2 by 5–38, 5–47 and 5–48%, respectively, within 1000 m above the ground in the coastal regions of China (Fig. 10). The vertical enhancements of OH, HO_2 and RO_2 at the same latitude were roughly uniform within the 1000 m (Fig. 10) due to strong vertical mixing in the daytime. Different $P_{unknown}$ distributions led to distinct differences in the enhancements of OH, HO_2 and RO_2, with a maximum located near 35 °N (Fig. 10).

3.4 $P_{unknown}$ impacts on the budgets of OH, HO_2 and RO_2

OH radicals are produced mainly through the reaction of HO_2 + NO, the photolysis of O_3 and HONO, and the reactions between O_3 and alkenes (Fig. 11). For case R, the predominant contribution to P(OH) [production rate of OH] was the reaction of HO_2 + NO, with a diurnal peak of 4.04 ppb h^{-1} in Beijing, 1.52 ppb h^{-1} in Shanghai, and 3.91 ppb h^{-1} in Guangzhou at noon (Fig. S1a, c, e in the Supplement).

The photolysis of O_3 was the second most important sources of OH, which was dominant (0.91 ppb h^{-1} in Beijing, 0.52 ppb h^{-1} in Shanghai, and 1.20 ppb h^{-1} in Guangzhou) at noon (Fig. S1a, c, e). Compared with the two OH sources above, the contributions of the reactions of O_3 + alkenes, HONO photolysis and others were small, lower than 0.15 ppb h^{-1} (Fig. S1a, c, e). When the additional HONO sources were added, the most important source was the reaction of HO_2 + NO, with a diurnal maximum conversion rate reaching 9.38 [7.23 due to the $P_{unknown}$] ppb h^{-1} in Beijing, 2.63 [1.15] ppb h^{-1} in Shanghai, and 4.88 [1.43] ppb h^{-1} in Guangzhou near noon (Fig. 11a, c, e). The photolysis of HONO became the second important source of OH in Beijing and Guangzhou before 10:00 LST, and in Shanghai before 12:00 LST; the diurnal peaks were 3.72 [3.06] ppb h^{-1} in Beijing at 09:00 LST, 0.89 [0.62] ppb h^{-1} in Shanghai at 11:00 LST, and 0.97 [0.78] ppb h^{-1} in Guangzhou at 09:00 LST (Fig. 11a, c, e), which were comparable to or lower than the 3.10 ppb h^{-1} reported by Elshorbany et al. (2009). The contributions of the photolysis of O_3, the reactions of O_3 + alkenes and others to P(OH) showed minor changes in comparison with case R (Figs. 11a, c, e and S1a, c, e). Kanaya et al. (2009), who also conducted similar studies at Mount Tai (located in a rural area) of China, suggested that the reaction of HO_2 + NO was the predominant OH source, with a daytime average of 3.72 ppb h^{-1}, more than the 1.38 ppb h^{-1} of the photolysis of O_3. Hens et al. (2014) reported similar results in a boreal forest, in which the dominant contributor to OH was the reaction of HO_2 + NO, ranging from 0.23 to 1.02 ppb h^{-1} during daytime. The production rates of OH in our study were higher than in Kanaya et al. (2009) and

Hens et al. (2014) due to higher NO_x emissions in urban areas than in rural areas.

The dominant loss rate of OH was the reaction of OH + NO_2 for both cases R and R_p (Figs. 11b, d, f and S1b, d, f). The diurnal maximum loss rates were 1.98 ppb h^{-1} in Beijing, 1.12 ppb h^{-1} in Shanghai, and 1.70 ppb h^{-1} in Guangzhou for case R (Fig. S1b, d, f), whereas these values were 5.61 [4.38 due to the $P_{unknown}$] ppb h^{-1} in Beijing, 2.00 [1.00] ppb h^{-1} in Shanghai, and 2.65 [1.02] ppb h^{-1} in Guangzhou for case R_p (Fig. 11b, d, f). The reactions of OH + VOCs to form HO_2 and RO_2 were the second most important loss path of OH, with a diurnal maximum of 0.75–1.73 ppb h^{-1} for case R (Fig. S1b, d, f) and 1.57 [0.82 due to the $P_{unknown}$] to 5.37 [4.05] ppb h^{-1} for case R_p in Beijing, Shanghai and Guangzhou (Fig. 11b, d, f). The third most important OH loss path was the reaction of OH + CO to form HO_2; the diurnal maximum rates were 0.46–1.47 ppb h^{-1} for case R (Fig. S1b, d, f) and 0.93 [0.49 due to the $P_{unknown}$] to 3.58 [2.86] ppb h^{-1} for case R_p in Beijing, Shanghai and Guangzhou (Fig. 11b, d, f).

The averaged radical conversion rates in the daytime (06:00–18:00 LST) are illustrated in Fig. 12. OH radicals are produced mainly via the photolysis of O_3, HONO and hydrogen peroxide (H_2O_2), and the reactions between O_3 and alkenes, after which OH radicals enter the RO_x (= OH + HO_2 + RO_2) cycle (Fig. 12 and Tables 4, S2 and S3 in the Supplement). In the cycle, the transfer among OH, HO_2 and RO_2 radicals oxidizes VOCs and converts NO to NO_2, accomplishing major oxidation processes. The OH, HO_2 and RO_2 radicals are eliminated by the termination reactions, ultimately leading to the formation and deposition of reservoir species (e.g. HNO_3, organic acid, PANs, and H_2O_2).

For case R, the reaction of HO_2 + NO was the major source of OH [2.78 ppb h^{-1} (81.73% of the total daytime average production rate of OH) in Beijing, 0.73 ppb h^{-1} (67.09%) in Shanghai, and 1.75 ppb h^{-1} (71.54%) in Guangzhou] (Fig. 12a and Table 4). The second largest source of OH was the photolysis of O_3 [0.47 ppb h^{-1} (13.68%) in Beijing, 0.31 ppb h^{-1} (28.17%) in Shanghai, and 0.62 ppb h^{-1} (25.27%) in Guangzhou] (Table 4). OH radicals were removed mainly through the reaction of OH + NO_2 [1.12 ppb h^{-1} (39.31% of the total daytime average loss rate of OH) in Beijing, 0.47 ppb h^{-1} (46.63%) in Shanghai, and 0.77 ppb h^{-1} (38.33%) in Guangzhou] (Table 4), whereas those were converted to HO_2 mainly via the reaction of OH + CO [0.79 ppb h^{-1} (27.65%) in Beijing, 0.20 ppb h^{-1} (19.97%) in Shanghai, and 0.58 ppb h^{-1} (28.67%) in Guangzhou] (Table 4). The total daytime average conversion rate of OH to HO_2 was 0.40–1.35 ppb h^{-1}, and that of OH to RO_2 was 0.21–0.69 ppb h^{-1} in Beijing, Shanghai and Guangzhou (Fig. 12a). For HO_2, the predominant production pathways were the reactions of OH + CO [0.79 ppb h^{-1} (33.42%) in Beijing, 0.20 ppb h^{-1} (28.27%) in Shanghai, and 0.58 ppb h^{-1} (38.26%) in Guangzhou] and CH_3O_2 + NO [0.54 ppb h^{-1} (23.12%) in Beijing, 0.16 ppb h^{-1} (22.53%) in Shanghai, and 0.33 ppb h^{-1} (21.75%) in Guangzhou] and the photolysis of formaldehyde (HCHO) [0.24 ppb h^{-1} (10.34%) in Beijing, 0.09 ppb h^{-1} (11.97%) in Shanghai, and 0.11 ppb h^{-1} (7.42%) in Guangzhou] (Table S2). HO_2 radicals were consumed primarily via the reaction of HO_2 + NO [2.78 ppb h^{-1} (99.34%) in Beijing, 0.73 ppb h^{-1} (99.61%) in Shanghai, and 1.75 ppb h^{-1} (98.29%) in Guangzhou] (Table

S2). RO_2 radicals were formed mainly from the reactions of OH + OLET (terminal olefin carbons)/OLEI (internal olefin carbons) [0.19 ppb h^{-1} (22.45%) in Beijing, 0.05 ppb h^{-1} (21.07%) in Shanghai, and 0.06 ppb h^{-1} (14.88%) in Guangzhou], OH + ETH (ethene) [0.16 ppb h^{-1} (18.36%) in Beijing, 0.03 ppb h^{-1} (11.91%) in Shanghai, and 0.04 ppb h^{-1} (10.24%) in Guangzhou], OH + methane (CH_4) [0.10 ppb h^{-1} (12.09%) in Beijing, 0.06 ppb h^{-1} (22.44%) in Shanghai, and 0.14 ppb h^{-1} (33.97%) in Guangzhou], and OH + AONE (acetone) [0.09 ppb h^{-1} (10.76%) in Beijing, 0.02 ppb h^{-1} (7.09%) in Shanghai, and 0.05 ppb h^{-1} (11.24%) in Guangzhou]. RO_2 radicals were consumed primarily via the reaction of CH_3O_2 + NO [0.54 ppb h^{-1} (94.56%) in Beijing, 0.16 ppb h^{-1} (95.28%) in Shanghai, and 0.33 ppb h^{-1} (96.07%) in Guangzhou] (Table S3).

When the additional HONO sources were inserted into the WRF-Chem model (case R_p), the daytime average OH production rate was enhanced by 4.32 (= 7.10 − 2.78) [3.86 due to the $P_{unknown}$] ppb h^{-1} in Beijing, 0.67 (= 1.40 − 0.73) [0.64] ppb h^{-1} in Shanghai, and 0.80 (= 2.55 − 1.75) [0.68] ppb h^{-1} in Guangzhou via the reaction of HO_2 + NO, and by 1.86 (= 1.86 − 0) [1.86] ppb h^{-1} in Beijing, 0.50 (= 0.50 − 0) [0.50] ppb h^{-1} in Shanghai, and 0.49 (= 0.49 − 0) [0.47] ppb h^{-1} in Guangzhou via the photolysis of HONO, respectively (Table 4). The enhancements of the daytime average OH production rate due to the photolysis of HONO were comparable to or lower than the 2.20 ppb h^{-1} obtained by Liu et al. (2012). The daytime average OH loss rate was increased by 2.03 (= 3.15 − 1.12) [1.92 due to the $P_{unknown}$] ppb h^{-1} in Beijing, 0.58 (= 1.05 − 0.47) [0.55] ppb h^{-1} in Shanghai, and 0.65 (= 1.42 − 0.77)

[0.58] ppb h^{-1} in Guangzhou via the reaction of OH + NO_2, and by 1.78 (= 2.57 − 0.79) [1.64] ppb h^{-1} in Beijing, 0.31 (= 0.51 − 0.20) [0.28] ppb h^{-1} in Shanghai, and 0.42 (= 1.00 − 0.58) [0.36] ppb h^{-1} in Guangzhou via the reaction of OH + CO, respectively (Table 4). Similarly, the daytime average HO_2 production rate was increased by 0.31 [0.28 due to the $P_{unknown}$] to 1.78 [1.64] ppb h^{-1} in Beijing, Shanghai and Guangzhou via the reaction of OH + CO, and by 0.63 (= 1.17 − 0.54) [0.59] ppb h^{-1} in Beijing, 0.10 (= 0.26 − 0.16) [0.09] ppb h^{-1} in Shanghai, and 0.19 (= 0.52 − 0.33) [0.17] ppb h^{-1} in Guangzhou via the reaction of CH_3O_2 + NO; whereas, the daytime average HO_2 loss rate was enhanced by 0.67 [0.61 due to the $P_{unknown}$] to 4.32 [4.27] ppb h^{-1} in Beijing, Shanghai and Guangzhou via the reaction of HO_2 + NO (Table S2). The additional HONO sources also led to an increase of 0.06 (= 0.11 − 0.05) [0.04 due to the $P_{unknown}$] to 0.35 (= 0.54 − 0.19) [0.28] ppb h^{-1} via the reaction of OH + OLET/OLEI, 0.04 (= 0.07 − 0.03) [0.03] to 0.32 (= 0.48 − 0.16) [0.28] ppb h^{-1} via the reaction of OH + ETH, 0.06 (= 0.12 − 0.06) [0.06] to 0.16 (= 0.26 − 0.10) [0.15] ppb h^{-1} via the reaction of OH + CH_4, and 0.03 (= 0.05 − 0.02) [0.03] to 0.23 (= 0.32 − 0.09) [0.21] ppb h^{-1} via the reaction of OH + AONE in the daytime average RO_2 production rate, and 0.10 [0.09 due to the $P_{unknown}$] to 0.63 [0.59] ppb h^{-1} via the reaction of CH_3O_2 + NO in the daytime average RO_2 loss rate in Beijing, Shanghai and Guangzhou (Table S3).

Overall, the net daytime production rate of RO_x was increased to 3.48 (= 2.56 + 0.71 + 0.21) [2.06 due to the $P_{unknown}$] from 1.20 (= 0.60 + 0.43 + 0.17) ppb h^{-1} in Beijing, 1.09 (= 0.86 + 0.19 + 0.04) [0.45] from 0.54 (= 0.36 + 0.14 + 0.04) ppb h^{-1}

in Shanghai, and 1.52 (= 1.21 + 0.26 + 0.05) [0.58] from 0.92 (= 0.68 + 0.20 + 0.04) ppb h^{-1} in Guangzhou (Fig. 12) due to the additional HONO sources, indicating that the RO_x source was mainly from OH production, especially via the photolysis of HONO (Tables 4, S2 and S3). This result is different from the conclusion of Liu et al. (2012) that the photolysis of HONO and oxygenated VOCs is the largest RO_x source. One of the primary reasons for this is the underestimation of anthropogenic VOCs (Wang et al., 2014). For Beijing, the net production rate of RO_x was 3.48 ppb h^{-1}, lower than the 6.60 ppb h^{-1} from the field studies of Liu et al. (2012). Our results reconfirmed the view of Ma et al. (2012) that the North China Plain acts as an oxidation pool. The additional HONO sources produced an increase in the net loss rate of RO_x from 1.25 (= 1.23 + 0.01 + 0.01) to 3.28 (3.24+0.03+0.01) [1.96 due to the $P_{unknown}$] ppb h^{-1} in Beijing, 0.53 (= 0.51 + 0.01 + 0.01) to 1.09 (= 1.07 + 0.01 + 0.01) [0.54] ppb h^{-1} in Shanghai, and 0.85 (= 0.82 + 0.02 + 0.01) to 1.51 (= 1.47 + 0.03 + 0.01) [0.59] ppb h^{-1} in Guangzhou (Fig. 12).

4. Conclusions

The relationship between the $P_{unknown}$, NO_2 mixing ratios and $J(NO_2)$ was investigated using available data from 13 field studies across the globe. The formula $P_{unknown} \approx 19.60[NO_2] \cdot J(NO_2)$ was obtained, and then the additional HONO sources (i.e., the $P_{unknown}$, HONO emissions and nighttime hydrolysis conversion of NO_2 on aerosols) were inserted into the WRF-Chem model, to assess the $P_{unknown}$ impacts on the concentrations and budgets of HONO and RO_x in the coastal regions of China. The results showed that:

(1) The additional HONO sources led to significant improvements in the simulations of HONO and OH, especially in the daytime.

(2) Elevated daytime average $P_{unknown}$ values were found in the coastal regions of China, reaching 2.5 ppb h^{-1} in the BTH region, 2.0 ppb h^{-1} in the YRD region, and 1.2 ppb h^{-1} in the PRD region.

(3) When the additional HONO sources were considered, nighttime HONO was produced primarily via Reaction (R4) (0.20–1.42 ppb h^{-1} in Beijing, Shanghai and Guangzhou). Simulated $P_{unknown}$ values lay between 0.42 and 2.98 ppb h^{-1} in Beijing, between 0.18 and 2.58 ppb h^{-1} in Shanghai, and between 0.06 and 1.66 ppb h^{-1} in Guangzhou. HONO emissions contributed 0.04–0.62 ppb h^{-1} to HONO production.

(4) The additional HONO sources substantially enhanced the production and loss rates of HONO. The maximum production rate of HONO was increased to 4.70 [1.44 due to the $P_{unknown}$] from 0.69 ppb h^{-1} in Beijing, 4.25 [3.13] from 1.20 ppb h^{-1} in Shanghai, and 1.58 [0.40] from 0.72 ppb h^{-1} in Guangzhou via the reaction of OH and NO in the morning; whereas, the maximum loss rate of HONO was increased to 5.82 [1.97] from 0.62 ppb h^{-1} in Beijing, 5.40 [1.44] from 1.09 ppb h^{-1} in Shanghai, and 2.61 [1.18] from 0.65 ppb h^{-1} in Guangzhou via the photolysis of HONO. Dry deposition of HONO contributed 0.28–0.45 ppb h^{-1} to the loss rate of HONO, approximately equivalent to the contribution of HONO emissions, emphasizing the importance of dry deposition of HONO in high NO_x emission areas.

(5) The $P_{unknown}$ produced a 60–210% enhancement of OH, a 60–250% enhancement of HO_2, and a 60–180% enhancement of RO_2 near the ground in the

major cities of the coastal regions of China. Vertically, the $P_{unknown}$ enhanced the daytime meridional-mean mixing ratios of OH, HO_2 and RO_2 by 5–38, 5–47 and 5–48%, respectively, within 1000 m above the ground.

(6) When the additional HONO sources were added, the photolysis of HONO became the second important source of OH in Beijing and Guangzhou before 10:00 LST, and in Shanghai before 12:00 LST, with a maximum of 3.72 [3.06 due to the $P_{unknown}$] ppb h^{-1} in Beijing, 0.89 [0.62] ppb h^{-1} in Shanghai, and 0.97 [0.78] ppb h^{-1} in Guangzhou; whereas, the reaction of HO_2 + NO was the most important source of OH, dominated in Beijing and Guangzhou after 10:00 LST and in Shanghai after 12:00 LST, with a maximum of 9.38 [7.23] ppb h^{-1} in Beijing, 2.63 [1.15] ppb h^{-1} in Shanghai, and 4.88 [1.43] ppb h^{-1} in Guangzhou.

(7) The additional HONO sources, especially the $P_{unknown}$, accelerated the whole RO_x cycle. The daytime average OH production rates were enhanced by 4.32 [3.86 due to the $P_{unknown}$] ppb h^{-1} in Beijing, 0.67 [0.64] ppb h^{-1} in Shanghai, and 0.80 [0.68] ppb h^{-1} in Guangzhou via the reaction of HO_2 + NO, and by 1.86 [1.86] ppb h^{-1} in Beijing, 0.50 [0.50] ppb h^{-1} in Shanghai, and 0.49 [0.47] ppb h^{-1} in Guangzhou via the photolysis of HONO. The daytime average OH loss rates were increased by 2.03 [1.92 due to the $P_{unknown}$] ppb h^{-1} in Beijing, 0.58 [0.55] ppb h^{-1} in Shanghai, and 0.65 [0.58] ppb h^{-1} in Guangzhou via the reaction of OH + NO_2, and by 1.78 [1.64] ppb h^{-1} in Beijing, 0.31 [0.28] ppb h^{-1} in Shanghai, and 0.42 [0.36] ppb h^{-1} in Guangzhou via the reaction of OH + CO.

(8) The additional HONO sources produced an increase of 0.31 [0.28 due to the

$P_{unknown}$] to 1.78 [1.64] ppb h^{-1} via the reaction of OH + CO and 0.10 [0.09] to 0.63 [0.59] ppb h^{-1} via the reaction of CH_3O_2 + NO in the daytime average HO_2 production rate, and 0.67 [0.61] to 4.32 [4.27] ppb h^{-1} via the reaction of HO_2 + NO in the daytime average HO_2 loss rate in Beijing, Shanghai and Guangzhou. Similarly, the additional HONO sources led to an enhancement of 0.06 [0.04] to 0.35 [0.28] ppb h^{-1} via the reaction of OH + OLET/OLEI, 0.04 [0.03] to 0.32 [0.28] ppb h^{-1} via the reaction of OH + ETH, 0.06 [0.06] to 0.16 [0.15] ppb h^{-1} via the reaction of OH + CH_4, and 0.03 [0.03] to 0.23 [0.21] ppb h^{-1} via the reaction of OH + AONE in the daytime average RO_2 production rate, and 0.10 [0.09] to 0.63 [0.59] ppb h^{-1} via the reaction of CH_3O_2 + NO in the daytime average RO_2 loss rate in Beijing, Shanghai and Guangzhou.

Overall, the above results suggest that the $P_{unknown}$ significantly enhances the atmospheric oxidation capacity in the coastal regions of China by increasing RO_x concentrations and accelerating RO_x cycles, and could lead to considerable increases in concentrations of inorganic aerosols and secondary organic aerosols and further aggravate haze events in these regions.

Acknowledgements

This research was partially supported by the National Natural Science Foundation of China (41175105, 41405121), a Key Project of the Chinese Academy of Sciences (XDB05030301), and the Carbon and Nitrogen Cycle Project of the Institute of Atmospheric Physics, Chinese Academy of Sciences, and the Beijing Municipal

Natural Science Foundation (8144054).

References

Acker, K., Möller, D.: Corrigendum to: Atmospheric variation of nitrous acid at different sites in Europe. Environmental Chemistry, 4(5), 364-364, 2007.

Acker, K., Möller, D., Wieprecht, W., Meixner, F. X., Bohn, B., Gilge, S., Plass-Dülmer, C., and Berresheim, H.: Strong daytime production of OH from HNO_2 at a rural mountain site, Geophys. Res. Lett., 33(2), doi: 10.1029/2005GL024643, 2006.

Alicke, B., Platt, U., and Stutz, J.: Impact of nitrous acid photolysis on the total hydroxyl radical budget during the limitation of oxidant production/Pianura padana produzione di ozono study in Milan, J. Geophys. Res. –Atmos., 107(D22): LOP9-1 – LOP9-17, doi: 10.1029/2000JD000075, 2002.

Amedro, D., Parker, A. E., Schoemaecker, C., Fittschen, C.: Direct observation of OH radicals after 565nm multi-photon excitation of NO_2 in the presence of H_2O. Chemical Physics Letters, 513(1), 12-16, 2011.

Ammann, M., Kalberer, M., Jost, D. T., Tobler, L., Rössler, E., Piguet, D., Gäggeler, H., Baltensperger, U.: Heterogeneous production of nitrous acid on soot in polluted air masses. Nature, 395(6698), 157-160, 1998.

An, J., Li, Y., Wang, F., and Xie, P.: Impacts of photoexcited NO_2 chemistry and heterogeneous reactions on concentrations of O_3 and NO_y in Beijing, Tianjin and Hebei province of China, Air Quality-Models and Applications, Prof.

Dragana Popovic (Ed.), InTech, ISBN: 978-953-307-307-1, doi: 10.5772/16858, 2011.

An, J., Li, Y., Chen, Y., Li, J., Qu, Y., Tang, Y.: Enhancements of major aerosol components due to additional HONO sources in the North China Plain and implications for visibility and haze. Advances in Atmospheric Science, 30, 57-66, 2013.

Atkinson, R., Aschmann, S. M.: Hydroxyl radical production from the gas-phase reactions of ozone with a series of alkenes under atmospheric conditions. Environmental science & technology, 27(7), 1357-1363, 1993.

Carr, S., Heard, D., Blitz, M.: Comment on “Atmospheric Hydroxyl Radical Production from Electronically Excited NO_2 and H_2O”. Science, 324, 5925, doi:10.1126/science.1166669, 2009.

Crutzen, P. J., Zimmermann, P. H.: The changing photochemistry of the troposphere. Tellus B, 43(4), 136-151, 1991.

Czader, B. H., Rappenglück, B., Percell, P., Byun, D. W., Ngan, F., Kim, S.: Modeling nitrous acid and its impact on ozone and hydroxyl radical during the Texas Air Quality Study 2006. Atmospheric Chemistry and Physics, 12(15), 6939-6951, 2012.

Dentener, F. J., Crutzen, P. J.: Reaction of N_2O_5 on tropospheric aerosols: Impact on the global distributions of NO_x, O_3, and OH. Journal of Geophysical Research: Atmospheres (1984–2012), 98(D4), 7149-7163, 1993.

Elshorbany, Y. F., Kurtenbach, R., Wiesen, P., Lissi, E., Rubio, M., Villena, G., Gramsch, E., Rickard, A. R., Pilling, M. J., Kleffmann, J.: Oxidation capacity of the city air of Santiago, Chile. Atmospheric Chemistry and Physics, 9(6), 2257-2273, 2009.

Emmons, L. K., Walters, S., Hess, P. G., Lamarque, J. F., Pfister, G. G., Fillmore, D., Granier, C., Guenther, A., Kinnison, D., Laepple, T., Orlando, J., Tie, X., Tyndall, G., Wiedinmyer, C., Baughcum, S. L., Kloster, S.: Description and evaluation of the Model for Ozone and Related chemical Tracers, version 4 (MOZART-4). Geoscientific Model Development, 3(1), 43-67, 2010.

Fast, J. D., Gustafson, W. I., Easter, R. C., Zaveri, R. A., Barnard, J. C., Chapman, E. G., Grell, G. A., and Peckham, S. E.: Evolution of ozone, particulates, and aerosol direct radiative forcing in the vicinity of Houston using a fully coupled meteorology chemistry aerosol model, J. Geophys. Res. –Atmos., 111(D21), doi: 10.1029/2005JD006721, 2006.

Finlayson-Pitts, B. J., Wingen, L. M., Sumner, A. L., Syomin, D., Ramazan, K. A.: The heterogeneous hydrolysis of NO_2 in laboratory systems and in outdoor and indoor atmospheres: An integrated mechanism.Physical Chemistry Chemical Physics, 5(2), 223-242, 2003.

Fried, A., McKeen, S., Sewell, S., Harder, J., Henry, B., Goldan, P., Kuster, W., William, E., Baumann, K., Shett, R., Cantrell, C.: Photochemistry of formaldehyde during the 1993 Tropospheric OH Photochemistry Experiment. Journal of Geophysical Research: Atmospheres (1984–2012), 102(D5), 6283-6296, 1997.

George, C., Strekowski, R. S., Kleffmann, J., Stemmler, K., Ammann, M.: Photoenhanced uptake of gaseous NO_2 on solid organic compounds: a photochemical source of HONO?. Faraday discussions, 130, 195-210, 2005.

Gonçalves, M., Dabdub, D., Chang, W. L., Jorba, O., Baldasano, J. M.: Impact of HONO sources on the performance of mesoscale air quality models. Atmospheric Environment, 54, 168-176, 2012.

Grell, G. A., Peckham, S. E., Schmitz, R., McKeen, S. A., Frost, G., Skamarock, W. C., Eder, B.: Fully coupled "online" chemistry within the WRF model. Atmospheric Environment, 39(37), 6957-6975, 2005.

Hens, K., Novelli, A., Martinez, M., Auld, J., Axinte, R., Bohn, B., Fischer, H., Keronen, P., Kubistin, D., Nölscher, A. C., Oswald, R., Paasonen, P., Petäjä, T., Regelin, E., Sander, R., Sinha, V., Sipilä, M., Taraborrelli, D., Tatum Ernest, C., Williams, J., Lelieveld, J., Harder, H.: Observation and modeling of HO_x radicals in a boreal forest. Atmospheric Chemistry and Physics, 14, 8723–8747, 2014.

Jacob, D. J.: Heterogeneous chemistry and tropospheric ozone. Atmospheric Environment, 34(12), 2131-2159, 2000.

Kanaya, Y., Pochanart, P., Liu, Y., Li, J., Tanimoto, H., Kato, S., Suthawaree. J., Inomata, S., Taketani, F., Okuzawa, K., Kawamura, K., Akimoto, H., Wang, Z. F.: Rates and regimes of photochemical ozone production over Central East China in June 2006: a box model analysis using comprehensive measurements of ozone precursors. Atmospheric Chemistry and Physics, 9, 7711–7723, 2009.

Kerbrat, M., Legrand, M., Preunkert, S., Gallée, H., and Kleffmann, J.: Nitrous acid at Concordia (inland site) and Dumont d'Urville (coastal site), East Antarctica, J. Geophys. Res. –Atmos., 117(D8), doi: 10.1029/2011JD017149, 2012.

Kleffmann, J., Gavriloaiei, T., Hofzumahaus, A., Holland, F., Koppmann, R., Rupp, L.,Schlosser, E., Siese, M., and Wahner, A.: Daytime formation of nitrous acid: a major source of OH radicals in a forest, J. Geophys. Res. Lett., 32(5), doi: 10.1029/2005GL022524, 2005.

Kleffmann, J., Gavriloaiei, T., Hofzumahaus, A., Holland, F., Koppmann, R., Rupp, L., Schlosser, E., Siese, M., Wahner, A.: Daytime formation of nitrous acid: A major source of OH radicals in a forest. Geophysical Research Letters, 32(5), 2005.

Li, G., Lei, W., Zavala, M., Volkamer, R., Dusanter, S., Stevens, P., Molina1, L. T.: Impacts of HONO sources on the photochemistry in Mexico City during the MCMA-2006/MILAGO Campaign. Atmospheric Chemistry and Physics, 10, 6551–6567, 2010.

Li, L., Chen, C. H., Huang, C., Huang, H. Y., Zhang, G. F., Wang, Y. J., Wang, H. L., Lou, S. R., Qiao, L. P., Zhou, M., Chen, M. H., Chen, Y. R., Fu, J. S., Streets, D. G., Jang, C. J.: Process analysis of regional ozone formation over the Yangtze River Delta, China using the Community Multi-scale Air Quality modeling system. Atmospheric Chemistry and Physics, 12, 10971-10987, 2012.

Li, S., J. Matthews, and A. Sinha.: Atmospheric hydroxyl radical production from electronically excited NO_2 and H_2O. Science, 319, 1657–1660, 2008.

Li, X., Brauers, T., Häseler, R., Bohn, B., Fuchs, H., Hofzumahaus, A., Holland, F., Lou, S., Lu, K. D., Rohrer, F., Hu, M., Zeng, L. M., Zhang, Y. H., Garland, R. M., Su, H., Nowak, A., Wiedensohler, A., Takegawa, N., Shao, M., Wahner, A.: Exploring the atmospheric chemistry of nitrous acid (HONO) at a rural site in Southern China. Atmospheric Chemistry and Physics, 12(3), 1497-1513, 2012.

Li, Y., An, J., Min, M., Zhang, W., Wang, F., Xie, P.: Impacts of HONO sources on the air quality in Beijing, Tianjin and Hebei Province of China. Atmospheric Environment, 45(27), 4735-4744, 2011.

Liu, Z., Wang, Y., Gu, D., Zhao, C., Huey, L. G., Sticke, R., Liao, J., Shao, M., Zhu, T., Zeng, L., Amoroso, A., Costabile, F., Chang, C.-C., Liu, S.-C.: Summertime photochemistry during CARE Beijing-2007: RO_x budgets and O_3 formation. Atmospheric Chemistry and Physics, 12, 7737–7752, 2012.

Lu, K. D., Rohrer, F., Holland, F., Fuchs, H., Bohn, B., Brauers, T., Chang, C. C., Haseler, R., Hu, M., Kita, K., Kondo, Y., Li, X., Lou, S. R., Nehr, S., Shao, M., Zeng, L. M., Wahner, A., Zhang, Y. H., Hofzumahaus, A.: Observation and modelling of OH and HO_2 concentrations in the Pearl River Delta 2006: a missing OH source in a VOC rich atmosphere. Atmospheric Chemistry and Physics, 12(3), 1541-1569, 2012.

Ma, J. Z., Wang, W., Chen, Y., Liu, H. J., Yan, P., Ding, G. A., Wang, M. L., Sun, J., Lelieveld, J.: The IPAC-NC field campaign: a pollution and oxidization pool in the lower atmosphere over Huabei, China. Atmospheric Chemistry and Physics, 12, 3883–3908, 2012.

Michoud, V., Colomb, A., Borbon, A., Miet, K., Beekmann, M., Camredon, M., Aumont, B., Perrier, S., Zapf, P., Siour, G., Ait-Helal, W., Afif, C., Kukui, A., Furger, M., Dupont, J. C., Haeffelin, M., Doussin, J. F.: Study of the unknown HONO daytime source at a European suburban site during the MEGAPOLI summer and winter field campaigns. Atmospheric Chemistry and Physics, 14(6), 2805-2822, 2014.

Monge, M. E., D'Anna, B., Mazri, L., Giroir-Fendler, A., Ammann, M., Donaldson, D. J., George, C.: Light changes the atmospheric reactivity of soot. Proceedings of the National Academy of Sciences, 107(15), 6605-6609, 2010.

Oswald, R., Behrendt, T., Ermel, M., Wu, D., Su, H., Cheng, Y., Breuninger, C., Moravek, A., Mougin, E., Delon, C., Loubet, B., Pommerening-Röser, A., Sörgel, M., Pöschl, U., Hoffmann, T., Andreae, M.O., Meixner, F.X., Trebs, I.: HONO emissions from soil bacteria as a major source of atmospheric reactive nitrogen. Science 341, 1233-1235, 2013.

Paulson, S. E., Sen, A. D., Liu, P., Fenske, J. D., Fox, M. J.: Evidence for formation of OH radicals from the reaction of O_3 with alkenes in the gas phase. Geophysical research letters, 24(24), 3193-3196, 1997.

Platt, U., Perner, D., Harris, G. W., Winer, A. M., Pitts, J. N.: Observations of nitrous acid in an urban atmosphere by differential optical absorption. Nature 285, 312-314 (29 May 1980); doi: 10.1038/285312a0, 1980.

Qin, M., Xie, P. H., Liu, W. Q., Li, A., Dou, K., Fang, W., Liu, J., Zhang, W. J.:

Observation of atmospheric nitrous acid with DOAS in Beijing, China. Journal of Environmental Sciences, 18(1), 69-75, 2006.

Qin, M., Xie, P., Su, H., Gu, J., Peng, F., Li, S., Zengb, L., Liua, J., Liua W., Zhang, Y.: An observational study of the HONO–NO_2 coupling at an urban site in Guangzhou City, South China. Atmospheric Environment, 43(36), 5731-5742, 2009.

Ren, X., Gao, H., Zhou, X., Crounse, J. D., Wennberg, P. O., Browne, E. C., LaFranchi, B. W., Cohen, R. C., McKay, M., Goldstein, A. H., Mao, J.: Measurement of atmospheric nitrous acid at Bodgett Forest during BEARPEX2007. Atmospheric Chemistry and Physics, 10(13), 6283-6294, 2010.

Ren, X., Harder, H., Martinez, M., Lesher, R. L., Oliger, A., Simpas, J. B., Brunea, W. H., Schwab, J. J., Demerjian, K. L., He, Y., Zhou, X., Gao, H.: OH and HO_2 Chemistry in the urban atmosphere of New York City. Atmospheric Environment, 37(26), 3639-3651, 2003.

Ren, X., Sanders, J. E., Rajendran, A., Weber, R. J., Goldstein, A.H., Pusede, S. E., Browne, E. C., Min, K.-E., and Cohen, R.C.: A relaxed eddy accumulation system for measuring vertical fluxes of nitrous acid, Atmos. Meas. Tech., 4, 2093–2103, doi:10.5194/amt-4-2093-2011, 2011.

Rohrer, F., Bohn, B., Brauers, T., Brüning, D., Johnen, F. J., Wahner, A., Kleffmann, J.: Characterisation of the photolytic HONO-source in the atmosphere simulation chamber SAPHIR. Atmospheric Chemistry and Physics, 5(8), 2189-2201, 2005.

Sörgel, M., Regelin, E., Bozem, H., Diesch, J. M., Drewnick, F., Fischer, H., Harder, H., Held, A., Hosaynali-Beygi, Z., Martinez, M., Zetzsch, C.: Quantification of the unknown HONO daytime source and its relation to NO_2. Atmospheric Chemistry and Physics, 11(20), 10433-10447, 2011.

Sarwar, G., Roselle, S. J., Mathur, R., Appel, W., Dennis, R. L., Vogel, B.: A comparison of CMAQ HONO predictions with observations from the Northeast Oxidant and Particle Study. Atmospheric Environment, 42(23), 5760-5770, 2008.

Spataro, F., Ianniello, A., Esposito, G., Allegrini, I., Zhu, T., Hu, M.: Occurrence of atmospheric nitrous acid in the urban area of Beijing (China).Science of the Total Environment, 447, 210-224, 2013.

Stemmler, K., Ammann, M., Donders, C., Kleffmann, J., George, C.: Photosensitized reduction of nitrogen dioxide on humic acid as a source of nitrous acid. Nature, 440(7081), 195-198, 2006.

Stemmler, K., Ndour, M., Elshorbany, Y., Kleffmann, J., D'anna, B., George, C., Bohn, B., Ammann, M.: Light induced conversion of nitrogen dioxide into nitrous acid on submicron humic acid aerosol. Atmospheric Chemistry and Physics, 7(16), 4237-4248, 2007.

Stone, D., Whalley, L. K., Heard, D. E.: Tropospheric OH and HO_2 radicals: field measurements and model comparisons. Chemical Society Reviews, 41, 6348-6404, 2012.

Su, H., Cheng, Y., Oswald, R., Behrendt, T., Trebs, I., Meixner, F. X., Andreae, M. O., Cheng, P., Zhang, Y., Pöschl, U.: Soil nitrite as a source of atmospheric HONO and OH radicals. Science, 333(6049), 1616-1618, 2011.

Su, H., Cheng, Y. F., Shao, M., Gao, D. F., Yu, Z. Y., Zeng, L. M., Slanina, J., Zhang, Y. H., and Wiedensohler, A.: Nitrous acid (HONO) and its daytime sources at a rural site during the 2004 PRIDE-PRD experiment in China, J. Geophys. Res. –Atmos., 113(D14), doi: 10.1029/2007JD009060, 2008.

Tang, Y., An, J., Li, Y., Wang, F.: Uncertainty in the uptake coefficient for HONO formation on soot and its impacts on concentrations of major chemical components in the Beijing–Tianjin–Hebei region. Atmospheric Environment, 84, 163-171, 2014.

VandenBoer, T. C., Brown, S. S., Murphy, J. G., Keene, W. C., Young, C. J., Pszenny, A. A. P., Kim, S., Warneke, C., de Gouw, J. A., Maben, J. R., Wagner, N. L., Riedel, T. P., Thornton, J. A., Wolfe, D. E., Dubé, W. P., Öztürk, F., Brock, C. A., Grossberg, N., Lefer, B., Lerner, B. Middlebrook, A. M., Roberts, J. M.: Understanding the role of the ground surface in HONO vertical structure: High resolution vertical profiles during NACHTT-11. Journal of Geophysical Research: Atmospheres, 118, 10,155–10,171, doi:10.1002/jgrd.50721, 2013.

Villena, G., Wiesen, P., Cantrell, C. A., Flocke, F., Fried, A., Hall, S. R., Hornbrook, R. S., Knapp, D., Kosciuch, E., Mauldin, R. L., McGrath, J. A., Montzka, D., Richter, D., Ullmann, K., Walega, J., Weibring, P., Weinheimer, A., Staebler, R. M., Liao, J., Huey, L. G., and Kleffmann, J.: Nitrous acid (HONO) during polar spring in Barrow, Alaska: a net source of OH radicals?, J. Geophys. Res. –Atmos., 116(D14), doi: 10.1029/2011JD016643, 2011.

Wang, F., An, J., Li, Y., Tang, Y., Lin, J., Qu, Y., Cheng, Y., Zhang, B., Zhai, J.: Impacts of Uncertainty in AVOC Emissions on the Summer RO_x Budget and Ozone Production Rate in the Three Most Rapidly-Developing Economic Growth Regions of China. Advances in Atmospheric Sciences, 31, 1331–1342, 2014.

Wang, X., Zhang, Y., Hu, Y., Zhou, W., Lu, K., Zhong, L., Zeng, L., Shao, M., Hu, M., Russell, A. G.: Process analysis and sensitivity study of regional ozone formation over the Pearl River Delta, China, during the PRIDE-PRD2004 campaign using the Community Multiscale Air Quality modeling system. Atmospheric Chemistry and Physics, 10(9), 4423-4437, 2010.

Wong, K. W., Oh, H. J., Lefer, B. L., Rappenglück, B., Stutz, J.: Vertical profiles of nitrous acid in the nocturnal urban atmosphere of Houston, TX. Atmospheric Chemistry and Physics, 11(8), 3595-3609, 2011.

Wong, K. W., Tsai, C., Lefer, B., Grossberg, N., Stutz, J.: Modeling of daytime HONO vertical gradients during SHARP 2009. Atmospheric Chemistry and Physics, 13(7), 3587-3601, 2013.

Wong, K. W., Tsai, C., Lefer, B., Haman, C., Grossberg, N., Brune, W. H., Ren, X., Luke, W., Stutz, J.: Daytime HONO vertical gradients during SHARP 2009 in Houston, TX. Atmospheric Chemistry and Physics, 12(2), 635-652, 2012.

Wu, J., Xu, Z., Xue, L., Wang, T.: Daytime nitrous acid at a polluted suburban site in Hong Kong: Indication of heterogeneous production on aerosol. Proceedings of 12th international conference on atmospheric sciences and applications to air quality, Seoul, Korea, June 3-5, 2013, p. 52, 2013.

Zaveri, R. A., Peters, L. K.: A new lumped structure photochemical mechanism for large‐scale applications. Journal of Geophysical Research: Atmospheres (1984–2012), 104(D23), 30387-30415, 1999.

Zaveri, R. A., Easter, R. C., Fast, J. D., and Peters, L. K.: Model for simulating aerosol interactions and chemistry (MOSAIC), J. Geophys. Res. –Atmos., 113(D13), doi: 10.1029/2007JD008782, 2008.

Zhang, B., Tao, F.: Direct homogeneous nucleation of NO_2, H_2O, and NH_3 for the production of ammonium nitrate particles and HONO gas. Chemical Physics Letters, 489, 4-6, 143, 2010.

Zhang, H., Li, J., Ying, Q., Yu, J. Z., Wu, D., Cheng, Y., Kebin Hed, Jiang, J.: Source apportionment of $PM_{2.5}$ nitrate and sulfate in China using a source-oriented chemical transport model. Atmospheric Environment, 62, 228-242, 2012.

Zhang, N., Zhou, X., Bertman, S., Tang, D., Alaghmand, M., Shepson, P. B., Carroll, M. A.: Measurements of ambient HONO concentrations and vertical HONO flux above a northern Michigan forest canopy. Atmospheric Chemistry and Physics, 12(17), 8285-8296, 2012.

Zhang, Q., Streets, D. G., Carmichael, G. R., He, K., Huo, H., Kannari, A., Klimont, Z., Park, I., Reddy, S., Fu, J. S., Chen, D., Duan, L., Lei, Y., Wang, L., Yao, Z.:

Asian emissions in 2006 for the NASA INTEX-B mission. Atmospheric Chemistry and Physics, 9, 5131-5153, 2009.

Zhou, X., Civerolo, K., Dai, H., Huang, G., Schwab, J., and Demerjian, K: Summertime nitrous acid chemistry in the atmospheric boundary layer at a rural site in New York State, J. Geophys. Res. –Atmos., 107(D21), ACH13-1 – ACH13-11, doi: 10.1029/2001JD001539, 2002a.

Zhou, X., Gao, H., He, Y., Huang, G., Bertman, S. B., Civerolo, K., and Schwab, J.: Nitric acid photolysis on surfaces in low-NO_x environments: significant atmospheric implications, Geophys. Res. Lett., 30(23), doi: 10.1029/2003GL018620, 2003.

Zhou, X., He, Y., Huang, G., Thornberry, T. D., Carroll, M. A., and Bertman, S. B.: Photochemical production of nitrous acid on glass sample manifold surface, Geophys. Res. Lett., 29, 26-1 – 26-4, doi: 10.1029/2002GL015080, 2002b.

Zhou, X., Zhang, N., TerAvest, M., Tang, D., Hou, J., Bertman, S., Alaghmand, M., Shepson, P. B. Carroll, M. A. Griffith, S., Dusanter, S., Stevens, P. S.: Nitric acid photolysis on forest canopy surface as a source for tropospheric nitrous acid. Nature Geoscience, 4(7), 440-443, 2011.

Table 1. Model performance statistics for O_3 and NO_2 in Beijing in August 2007 and Guangzhou in July 2006.

Species	Case	MB (ppb)	ME (ppb)	RMSE (ppb)	NMB (%)	NME (%)	IOA
O_3	R_p	−0.65	19.40	25.44	−2.20	66.10	0.80
	R	−6.69	17.21	25.24	−22.80	58.70	0.79
NO_2	R_p	−9.50	17.31	21.40	−29.10	53.00	0.51
	R	−4.40	13.75	17.61	−13.50	42.10	0.57

MB: mean bias; ME: mean error; RMSE: root-mean-square error; NMB: normalized mean bias; NME: normalized mean error; IOA: index of agreement.

Table 2. Model performance statistics for daytime (06:00–18:00 LST) and nighttime (19:00–05:00 LST) HONO in Beijing in August 2007 and Guangzhou in July 2006.

Species	Case	MB (10^6 molec cm^{-3})	ME (10^6 molec cm^{-3})	RMSE (10^6 molec cm^{-3})	NMB (%)	NME (%)	IOA	CC
$\mathrm{HONO}_{\mathrm{daytime}}$ (Beijing)	R_p	−0.54	0.98	1.41	−24.30	44.50	0.73	0.57
	R_{wop}	−1.37	1.41	1.83	−62.00	64.10	0.64	0.63
	R	−2.07	2.07	2.58	−93.80	93.80	0.46	0.31
$\mathrm{HONO}_{\mathrm{nighttime}}$ (Beijing)	R_p	−0.73	0.84	1.09	−42.20	49.10	0.77	0.74
	R_{wop}	−0.82	0.91	1.16	−47.90	53.20	0.75	0.75
	R	−1.68	1.68	2.06	−97.90	97.90	0.46	0.76
$\mathrm{HONO}_{\mathrm{daytime}}$ (Guangzhou)	R_p	−0.38	0.43	0.58	−61.20	69.60	0.58	0.56
	R_{wop}	−0.48	0.49	0.65	−76.50	77.70	0.55	0.56
	R	−0.60	0.60	0.80	−95.60	96.20	0.43	-0.30
$\mathrm{HONO}_{\mathrm{nighttime}}$ (Guangzhou)	R_p	−0.42	0.75	1.05	−32.90	58.50	0.66	0.43
	R_{wop}	−0.49	0.83	1.15	−38.40	64.30	0.63	0.38
	R	−1.25	1.25	1.59	−97.20	97.20	0.45	-0.01

CC: correlation coefficient.

Table 3. Model performance statistics for OH and HO_2 in Guangzhou in July 2006.

Species	Case	MB (10^6 molec cm^{-3})	ME (10^6 molec cm^{-3})	RMSE (10^6 molec cm^{-3})	NMB (%)	NME (%)	IOA	CC
OH	R_p	−1.35	4.37	6.22	−17.60	57.00	0.84	0.75
	R_{wop}	−3.00	4.58	6.25	−112.20	126.50	0.81	0.72
	R	−3.36	4.85	6.55	−123.00	136.60	0.79	0.70
HO_2	R_p	−3.80	3.81	5.59	−78.50	78.60	0.61	0.66
	R_{wop}	−4.19	4.20	6.14	−86.60	86.70	0.54	0.59
	R	−4.22	4.23	6.16	−87.20	87.30	0.54	0.57

Table 4. Daytime (06:00–18:00 LST) average OH budgets in Beijing/Shanghai/Guangzhou in August 2007.

Reaction	Case R		Case R_{wop}		Case R_p	
	Rate (ppb h^{-1})	Contribution (%)	Rate (ppb h^{-1})	Contribution (%)	Rate (ppb h^{-1})	Contribution (%)
OH production						
HO_2+NO	**2.778/0.732/1.748**	**81.73/67.09/71.54**	**3.242/0.760/1.871**	**83.74/68.00/72.02**	**7.101/1.402/2.553**	**73.34/61.95/67.55**
$^*(HONO+hv)_{net}$	**--/--/--**	**--/--/--**	**--/--/0.017**	**--/--/0.66**	**1.855/0.497/0.489**	**19.16/21.98/12.93**
O^1D+H_2O	**0.465/0.307/0.617**	**13.68/28.17/25.27**	**0.479/0.306/0.630**	**12.36/27.38/24.24**	**0.568/0.312/0.651**	**5.86/13.80/17.23**
O_3+OLET/OLEI	0.101/0.024/0.027	2.98/2.16/1.11	0.095/0.023/0.027	2.45/2.08/1.03	0.080/0.021/0.025	0.83/0.91/0. 65
$^*(H_2O_2+hv)_{net}$	0.035/0.023/0.029	1.02/2.07/1.17	0.035/0.023/0.030	0.91/2.03/1.16	0.037/0.022/0.032	0.38/0.97/0.19
HO_2+O_3	0.009/0.001/0.014	0.28/0.07/0.59	0.010/0.001/0.015	0.26/0.06/0.58	0.026/0.001/0.019	0.27/0.05/0.51
$^*(HNO_3+hv)_{net}$	0.005/0.001/0.002	0.15/0.06/0.10	0.005/0.001/0.002	0.13/0.06/0.09	0.007/0.001/0.003	0.07/0.04/0.07
ROOH+hv	0.003/0.004/0.005	0.09/0.36/0.19	0.003/0.004/0.005	0.09/0.38/0.19	0.007/0.007/0.007	0.07/0.29/0.19
O_3+ETH	0.002/<0.001/<0.001	0.05/0.02/0.01	0.002/<0.001/<0.001	0.04/0.02/0.01	0.001/<0.001/<0.001	0.02/0.01/0.01
HO_2+NO_3	<0.001/<0.001/<0.001	<0.01/<0.01/0.01	<0.001/<0.001/<0.001	<0.01/<0.01/<0.01	<0.001/<0.001/<0.001	<0.01/<0.01/<0.01
O_3+ISOP	<0.001/<0.001/<0.001	0.01/<0.01/<0.01	<0.001/<0.001/<0.001	0.01/<0.01/<0.01	<0.001/<0.001/<0.001	<0.01/<0.01/<0.01
Total	3.399/1.091/2.443	100/100/100	3.873/1.118/2.598	100/100/100	9.683/2.263/3.779	100/100/100
OH loss						
$OH+NO_2$	**1.116/0.474/0.770**	**39.31/46.63/38.33**	**1.225/0.501/0.844**	**38.11/45.86/38.86**	**3.146/1.045/1.424**	**38.08/44.29/40.76**
OH+CO	**0.785/0.203/0.576**	**27.65/19.97/28.67**	**0.932/0.227/0.637**	**29.00/20.78/29.33**	**2.573/0.506/1.001**	**31.14/21.45/28.65**
OH+OLET/OLEI	**0.192/0.054/0.059**	**6.76/5.31/2.94**	**0.264/0.065/0.077**	**8.21/5.95/3.55**	**0.537/0.206/0.095**	**6.50/8.73/2.72**
OH+HCHO	**0.150/0.050/0.146**	**5.28/4.92/7.27**	**0.166/0.053/0.156**	**5.16/4.85/7.18**	**0.544/0.096/0.242**	**6.59/4.07/6.93**
$OH+CH_4$	0.103/0.057/0.135	3.63/5.61/6.72	0.109/0.059/0.142	3.39/5.40/6.54	0.260/0.115/0.223	3.15/4.87/6.38
OH+ALD2/MGLY/ANOE	0.092/0.018/0.045	3.24/1.77/2.24	0.109/0.020/0.049	3.39/1.83/2.26	0.323/0.047/0.081	3.91/1.99/2.32
$OH+SO_2$	0.054/0.030/0.035	1.90/2.95/1.74	0.064/0.034/0.041	1.99/3.11/1.89	0.172/0.116/0.072	2.08/4.92/2.06

OH+XYL	0.052/0.022/0.023	1.83/2.16/1.14	0.066/0.026/0.029	2.05/2.38/1.34	0.141/0.078/0.045	1.71/3.31/1.29
OH+H_2	0.038/0.021/0.050	1.34/2.07/2.49	0.040/0.022/0.052	1.24/2.01/2.39	0.095/0.027/0.075	1.15/1.14/2.15
OH+TOL	0.027/0.007/0.011	0.95/0.69/0.55	0.034/0.008/0.014	1.06/0.73/0.64	0.086/0.025/0.024	1.04/1.06/0.69
OH+HONO	0.003/0.003/0.005	0.11/0.30/0.25	0.006/0.004/0.007	0.19/0.37/0.32	0.069/0.023/0.032	0.84/0.97/0.92
OH+HNO_x	0.005/0.001/0.005	0.18/0.10/0.25	0.005/0.001/0.005	0.16/0.09/0.23	0.015/0.002/0.008	0.18/0.08/0.23
OH+O_3	0.028/0.006/0.035	0.99/0.59/1.70	0.029/0.006/0.036	0.90/0.55/1.66	0.072/0.005/0.046	0.87/0.21/1.32
OH+H_2O_2	0.015/0.008/0.027	0.53/0.79/1.34	0.016/0.008/0.029	0.50/0.73/1.34	0.040/0.010/0.043	0.48/0.42/1.23
OH+ETH/OPEN	0.007/0.002/0.004	0.25/0.20/0.20	0.008/0.002/0.005	0.25/0.18/0.23	0.036/0.009/0.011	0.44/0.38/0.31
OH+CH_3OOH/ROOH	0.010/0.011/0.014	0.35/1.08/0.70	0.011/0.012/0.014	0.34/1.10/0.64	0.022/0.020/0.022	0.27/0.85/0.63
OH+ISOP	0.019/0.004/0.002	0.67/0.39/0.10	0.020/0.004/0.003	0.62/0.37/0.14	0.017/0.007/0.003	0.21/0.30/0.09
OH+PAR	0.005/0.002/0.004	0.18/0.20/0.20	0.007/0.003/0.005	0.22/0.27/0.23	0.015/0.005/0.007	0.18/0.21/0.20
OH+ONIT /ISOPRD	0.028/0.005/0.016	0.99/0.49/0.80	0.030/0.005/0.018	0.93/0.46/0.83	0.077/0.013/0.025	0.93/0.55/0.72
OH+C_2H_6	0.002/0.001/0.002	0.07/0.10/0.10	0.003/0.001/0.002	0.09/0.09/0.09	0.008/0.002/0.004	0.10/0.08/0.11
OH+CH_3OH/ANOL/CRES	0.002/0.001/0.002	0.07/0.10/0.10	0.002/0.001/0.002	0.06/0.09/0.09	0.007/0.002/0.003	0.08/0.08/0.09
OH+HO_2	0.001/<0.001/0.004	0.04/0.05/0.20	0.002/<0.001/0.005	0.06/0.05/0.23	0.006/<0.001/0.008	0.07/0.02/0.23
OH+NO	0.105/0.036/0.039	3.70/3.54/1.94	0.066/0.030/--	2.05/2.75/--	--/--/--	--/--/--
Total	2.839/1.017/2.009	100/100/100	3.214/1.093/2.172	100/100/100	8.261/2.360/3.495	100/100/100

OLET: internal olefin carbons (C=C); OLEI: terminal olefin carbons (C=C); ROOH: higher organic peroxide; ETH: ethene; ISOP: isoprene; ALD2: acetaldehyde; MGLY: methylglyoxal; ANOE: acetone; XYL: xylene; TOL: toluene; HNO_x: HNO_3 + HNO_4; OPEN: aromatic fragments; PAR: paraffin carbon –C–; ONIT: organic nitrate; ISOPRD: lumped intermediate species; ANOL: ethanol; CRES: cresol and higher molar weight phenols.

*The reactions of HONO+hv, H_2O_2+hv and HNO_3+hv are reversible, “net” in the subscript means subtracting the corresponding reverse reactions.

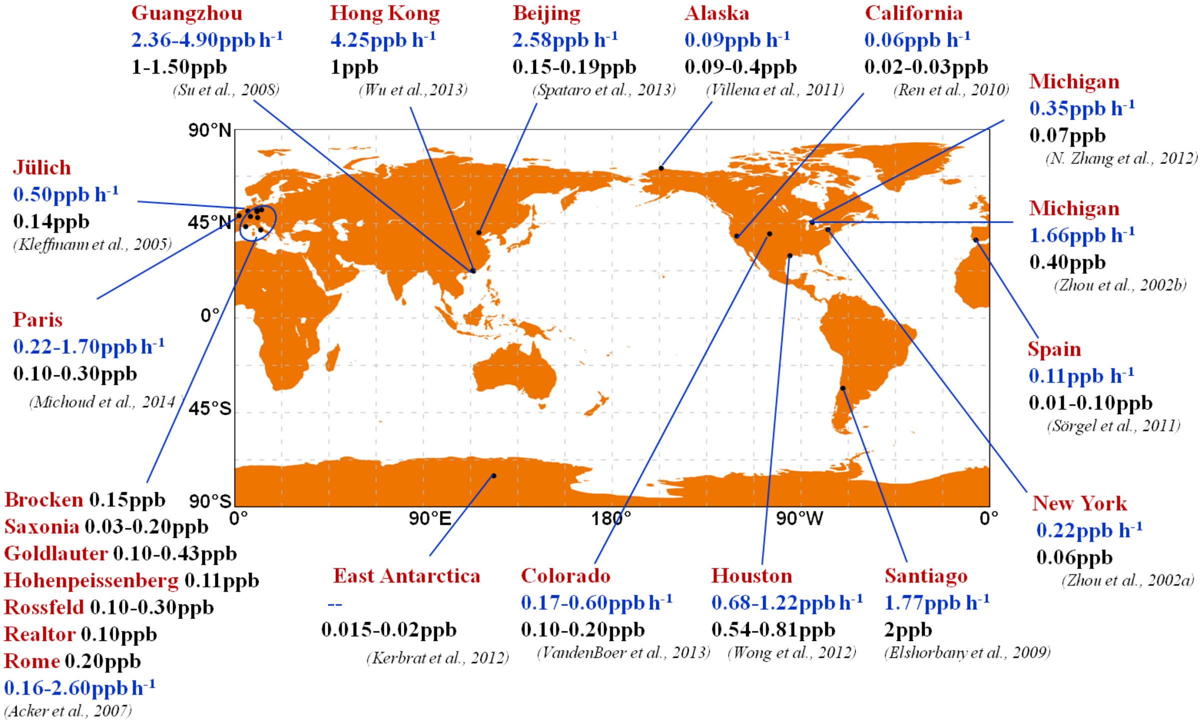

Fig. 1. Summary of observed HONO mixing ratios at noon (black font) and the calculated unknown daytime HONO source (blue font) from field studies.

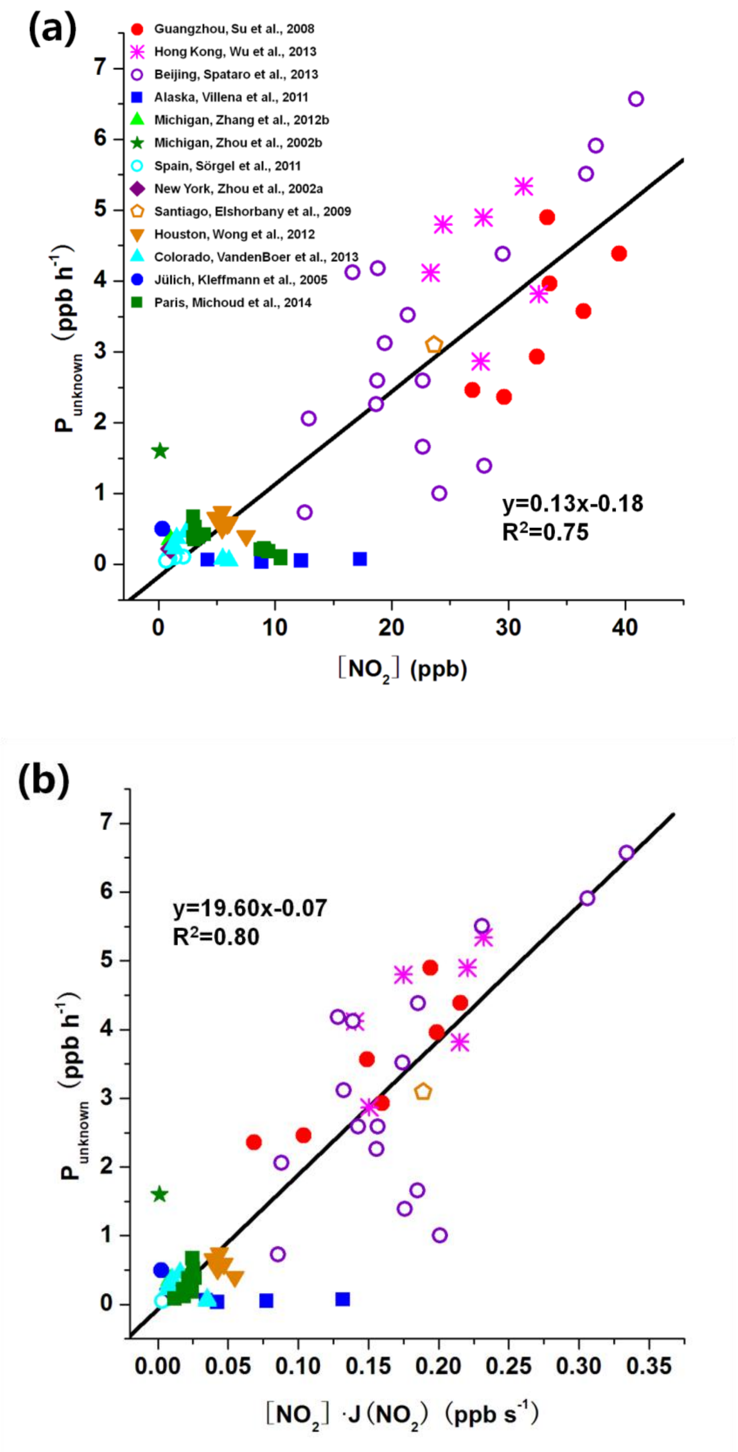

Fig. 2. Correlation of the unknown daytime HONO source ($P_{unknown}$) (ppb h^{-1}) with (a) NO_2 (ppb) and (b) $NO_2 \times J(NO_2)$ (ppb s^{-1}), based on the field experiment data shown in Fig. 1.

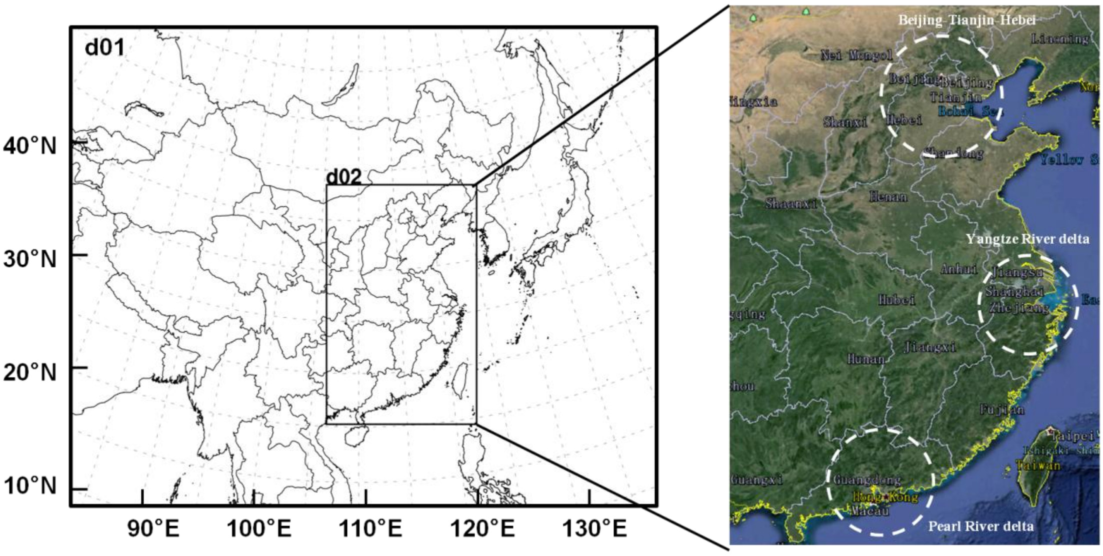

Fig. 3. Model domains used in this study. Domain 2 covers the Beijing–Tianjin–Hebei (BTH), Yangtze River delta (YRD), and Pearl River delta (PRD) regions.

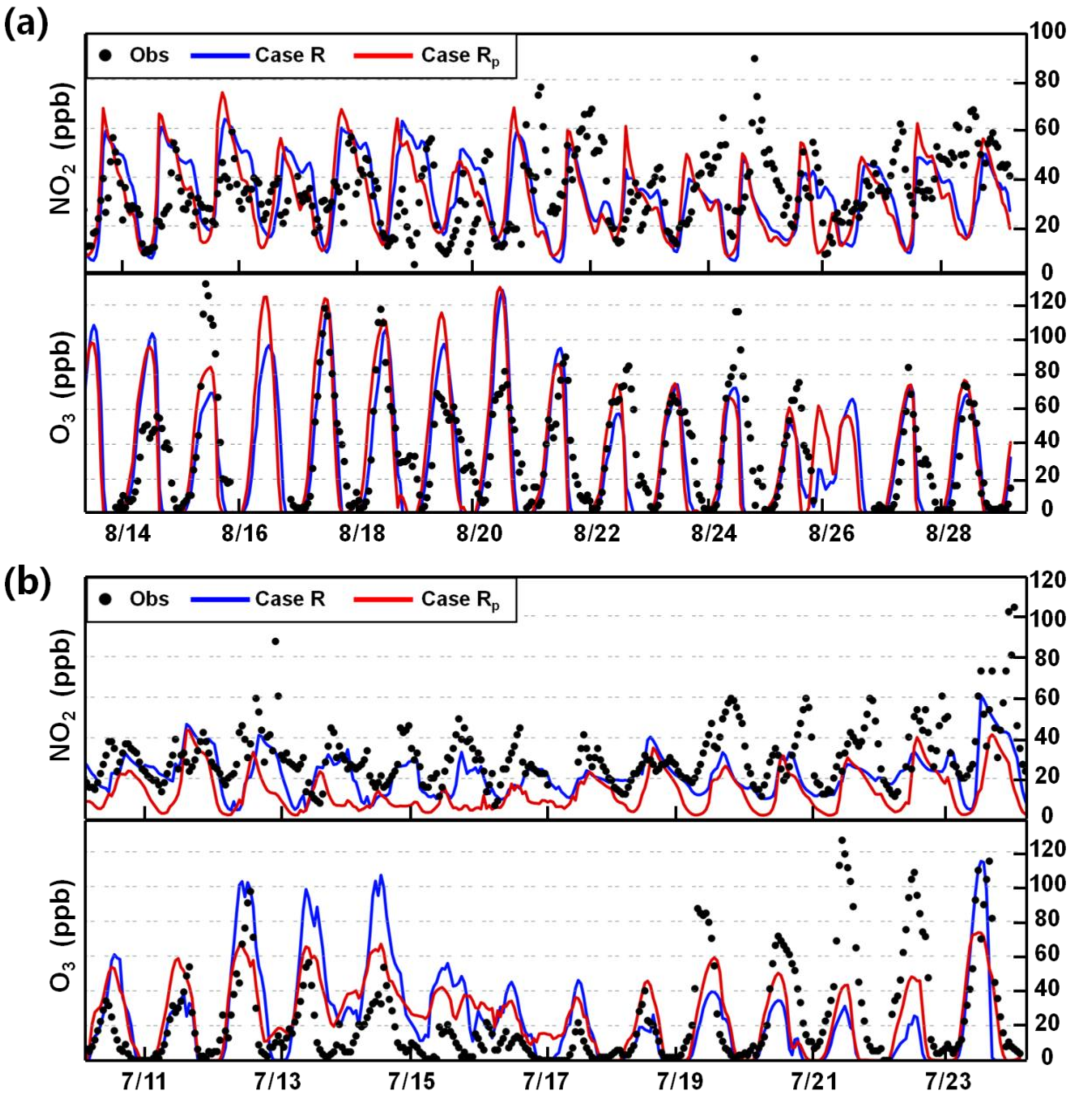

Fig. 4. Comparison of simulated and observed hourly-mean mixing ratios of NO_2 and O_3 in (a) Beijing on 14–28 August 2007 and (b) Guangzhou on 11–23 July 2006.

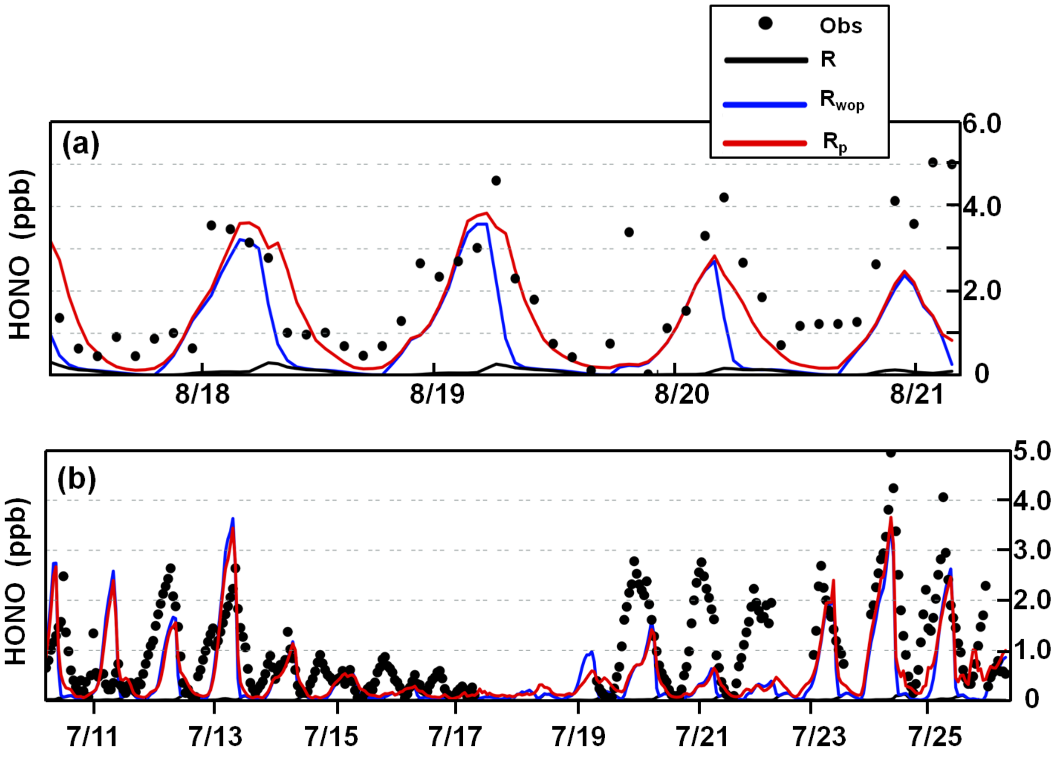

Fig. 5. Comparison of simulated and observed hourly-mean HONO mixing ratios at the Peking University site in (a) Beijing on 17–20 August 2007 (Spataro et al., 2013) and (b) the Backgarden site in Guangzhou on 11–25 July 2006 (X. Li et al., 2012).

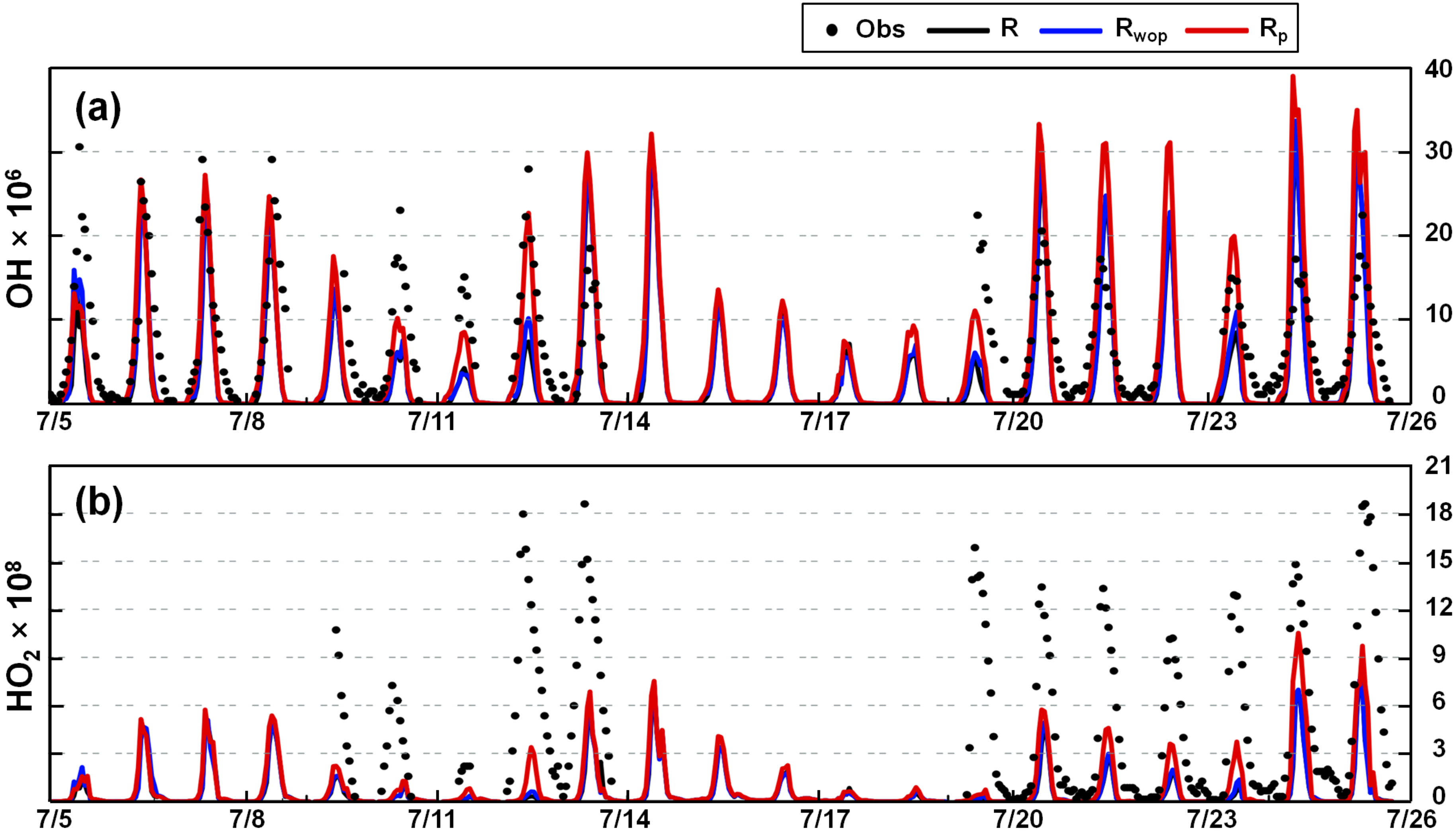

952

953 Fig. 6. Comparison of simulated and observed hourly-mean mixing ratios of OH and HO_2 at the Backgarden site in Guangzhou in July 2006 (Lu

et al., 2012).

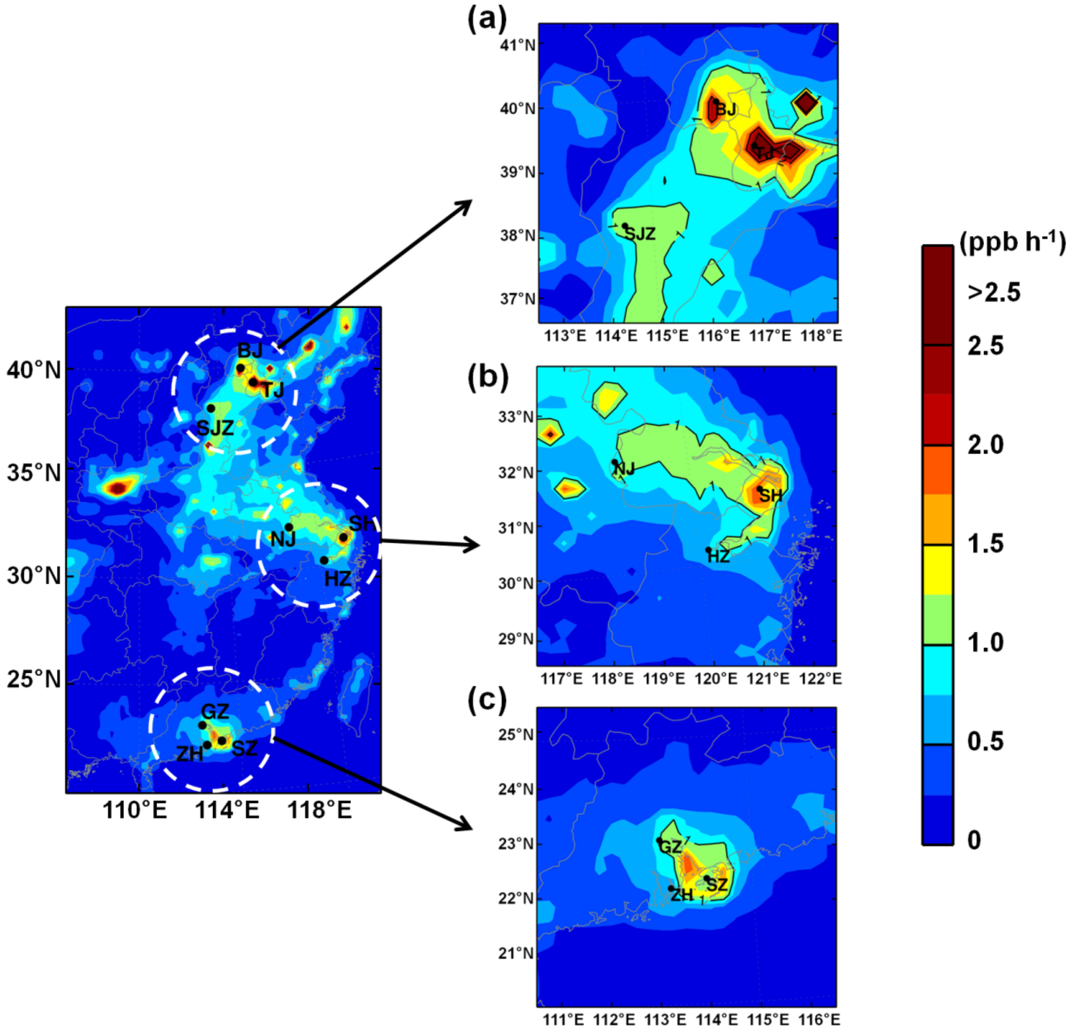

Fig. 7. Simulated unknown daytime HONO source (ppb h^{-1}) in the (a) BTH, (b) YRD, and (c) PRD regions in August 2007 (BJ, Beijing; TJ, Tianjin; SJZ, Shijiazhuang; SH, Shanghai; NJ, Nanjing; HZ, Hangzhou; GZ, Guangzhou; ZH, Zhuhai; SZ, Shenzhen).

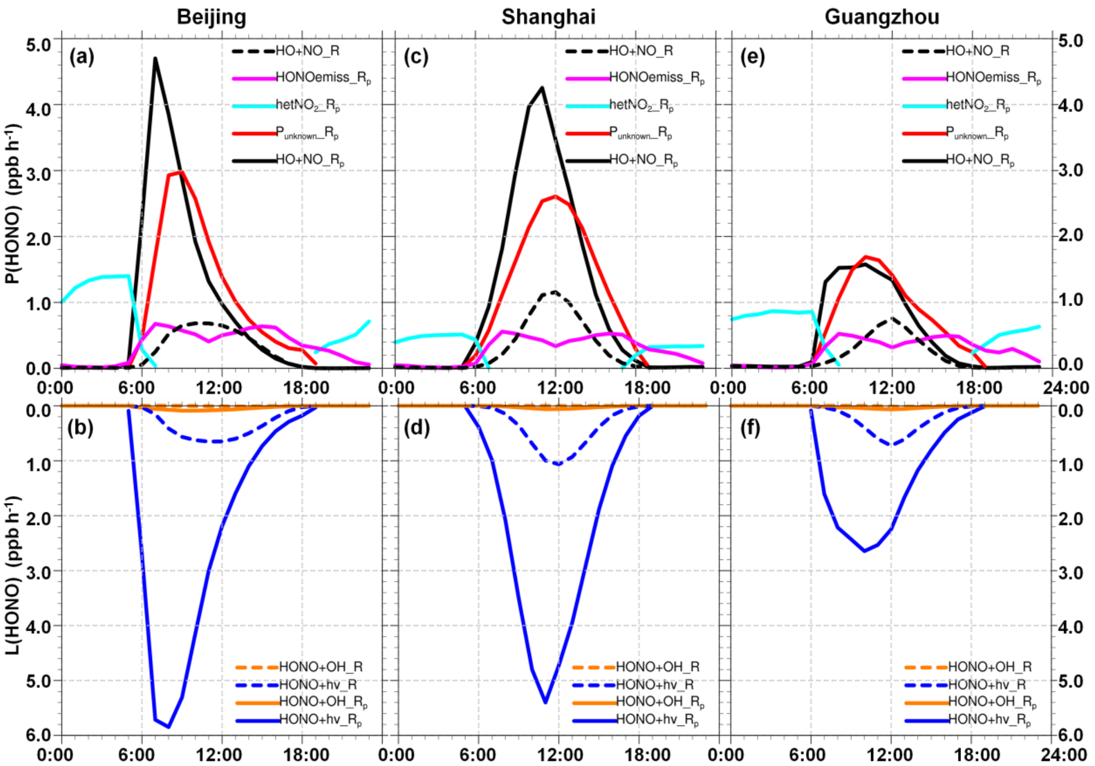

Fig. 8. Production [P(HONO)] and loss [L(HONO)] rates of HONO for cases R (dashed lines) and R_p (solid lines) in (a, b) Beijing, (c, d) Shanghai, and (e, f) Guangzhou in August 2007.

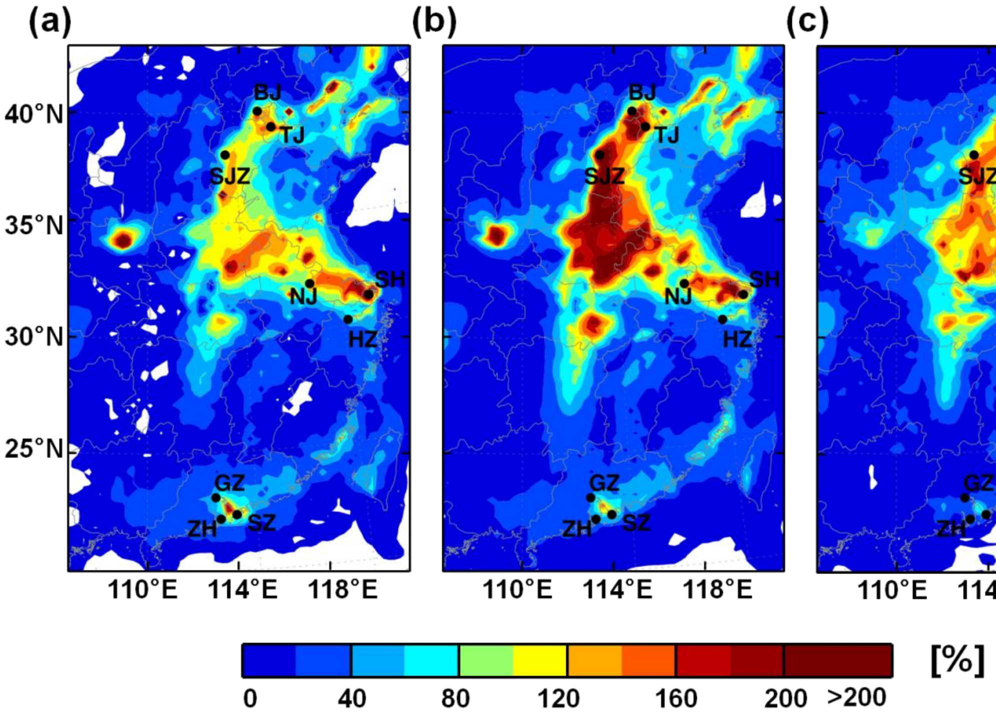

Fig. 9. Daytime (06:00–18:00 LST) percentage enhancements of (a) OH, (b) HO_2, and (c) RO_2 due to the unknown daytime HONO source (case R_p − case R_{wop}) in the coastal regions of China in August 2007.

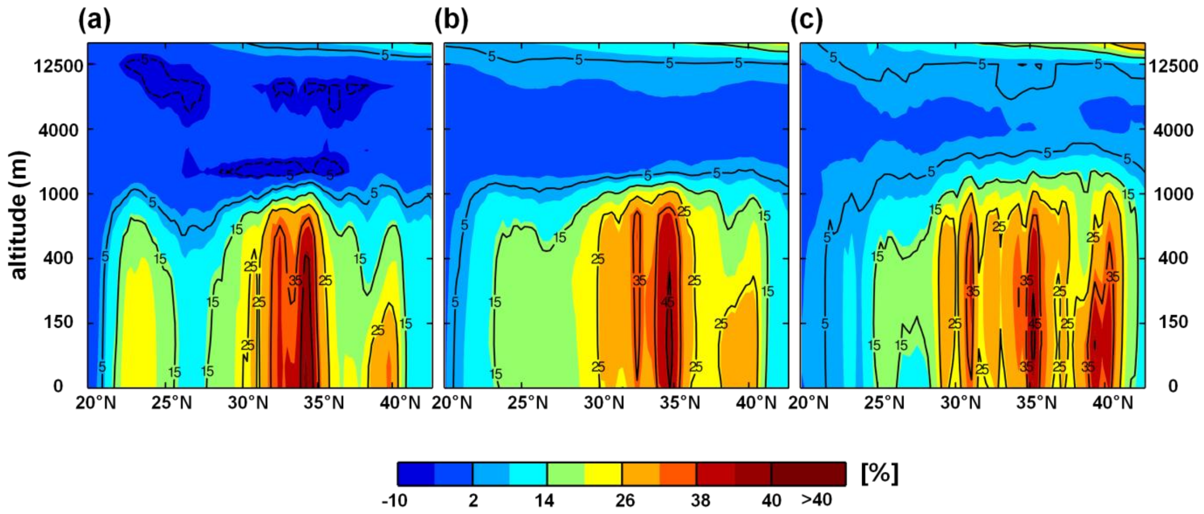

Fig. 10. Daytime (06:00–18:00 LST) meridional-mean percentage enhancements of (a) OH, (b) HO_2, and (c) RO_2 due to the unknown daytime HONO source (case R_p − case R_{wop}) in the coastal regions of China in August 2007.

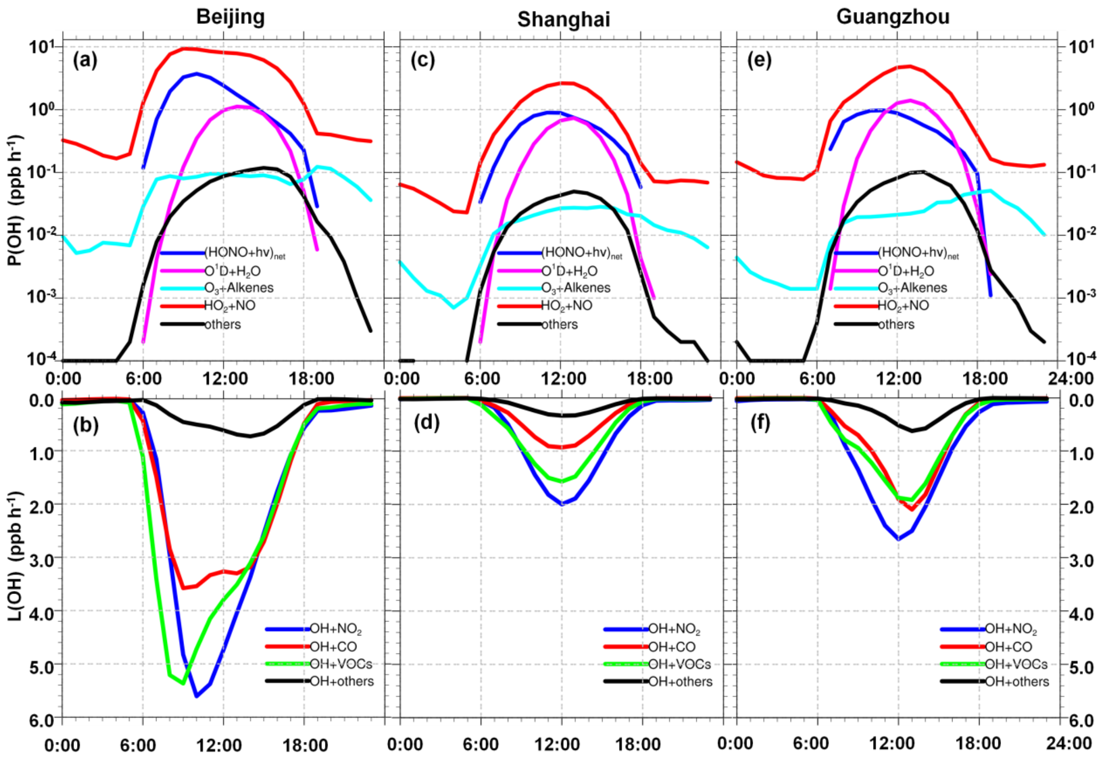

Fig. 11. Averaged production [P(OH)] and loss [L(OH)] rates of OH for case R_p in (a, b) Beijing, (c, d) Shanghai, and (e, f) Guangzhou in August 2007. $(HONO+hv)_{net}$ means the net OH production rate from HONO photolysis (subtracting OH + NO = HONO).

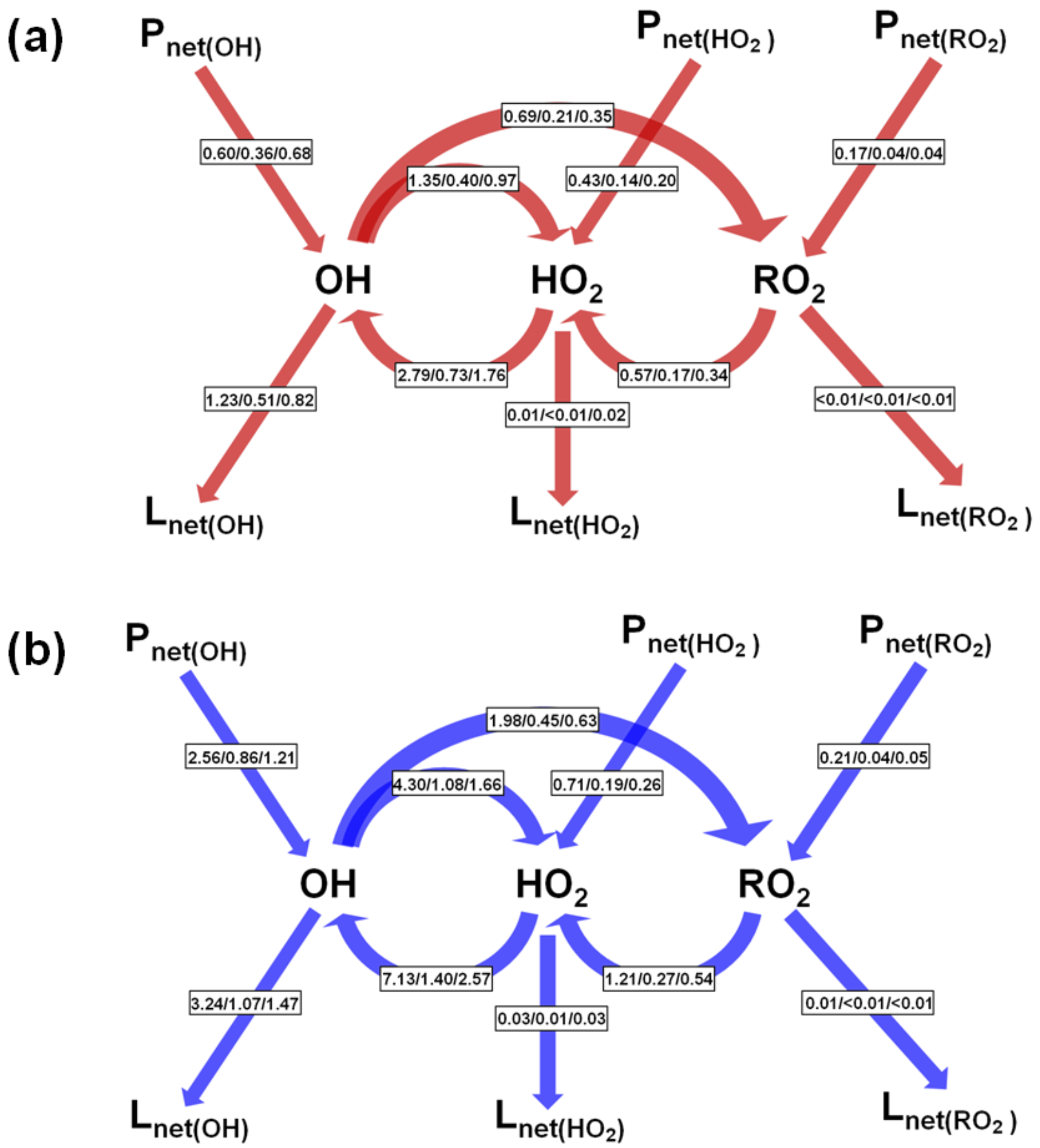

Fig. 12. Daytime (06:00–18:00 LST) average budgets of OH, HO_2 and RO_2 radicals (reaction rates, ppb h^{-1}) for cases (a) R and (b) R_p in Beijing/Shanghai/Guangzhou in August 2007.

1